Impact of aging and enriched environment on α-synuclein propagation

Doctoral thesis

to obtain a doctorate (PhD)

from the Faculty of Medicine

of the University of Bonn

Tanja Kraus

from Freising, Germany

2022

Written with authorization of

the Faculty of Medicine of the University of Bonn

First reviewer: Prof. Dr. Anja Schneider

Second reviewer: Prof. Dr. Tiago Fleming Outeiro

Day of oral examination: 28 March 2022

From the German Center for Neurodegenerative Diseases

Director: Prof. Dr. Dr. Pierluigi Nicotera

Table of contents

List of abbreviations

AD	Alzheimer's disease
AMB	nucleus ambiguous
ANOVA	analysis of variance
AP	area postrema
a-syn	α-synuclein
BCA	bicinchoninic acid assay
BDNF	brain-derived neurotrophic factor
BME	Basal Medium Eagle
BSA	bovine serum albumin
Ca^{2+}	calcium
CCR2	C-C chemokine receptor type 2
CD	cluster of differentiation
CHI	chromogenic immunohistochemistry
CLEC7A	C-type lectin domain family 7 member A
CNS	central nervous system
contra	contralateral
DAB	3-3’-diaminobenzidine
DAMP	damage-associated molecular pattern
DAPI	4’,6-diamidino-2-phenylindole
DMX	dorsal motor nucleus of the vagus nerve
DPBS	dulbecco’s phosphate buffered saline
ECL	electrochemiluminescence
EDTA	ethylenediaminetetra acetic acid
EE	enriched environment
ELISA	enzyme-linked immunosorbent assay
ER	endoplasmic reticulum
EtOH	ethanol
FAM	fluorescein amidites
FB	forebrain
FBS	fetal bovine serum
FC	Flow cytometry

FcγR	Fc gamma receptor
FSC	forward scatter
GAPDH	glyceraldehyde 3-phosphate dehydrogenase
GC	genome copies
GDNF	glial cell-derived neurotrophic factor
GEO	geometric mean
GFP	green fluorescent protein
ha-syn	human α-synuclein
HBSS	hanks' Balanced Salt Solution
HRP	horseradish peroxidase
Iba1	ionized calcium-binding adapter molecule 1
IF	immunofluorescence
IgG	immunoglobulin G
IGX	inferior ganglion of the vagus
IHC	immunohistocemistry
Il	interleukin
ipsi	ipsilateral
ITR	inverted terminal repeats
LB	lewy body
LC	locus coeruleus
LDH	lactate dehydrogenase
LN	lewy neurite
LRRK2	leucine-rich repeat serine/threonine-protein kinase 2
MAP	mitogen-activated protein
MB	midbrain
MEM	minimum Essential Medium Eagle
MFI	mean fluorescence intensity
MHC-II	major histocompatibility complex class II
MO	medulla oblongata
MOI	multiplicity of infection
MPTP	1-methyl-4-phenyl-1,2,3,6-tetrahydropyridine
n	number of biological replicates
NF-κB	nuclear factor kappa-light-chain-enhancer of activated B cells

NHS	normal horse serum
NLRP3	NLR family pyrin domain containing 3
NTS	nucleus of the solitary tract
OD	optical density
6-OHDA	6-hydroxydopamine
pA	polyadenylation signal sequence
PBS	phosphate-buffered saline
Pc	pars compacta
PD	Parkinson’s disease
PFA	para-formaldehyde
PFF	preformed-fibril
pH	potential hydrogen
PLL	poly-l lysine
PPN	pedunculopontine nucleus
rAAV	recombinant adeno-associated virus
RBD	rapid eye movement sleep behavior disorder
ROS	reactive oxygen species
rpm	revolutions per minute
RT	room temperature
RT-PCR	real time polymerase chain reaction
SDS	sodium dodecyl sulfate
SEM	standard error of the mean
SN	substantia nigra
SNARE	soluble N-ethylmaleimide-sensitive factor attachment protein receptor
Snca	gene encoding mouse α-synuclein
SPP1	secreted phosphoprotein 1
SSC	sideward scatter
TBS	tris-buffered saline
TH	tyrosine hydroxylase
TLR	toll like receptor
TNF	tumor necrosis factor
v/v	volume per volume
w/v	weight per volume

WPRE	woodchuck hepatitis virus post-transcriptional regulatory element
xg	times gravitational acceleration

1 Introduction

1.1 Parkinson's disease (PD)

Parkinson's disease (PD) and the associated motor symptoms were first described in 1817 by James Parkinson (Parkinson 2002). Presently PD is viewed as the most common movement disorder and the second most common neurodegenerative disease. The risk of developing PD rises steadily with increasing age. The prevalence of PD is approximately one percent at the age of 60 and increases to five percent by the age of 85 (de Lau & Breteler 2006). In 2015 around 6.1 million people were affected worldwide compared to 2.5 million people diagnosed with PD in 1990. However, the number of affected people is expected to rise due to higher life expectancy (Dorsey et al. 2018). The associated disease burden will impact health care systems and costs in the coming decades (Kowal et al. 2013, Bohingamu Mudiyanselage et al. 2017).

PD is a slowly progressive disease of the central nervous system (CNS) causing a broad range of non-motor and motor symptoms (Kalia & Lang 2015). These symptoms are linked to pathological changes which are described in chapter 1.4. Non-motor symptoms such as hypersomnia (Haehner et al. 2007), rapid eye movement sleep behavior disorder (RBD) (Janković et al. 2015), and constipation (Svensson et al. 2016, Stirpe et al. 2016) can precede the development of typical motor symptoms and subsequent diagnosis by more than ten years (Schrag et al. 2015). PD is defined by motor symptoms like resting tremor, rigidity, bradykinesia, shuffling gait, postural instability, and dysphagia (Postuma et al. 2015, Kalia & Lang 2015). In addition to the motor symptoms, neuropsychiatric features can evolve at later time points including fatigue, depression, obsessive-compulsive disorder, hallucinations, and cognitive impairment (Reijnders et al. 2008, Chahine et al. 2016).

Currently, no disease-modifying therapies are available. Symptomatic treatment targets dopamine dysbalance caused by the loss of dopaminergic neurons in the substantia nigra (SN) (Sveinbjornsdottir 2016). The drugs either increase the dopamine concentration (levodopa, monoamine oxidase B inhibitors) or stimulate dopamine receptors (dopamine agonists) (Rizek et al. 2016). Nevertheless, treatment can lead to psychotic symptoms and during disease progression, to fluctuations of motor function (e.g. wearing off as well

as dystonia) and the increase of non-motor symptoms, due to the loss of dopaminergic cells and elevated dopamine sensitivity (see Figure 1.1) (Hely et al. 2008).

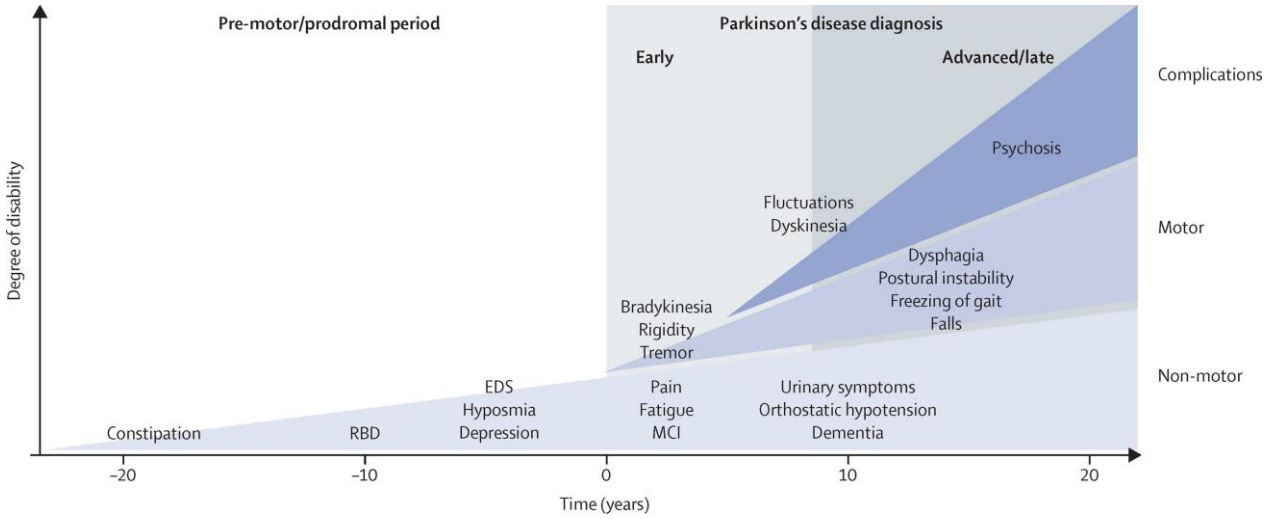

Figure 1.1: Typical symptoms in the progression of PD. The pre-motor period of PD can start around twenty to ten years before diagnosis with the appearance of non-motor symptoms like RBD and constipation. PD is diagnosed with the onset of motor symptoms like tremor and rigidity, which is followed by the development of a shuffling gait and postural instability. More neuropsychiatric characteristics can develop over time and complications often arise from the long-term side effects of symptomatic therapy. All of this increases the patient's level of disability. EDS: excessive daytime sleepiness; MCI: mild cognitive impairment; Reprinted from (Kalia & Lang 2015) with permission from Elsevier.

1.2 Forms of PD

PD can be either genetic or sporadic. Familial PD, which only accounts for approximately five percent of known PD cases, is an inherited form of this disease and might present with early-onset and a faster progression (Verstraeten et al. 2015, Deng et al. 2018). However, most cases of PD occur sporadically, due to an interplay of genetic, demographic, and environmental factors. These patients usually show a late-onset of the disease (Pang et al. 2019). In terms of clinical features, familial and sporadic PD have a broad overlap in the appearance of symptoms (Carr et al. 2003, Baba et al. 2006).

Familial PD underlies genetic causes and the first missense mutation linked to PD was found in the SNCA locus which encodes for the protein α-synuclein (a-syn) (Polymeropoulos et al. 1997). Up until now, six mutations in the SNCA gene have been identified as monogenic, i.e., just one of these mutations is sufficient for PD development (Krüger et al. 1998, Proukakis et al. 2013). Similarly, the multiplication of the SCNA gene leads to PD indicating the pivotal role of this gene and its dosage in disease development

(Singleton et al. 2003, Chartier-Harlin et al. 2004). In addition, 18 more genes have been identified and linked to PD although some follow a polygenic inheritance (Hernandez et al. 2016).

Sporadic PD is a multifactorial disorder and is presumed to be caused by a complex interaction of genetic susceptibility, age, sex, and environmental factors (Bennett et al. 1996, Ball et al. 2019, Selvaraj & Piramanayagam 2019). The genes accounting for the genetic vulnerability in sporadic cases are often similar to the genes affected in familial PD (Selvaraj & Piramanayagam 2019). Protective environmental factors are caffeine intake, cigarette smoking, and physical activity whereas pesticides and β-antagonists have been identified as environmental risk factors (Belvisi et al. 2020).

1.3 α-synuclein, the central protein involved in PD

Synucleinopathies including PD, dementia with Lewy bodies, multiple system atrophy, and further disorders are characterized by aggregated a-syn as the main component in Lewy bodies (LBs) (Spillantini et al., 1998). In PD, a-syn and more importantly aggregated a-syn is implicated in disease development and progression. Originally, the 140 amino acid long protein human a-syn was discovered in isolated amyloid plaques derived from Alzheimer's disease (AD) patient brains (Ueda et al. 1993). A few years later it was found in LBs and consequently linked to PD (Spillantini et al., 1997; Wakabayashi et al., 1997). The synuclein family is highly conserved and besides a-syn includes β-synuclein and γ-synuclein (Lavedan 1998). The homology of a-syn is furthermore conserved across species with human and mouse synuclein having a 95-% primary sequence match (Rochet et al. 2000).

1.3.1 Structure and function

The a-syn protein has a highly dynamic structure and in its physiological state, it mostly exists as an intrinsically disordered and soluble protein (Bertoncini et al. 2005). However, bound to phospholipids, the protein assembles a more structured and stabilized α-helical conformation (Davidson et al. 1998, Ulmer et al. 2005). The a-syn sequence can be divided into three distinct domains (see Figure 1.2 A). The N-terminus domain contains seven, eleven amino acid long sequence repeats predicted to form a helical secondary structure. This domain possesses lipid-binding properties (Bussell & Eliezer 2003).

Indeed, it has been shown that a-syn can bind to membranes and in particular binds preferentially to curved lipid membranes such as vesicles (Varkey et al. 2010). The middle domain of the a-syn sequence, the non-amyloid β component (NAC), exhibits a highly hydrophobic nature (Rodriguez et al. 2015). Therefore, this domain has a strong propensity to form β-sheet structures leading to the formation of aggregates (Giasson et al., 2001). The last domain at the C-terminus is unstructured, flexible, and highly negatively charged. It was shown to facilitate solubility and thus this domain is crucial in hindering the pathological aggregation process (Bertini et al. 2007, Wu et al. 2008).

The protein a-syn is ubiquitously expressed in the CNS, nevertheless, it is also found in blood circulating cells and in the hematopoietic cells of the bone marrow (Lavedan 1998, Nakai et al. 2007). In the brain, a-syn is vastly expressed in the synaptic terminals of neurons (Goedert, 2001; Iwai et al., 1995) and reported to be associated with synaptic vesicles there (Maroteaux & Scheller 1991). The physiological functions of a-syn are still not fully understood, but its function seems to be abundant.

In primary neurons from rats, an a-syn knockdown induced a decreased vesicle pool size (Murphy et al. 2000, Cabin et al. 2002). This effect was confirmed *in vivo* by the characterization of α-syn deficient mice. These mice displayed reduced dopamine levels in the presynaptic terminals of the SN and alterations in the vesicle pool size and mobilization (Abeliovich et al. 2000). However, overexpression of a-syn also led to a decrease in dopamine levels in mice. (Nemani et al. 2010). This was mediated by the reduced uptake of synaptic vesicles and a subsequent reduction in the vesicle recycling pool (Nemani et al. 2010, Scott & Roy 2012). In addition, a-syn has been found to interact with the assembly of the soluble N-ethylmaleimide-sensitive factor attachment protein receptor (SNARE) complex, which is involved in synaptic exocytosis (Burré et al. 2010, Garcia-Reitböck et al. 2010). In summary, a-syn was suggested to play a role in the regulation of vesicle trafficking, vesicle budding, and neurotransmitter release (Burré 2015).

1.3.2 Aggregation and toxicity

The native and soluble a-syn can undergo conformational changes that trigger aggregation. This development might be influenced by altered protein synthesis, gene

mutations, or changes in the cellular environment (Lashuel et al. 2013, Villar-Piqué et al. 2016). Aggregation of a-syn is a multistep process and begins with misfolding of monomeric a-syn. Subsequently, soluble oligomers are formed in a reversible process (Kalia et al. 2013). In a further step, the oligomers act as a seeding template. They gradually assemble more misfolded a-syn and eventually convert into large insoluble β-sheet structured amyloid fibrils (see Figure 1.2 B) (Villar-Piqué et al. 2016). These a-syn aggregates display a different subcellular distribution and are increasingly observed in the axons and the soma of neurons (Benskey et al. 2016).

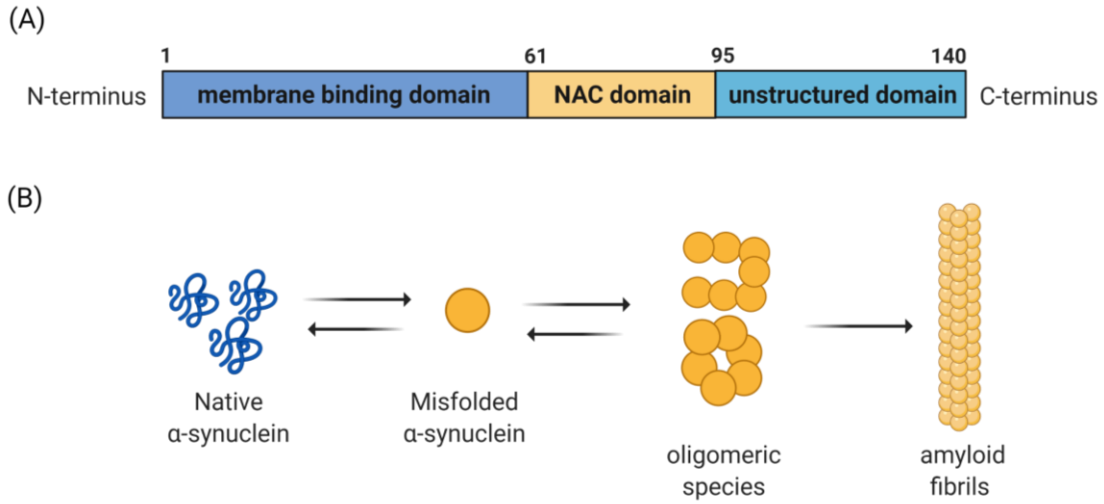

Figure 1.2: Schematic of SNCA sequence and aggregation process of a-syn. (A) The 140 amino acid sequence of a-syn is divided into three domains. At the N-terminus, there is a helical structured membrane-binding domain. The middle domain contains the non-amyloid β component (NAC) and is aggregation-prone. The last domain at the C-terminus has an unstructured conformation. **(B)** In its physiological state, native a-syn is present in a partially folded monomeric structure. However, under pathological conditions, it can misfold and then aggregate. Initially, soluble oligomeric species are formed. Then, more misfolded α-synuclein is recruited, leading to the formation of insoluble amyloid fibrils. Created with Biorender.

Aggregated a-syn is implicated in causing toxicity by disruption of several cellular mechanisms and consequently increasing cellular stress (Wong & Krainc, 2017). It is still controversial regarding which a-syn aggregates i.e. oligomers versus fibrils are the more toxic species (Conway et al. 2000, Winner et al. 2011, Pieri et al. 2012, Peelaerts et al. 2015). However, all aggregated a-syn species have proven to be capable of permeabilizing lipid membranes (Lashuel et al. 2002, Volles & Lansbury 2002, van Rooijen et al. 2010).

As expected from the localization and function of a-syn, synaptic homeostasis is one of the main pathways disrupted by a-syn aggregation. In this case, a-syn disrupts the dopamine release as well as the SNARE complex and alters the mobility of synaptic vesicles and the size of their pool (Choi et al., 2013; Nemani et al., 2010; Wang et al., 2014). Furthermore, the endoplasmic reticulum (ER) and associated Golgi pathway are affected by a-syn aggregates. Studies using different models indicate that a-syn overexpression and aggregation leads to ER stress, disrupts ER trafficking, and even induces Golgi fragmentation (Outeiro & Lindquist 2003, Cooper et al. 2006, Colla et al. 2012, Paiva et al. 2018). A-Syn aggregates can also trigger mitochondrial dysfunction. In cell and animal models, they have been described to cause mitochondrial DNA damage, enhance mitophagy, and even induce mitochondrial fragmentation (Martin et al. 2006, Choubey et al. 2011, Nakamura et al. 2011). This results in increased release of reactive oxygen species (ROS), which results in even more aggregation of a-syn (Giasson et al., 2000). The lysosomal-autophagy pathway is the main pathway for the clearance of a-syn aggregates (Lee et al., 2004). However, a-syn aggregates can block the formation of autophagosomes or impair enzymatic degradation in lysosomes leading to a-syn accumulation in the cell (Martinez-Vicente et al. 2008, Winslow et al. 2010, Tanik et al. 2013, Mazzulli et al. 2016).

1.3.3 Cell-to-cell transmission

Surprisingly, a-syn has been detected in the CSF and plasma of healthy individuals indicating that a-syn secretion is indeed a physiological process (El-Agnaf et al. 2003b, Llorens et al. 2016). The release of a-syn has also been demonstrated from wild-type and a-syn overexpressing neurons *in vitro* (El-Agnaf et al. 2003a). However, under pathological conditions, this mechanism of neuronal a-syn secretion has been proposed to act as an active clearing mechanism to reduce intracellular pathological a-syn levels (Ejlerskov et al. 2013). Lysosomal and mitochondrial dysfunction, impairment of the proteasomal function, or high levels of a-syn may trigger the increased secretion of a-syn (Jang et al., 2010; Lee et al., 2005; Reyes et al., 2015). On the one hand, this secreted a-syn can be degraded by extracellular proteases or by microglia phagocytosis (Kim et al., 2012; Lee et al., 2008a). On the other hand, it can be taken up by other cells like neurons

or microglia and accumulate (Choi et al., 2020; Danzer et al., 2009; Desplats et al., 2009b).

Depicted in Figure 1.3 are different molecular release and uptake mechanisms previously proposed for a-syn. Some mechanisms appear to be a-syn species-specific (Grozdanov & Danzer 2018). Monomeric a-syn can be released or taken up via a translocator in the cell membrane as a passive diffusion mechanism, whereas for aggregated a-syn a passive release mechanism is membrane leakage (Ahn et al., 2006; Lee et al., 2008a; Lee et al., 2005; Stöckl et al., 2013). A-syn sorted into multivesicular bodies can be released freely by non-classical exocytosis or inside of vesicles, i.e.: exosomes as an active release mechanism. In addition, a-syn can be released from the cell membrane within microvesicles (Emmanouilidou et al., 2010; Lee et al., 2005). Furthermore, tunneling nanotubes provide an active mechanism that facilitates the transfer of various a-syn species between two cells (Abounit et al. 2016, Dieriks et al. 2017).

Secreted a-syn in the extracellular space has been reported to be internalized by receptor-mediated endocytosis or directly at the membrane by pinocytosis (Hansen et al., 2011; Lee et al., 2008a; Mao et al., 2016; Shrivastava et al., 2015). For the extracellular vesicles, i.e. exosomes and microvesicles phagocytosis has been proposed as an internalization pathway (Danzer et al. 2012).

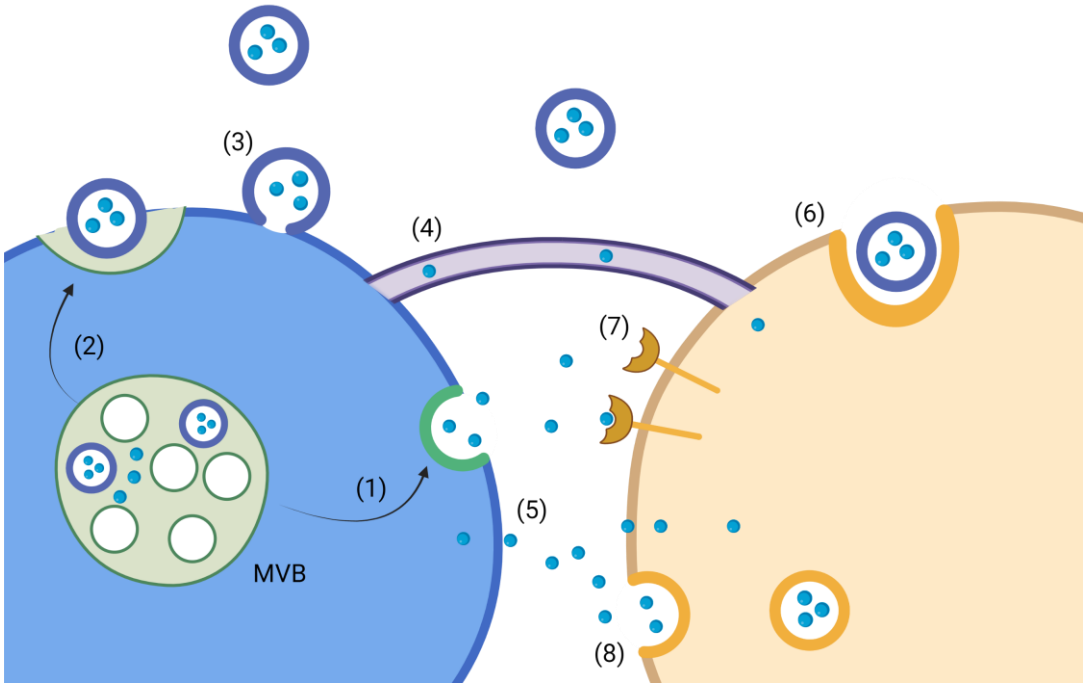

Figure 1.3: Release and uptake mechanisms of a-syn between cells. Different a-syn species can be released in extracellular vesicles either by the shedding of microvesicles from the cell membrane **(1)** or via the release of exosomes by the fusion of multivesicular bodies (MVB) with the membrane **(2)**. Naked a-syn can be released from these MVBs via the non-classical exocytosis pathway **(3)**. A direct transfer can occur via a tunneling nanotube between two cells **(4)**. A-Syn can be transferred by passive release, relying on a translocator in the cell membrane **(5)**. Free extracellular a-syn species can bind to receptors and be internalized **(7)** or taken up by pinocytosis **(8)**. Extracellular vesicles with a-syn are taken up by phagocytosis **(6)**. Schematic illustration based on (Grozdanov & Danzer 2018). Created with Biorender.

1.4 Pathology in PD

In PD the two main pathological hallmarks are LB pathology and the loss of dopaminergic neurons in the SN pars compacta (pc) (Braak & Del Tredici, 2009; Goedert et al., 2013). In addition, studies in recent years have recognized that neuroinflammation is a contributing factor in PD. However, it is controversial whether this process is beneficial and/or detrimental during disease progression (Dzamko et al. 2015, Rocha et al. 2015, Ransohoff 2016). The interplay of all these processes is crucial in the pathogenesis of PD.

1.4.1 Lewy body pathology

LBs were first identified in the post-mortem brains of PD patients in 1912 (Lewy 1912). They were characterized 50 years later as intracytoplasmic protein-rich depositions in neuronal somas (Duffy & Tennyson, 1965). Misfolded and aggregated a-syn was found to be the primary component in LBs and in addition, other neuronal proteins and lipid

membranes have been also associated with these inclusions (Shahmoradian et al., 2019; Wakabayashi et al., 2013). The deposits can also occur in neuronal processes, mostly in distal axons, where they are referred to as Lewy neurites (LN) (Martí et al. 2003). Until now evidence of LBs and LNs in PD patients has been detected not only in the CNS, but also in the peripheral nervous system, and the enteric nervous system (Braak & Del Tredici 2017).

Braak and colleagues analyzed post mortem brains of sporadic PD patients and described a stereotypical pattern of LB distribution at various time points during the course of the disease (Braak et al. 2003). The proposed model by Braak states that LB pathology originates in two distinct brain regions namely the dorsal motor nucleus of the vagus nerve (DMX) and the olfactory bulbs. From there LB pathology distributes in a spatial and temporal pattern to other anatomically connected brain regions (see Figure 1.4 A) (Braak et al. 2003, 2004). At present, however, in only about 50 % of postmortem PD brains does the pattern of LB distribution match that found by Braak (Beach et al., 2009; Jellinger, 2009; Kalaitzakis et al., 2008). Therefore, LB distribution and thus a-syn pathology cannot be explained by synaptic connectivity alone (Surmeier et al. 2017a). It has been suggested that, in addition to anatomical connectivity, certain types of neurons with defined intrinsic factors are more prone to develop LB pathology (Walsh & Selkoe 2016, Brundin & Melki 2017, Killinger & Kordower 2019).

Based on the stereotypical distribution pattern of LBs in PD, a prion-like spreading of a-syn pathology has been hypothesized. According to this hypothesis, a-syn misfolding and aggregation described in chapter 1.3.2 is triggered by an exogenous factor. Aggregated a-syn then acts as a template for the aggregation of native a-syn when transferred to other cells (Frost & Diamond 2010, Brettschneider et al. 2015). In chapter 1.3.3 different potential cellular mechanisms of a-syn cell-to-cell transfer are discussed. The prion-like spreading of a-syn is supported by the finding that PD patients, who received fetal mesencephalic neuron transplants in the striatum, exhibited proteinaceous deposits resembling LBs in these grafted neurons (Kordower et al., 2011; Li et al., 2008). In addition, animal experiments revealed that purified LBs from PD patient brains could induce aggregation of endogenous a-syn in mice and nonhuman primates (Recasens et al. 2014b).

1.4.2 Neuronal vulnerability

The second hallmark of PD is the loss of dopaminergic neurons in the SNpc. In general, the neuronal vulnerability of distinct neurons in different brain regions is part of the pathology in PDs progression (Surmeier et al. 2017b). This pattern of neuronal vulnerability only partially overlaps with the pattern of LB pathology in neurons (see Figure 1.4 B).

The average loss of dopaminergic neurons in the SNpc of diagnosed PD patients is approximately 68 %. Moreover, the neuronal loss in the SNpc correlates with the disease progression (Milber et al. 2012, Kordower et al. 2013, Kraemmer et al. 2014). Unfortunately, the extent of neuronal loss in other brain regions has not been consistently reported. In general neuronal loss has been reported in regions of the brain stem such as the locus coeruleus (LC), pedunculopontine nucleus (PPN), the area tegmentalis ventralis, and the DMX, but also in the basal forebrain (Giguère et al. 2018). This vulnerability does not necessarily affect entire brain regions, but often only particular populations of neurons. For instance, in the PPN only cholinergic neurons die but not dopaminergic, glutamatergic, or GABAergic neurons (Halliday et al. 1990). It is speculated that these vulnerable neuronal populations share common cell-autonomous features that may make them more vulnerable to aging, oxidative stress, and thus to cell death. The proposed common features of these vulnerable neurons are their highly branched morphology and their constant executed pace-making function (Surmeier et al. 2017b, Giguère et al. 2018).

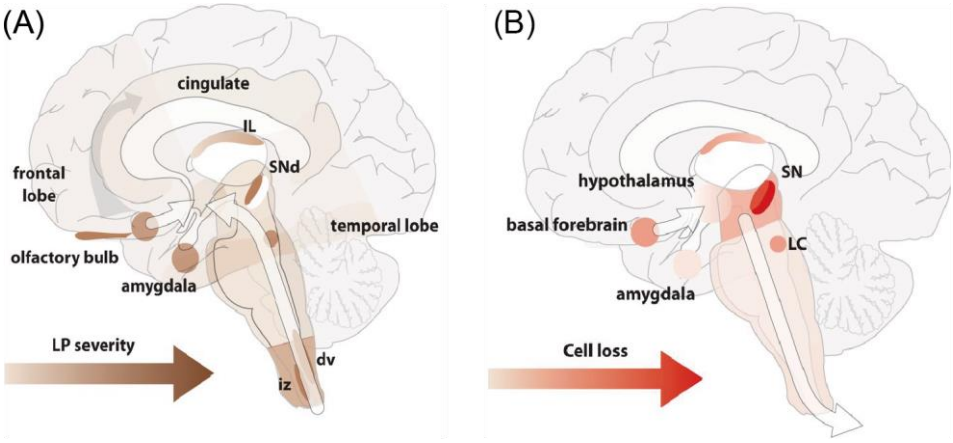

Figure 1.4: Stereotypical pattern of LB pathology and neuronal loss in PD. (A) Based on Braak, the propagation of LB pathology starts from the olfactory bulbs and the DMX. As the disease progresses, the pathology spreads to higher brain regions, indicated by the white arrow. The LB severity (marked in different shades of brown) differs in the brain regions. SNd: SNpc; dv: DMX; iz: intermediate reticular zone; IL: intralaminar thalamus **(B)** The pattern of neuron loss in specific brain regions in PD is shown by the white arrow. Neuron loss is almost confined to the brainstem and the severity is variable but most severe in the SN. LC: locus coeruleus. Reprinted from (Surmeier et al. 2017a).

1.4.3 Microglia and Neuroinflammation

Neuroinflammation contributes to the pathogenesis of neurodegenerative diseases such as PD, primarily through reactive microglia and astrocytes (McGeer et al. 1988, Imamura et al. 2003, Gerhard et al. 2006, Doorn et al. 2014). Microglia are the immune cells of the CNS and their central function is maintaining brain homeostasis and monitoring the brain for changes (Nimmerjahn et al. 2005). To maintain this homeostasis and immune balance in the brain microglia phagocytose pathogens as well as dysfunctional and dead neurons (Erwig & Henson 2007, Napoli & Neumann 2009). They can even trigger programmed cell death in neurons by releasing TNF-α, glutamate, superoxide, or nitric oxide (Marín-Teva et al. 2011). However, microglia exhibit both regional and age-related heterogeneity in their function, phenotype, and gene expression pattern (Keane et al., 2021; Li et al., 2019; Stratoulias et al., 2019).

In response to an endogenous or exogenous stimulus, microglia start the process of activation by changing their morphology and function (Hickman et al. 2018). In PD the activation of microglia is facilitated by extracellular monomeric or aggregated a-syn released by neurons (Emmanouilidou et al. 2010). This a-syn acts as a damage-associated molecular pattern (DAMP). Monomeric a-syn and oligomers bind mainly to toll-

like-receptor (TLR)2, TLR4, and the scavenger receptor cluster of differentiation (CD) 36 on microglia, whereas a-syn fibrils bind preferentially to the Fc gamma receptor (FcγR) (Choi et al., 2020; Fellner et al., 2013; Kim et al., 2013; Su et al., 2008).

This interaction induces diverse pathways like the nuclear factor kappa-light-chain-enhancer of activated B cells (NF-κB) and the mitogen-activated protein (MAP) kinase pathway. These cascades result in the activation of the NLR family pyrin domain containing 3 (NLRP3) inflammasome, an increase in ROS, and the expression and release of cytokines (see Figure 1.5) (Ferreira & Romero-Ramos 2018, Kam et al. 2020). Released pro-inflammatory cytokines include tumor necrosis factor (TNF)-α, interleukin (IL)-1β, IL-6, and along with other factors they create an inflammatory environment (Klegeris et al. 2008, Su et al. 2008, Couch et al. 2011). When inflammation and microglia activation becomes chronic, this toxic environment can contribute to neuronal death and neurodegeneration (Gao et al., 2011; Gordon et al., 2018; Wang et al., 2015; Zhang et al., 2005).

Importantly, binding of a-syn to the aforementioned receptors can activate microglia and facilitate uptake of a-syn by phagocytosis (see Figure 1.5) (Zhang et al., 2005). Indeed, microglia have been shown to have the highest degradative capacity for a-syn compared with other cells in the brain (Lee et al., 2008b). This degradation is facilitated by the autophagy pathway of the microglia (Choi et al., 2020). However, an excess of a-syn or fibrillar a-syn species can impede microglial phagocytosis (Choi et al., 2015; Haenseler et al., 2017) leading to a-syn accumulation in microglia (Croisier et al. 2005, Tanriöver et al. 2020). It is still unclear if microglia are also involved in the process of a-syn transmission. Recently two studies reported, that microglia release a-syn in extracellular vesicles and may propagate a-syn to nearby neurons (Guo et al. 2020, Xia et al. 2021). In another study, aggregated a-syn was previously shown to be transported between microglia by tunneling nanotubes (Scheiblich et al. 2021).

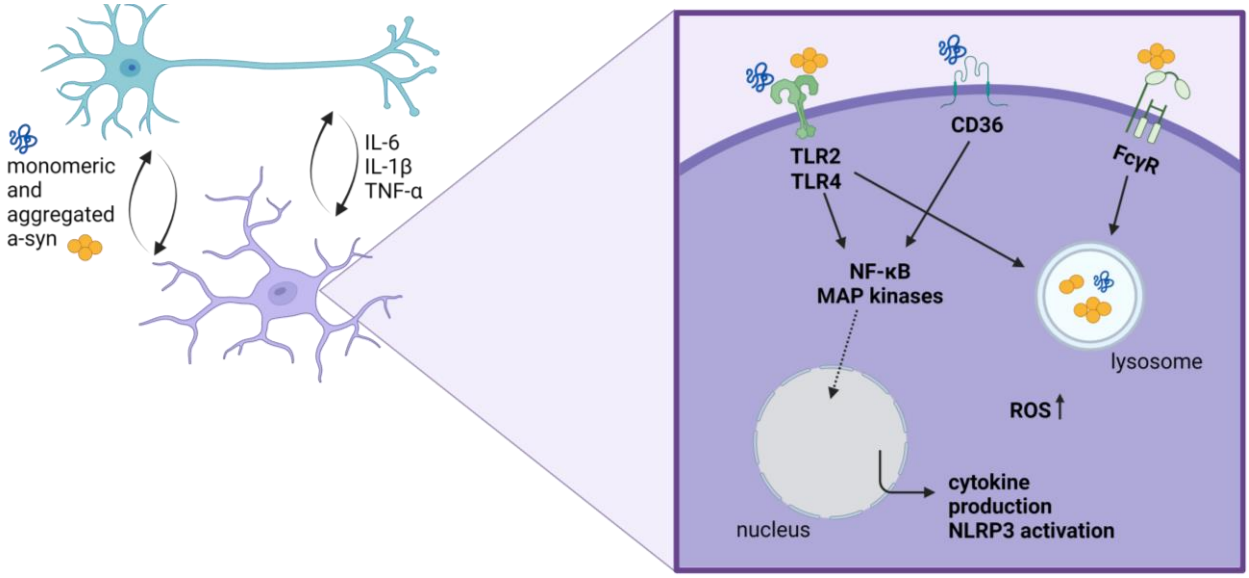

Figure 1.5: Microglia activation by neuronal released a-syn. Under pathological conditions aggregated and monomeric a-syn is released by neurons (blue) and activates microglia (purple) by binding to receptors like TLR2, TLR4, CD36, or FcγR on the microglia surface. Subsequently, NF-κB or MAP kinase pathways are activated, leading to transcriptional changes in the nucleus. As a result, cytokines are expressed and released such as IL-6, IL-1β, and TNF-α, the NLRP3 inflammasome is activated, and more reactive oxygen species (ROS) are produced. In addition, the receptor-bound a-syn is internalized by some receptors and degraded in the lysosome. Created with Biorender.

Ultimately, it remains controversial whether microglia play a beneficial or detrimental role in PD or if their role switches during disease progression. They release pro-inflammatory cytokines such as IL1β and TNF-α in a-syn pathology and can trigger neuronal cell death (Cardinale et al. 2021). Furthermore, microglia are known to phagocytose dead but also live and dysfunctional neurons in PD (Janda et al., 2018; Tremblay et al., 2019). In addition, microglia can phagocytose a-syn as described, but they may be also involved in the release and spread of a-syn.

1.5 Murine PD Models

There is no animal model available that fully recapitulates the heterogeneous PD pathology in humans. However, murine PD models provide a valuable tool to study various aspects of PD, disease pathology, and development. They are based on the administration of toxins, the use of transgenic models, the injection of viral vectors, or the injection of a-syn preformed fibrils (Chia et al. 2020).

Toxin-based models are the classic parkinsonian models and are the easiest to use. Local injection of the neurotoxin 6-hydroxydopamine (6-ODHA) into the brain or the systemic administration of 1-methyl-4-phenyl-1,2,3,6-tetrahydropyridine (MPTP) results in neuroinflammation, rapid and selective loss of dopaminergic neurons in the SN, and subsequent motor deficits (Ungerstedt et al. 1974, Sedelis et al. 2001). The model using the pesticide rotenone leads not only to dopaminergic neuronal loss in the SN and observable behavioral deficits but also to a-syn positive inclusions (Betarbet et al. 2000). However, compared to the neurotoxin models the rotenone model is not as consistent in terms of pathology features. In general, toxin-based models show consistent high dopaminergic neuron loss with associated motor deficits that resemble the late stages of PD. Unfortunately, they mostly fail to mimic the a-syn pathology and spreading as well as the slow progression of PD (Blandini & Armentero 2012).

Transgenic models utilize overexpression and/or silencing of genes or mutated genes that have been associated with familial PD (Li et al., 2010; Li et al., 2009; Masliah et al., 2000). Overexpression of wild-type or mutated a-syn is commonly used to study the function and aggregation of a-syn. This overexpression is often accompanied by neuroinflammation. Depending on the extent of expression, the regions, and the type of a-syn, this usually results in a-syn aggregation and mild motor impairments but generally is accompanied by very little dopaminergic neuronal loss in the SN (Richfield et al. 2002, Neumann et al. 2002, Emmer et al. 2011). Transgenic models using other gene mutations associated with familial PD often exhibit disruption of distinct molecular mechanisms such as mitochondrial or lysosomal dysfunction. However, they often fail to mimic PD pathology such as dopaminergic loss and motor deficits, and/or a-syn inclusion (Blandini & Armentero 2012).

Given the close relationship between a-syn pathology and PD, additional PD models have been developed that focus specifically on the role of a-syn in the disease. In these models, synthetic a-syn preformed-fibrils (PFFs) are generated and then administered preferably to the striatum or the SN of mice (Gómez-Benito et al. 2020). These exogenous a-syn fibrils trigger the aggregation of endogenous a-syn resulting in LB-like inclusions. Over time these a-syn inclusions were discovered to spread from the injected region to other brain regions. Moreover, neuroinflammation, mild dopaminergic loss in the SN, and motor

impairment were also detected (Breid et al., 2016; Duffy et al., 2018; Luk et al., 2012; Recasens et al., 2014a). Overall the PFF model mimics a-syn pathology and propagation under physiological a-syn levels but is triggered by an exogenous factor.

An alternative PD model to observe a-syn pathology is the overexpression of a-syn using viral vectors. In this case, the advantage is the targeted expression of a-syn in a brain region and a defined cell type such as neurons. The injection of viral vectors into the SN or striatum causes LB-like a-syn inclusions in neurons, variable neuronal loss, and associated motor dysfunction (Koprich et al. 2010, Oliveras-Salvá et al. 2013). However, this model is not only used to investigate neurodegeneration and a-syn pathology in the SN. To study the ability of a-syn transmission and propagation in the brain, a recombinant adeno-associated virus (rAAV) can be injected into the vagus nerve. This allows targeted a-syn overexpression in the medulla oblongata (MO), more specifically in the DMX and the area postrema (AP). Surprisingly, over time, this leads to a neuron-to-neuron transmission of a-syn to more rostral regions from the MO to the midbrain and the forebrain (Ulusoy et al. 2013, Helwig et al. 2016). As the DMX is one of the first brain regions affected by LB pathology this seems a compelling model to monitor a-syn propagation. However, no neuronal loss or a-syn inclusions in the nigrostriatal system or motor impairments are observed in this model even at longer time points (Rusconi et al. 2018).

1.6 Factors influencing PD development

As discussed in chapter 1.2, most cases of PD occur sporadically, with various environmental, demographic, and genetic factors influencing the prevalence of PD. Here, two important aspects and their role as risk or protective factors in PD are described in more detail.

1.6.1 Aging as a risk factor in PD

The number of people diagnosed with PD rises rapidly with age, making it the most crucial risk factor known in PD (Hirsch et al., 2016; Pringsheim et al., 2014). The process of aging, in general, is outlined as a time-dependent decline of various physiological functions and for humans nine hallmarks are defined to contribute to this phenotype on the cellular and molecular level (see Figure 1.6) (López-Otín et al. 2013). Interestingly, there are several

hallmarks such as loss of proteostasis, cellular senescence, genomic instability, mitochondrial dysfunction, and altered intercellular communication which are also implicated or perturbed in the development and progression of PD (Collier et al. 2017, Cherubini & Wade-Martins 2018).

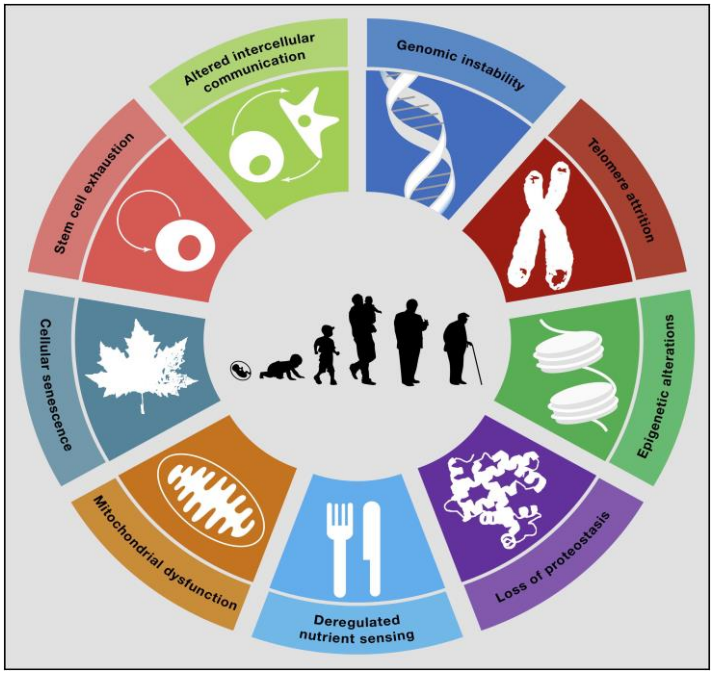

Figure 1.6: Factors impacting the process of aging. The phenotype of aging is defined on the molecular and cellular level by nine hallmarks. Reprinted from (López-Otín et al. 2013) with permission from Elsevier.

The aging process has widespread implications on the CNS. For instance, brain mass is known to decline during aging (Patterson 2015). Neuronal loss has been noted in the SN of aged but otherwise healthy people (Ma et al. 1999, Chen et al. 2000). One contributing factor may be that aging microglia are known to adopt a more reactive phenotype and produce pro-inflammatory cytokines. This gradual shift in aging has been termed "inflamm-aging" and can cause chronic inflammation and tissue damage (Franceschi et al., 2000; Franceschi et al., 2007).

Interestingly, studies have also detected a-syn depositions in a small number of elderly but otherwise healthy individuals (Buchman et al., 2012; Jellinger, 2004) and increased a-syn levels in the SN (Chu & Kordower, 2007; Li et al., 2004). In addition, a-syn has been found to be increasingly relocated from the synapses to the soma of neurons during aging (Chu & Kordower 2007). Taken together, this suggests that aging plays a central role in

the development and progression of PD (Collier et al. 2017). Surprisingly, little attention has been paid to the role of aging in the context of a-syn pathology and propagation in PD animal models.

1.6.2 Physical activity and enriched environment as a protective factor in PD

Physical activity is related to a reduction in the risk of developing PD. Many studies have found that moderate and high levels of physical activity are inversely correlated with the prevalence of PD (Ascherio & Schwarzschild, 2016; Bellou et al., 2016; Logroscino et al., 2006; Xu et al., 2010; Yang et al., 2015). Consequently, the increase in physical activity has been suggested as a simple and low-risk intervention to minimize the total number of PD cases (Marras et al. 2019). It has also been reported that physical activity can influence the development of diseases in patients. It has been shown that motor symptoms such as gait and balance and non-motor symptoms such as cognitive decline can be slowed in their progression and even improved by regular physical activity (Herman et al. 2007, Oguh et al. 2014, Combs-Miller & Moore 2019, Paul et al. 2019). In addition, cognitive training as an early intervention in the development of PD has also been shown to reduce symptom progression (Leung et al. 2015, Glizer & MacDonald 2016).

Enriched environment (EE) is an experimental paradigm that combines cognitive training and physical exercise to investigate the beneficial effects of these aspects on the brain. In rodent models, this is achieved by providing animals with a complex and changing environment with different objects and wheels to enhance sensory, cognitive, and physical stimulation. However, the paradigm is not standardized, and there is wide variation in components like object properties, social stimulation, larger space, and duration of stimulation (Nithianantharajah & Hannan 2006, Kempermann 2019).

Overall, EE has a variety of effects on the healthy brain in different brain regions as depicted in Figure 1.7. In rodents, EE has been shown to enhance synaptic plasticity (van Praag et al. 2000), increase the branching of dendrites (Faherty et al. 2003), and the number of dendritic spines in the cortex and the hippocampus (Leggio et al. 2005). In the hippocampus, adult neurogenesis was enhanced by EE by increasing the number of proliferating neurons (Kempermann et al. 2002, Bruel-Jungerman et al. 2005). In addition,

there are reports of increased numbers of astrocytes, microglia, and oligodendrocytes in various brain regions after EE treatment (Sirevaag & Greenough 1987, Ehninger & Kempermann 2003, Kronenberg et al. 2007). All these changes are likely mediated by the alteration of cellular and molecular mechanisms by EE. At the molecular level, EE alters gene expression (Rampon et al., 2000; Wassouf et al., 2018; Zhang et al., 2018). Similarly, cellular processes are changed by EE such as the level of neurotransmitters (Ragu Varman & Rajan 2015), immune factors (Singhal et al. 2014), or neurotrophic elements such as brain-derived neurotrophic factor (BDNF) (Gualtieri et al. 2017).

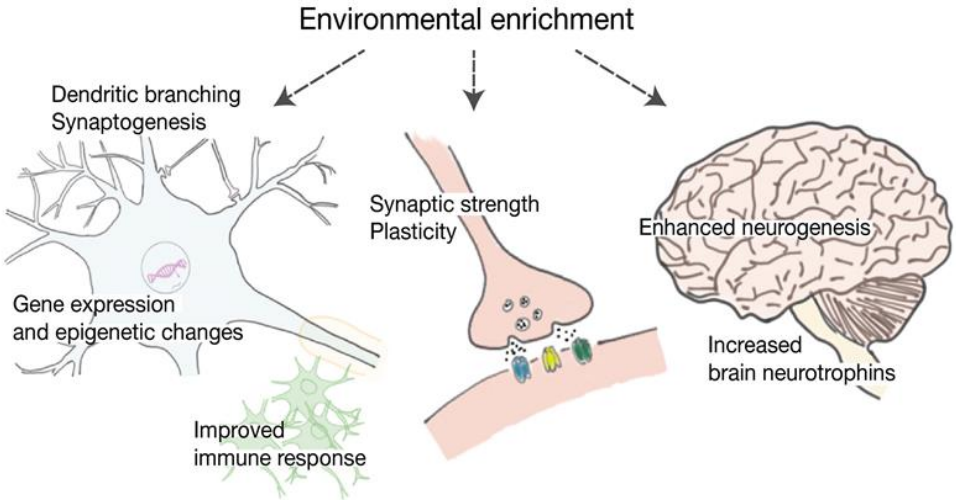

Figure 1.7: Effect of enriched environment on brain structure and function. EE has been shown to enhance synaptic plasticity and neurogenesis in the hippocampus. This is also mediated by an increase in neurotrophic factors. In addition, increased branching of dendrites and numbers of synapses were found. EE was also suggested to alter immune factors and thus improve the immune response. On the molecular level, EE was demonstrated to alter gene expression. Reprinted from (Wassouf & Schulze-Hentrich 2019).

Several studies have demonstrated a beneficial effect of EE in neurodegenerative diseases such as PD, AD, and Huntington (van Dellen et al. 2000, Brown et al. 2013, Fischer 2016) and in various forms of brain injury (Hicks et al. 2007, Kovesdi et al. 2011, de Boer et al. 2020). The effect of EE in PD was first studied in rodents in toxin-based PD models. They reported reduced neuronal loss, attenuated glia insult, and improved motor behavior upon exposure to EE (Bezard et al. 2003, Steiner et al. 2006, Anastasía et al. 2009, Goldberg et al. 2011). These improvements are associated with augmented levels of BDNF and glial cell-derived neurotrophic factor (GDNF) (Cohen et al. 2003, Faherty et al. 2005). However, the underlying mechanisms of EE and the beneficial alterations in neurodegenerative diseases remain enigmatic.

To better understand EE and its effect on PD also in the context of a-syn pathology, recent studies have examined EE in a-syn overexpressing mice. They demonstrated that EE exposure reduced oxidative stress and recovered the olfactory function in an a-syn overexpression mouse model (Wi et al. 2018). Furthermore, Wassouf *et al*. showed that long-term EE could offset alterations caused by a-syn overexpression at the mRNA level in neurons, microglia, and astrocytes (Wassouf et al. 2018). Nevertheless, it remains unclear whether EE has a direct impact on a-syn propagation and microglial activation in the context of a-syn pathology.

1.7 Aim

A-syn is an important aspect of PD development and one of the main drivers of PD progression. In particular, the distribution of a-syn to restricted brain regions during disease progression appears to be an important mechanism in the development of the disease. Therefore, in this study, we used an rAAV-based ha-syn overexpression model showing the propagation of ha-syn from the brainstem, more specifically in DMX, to higher brain regions.

However, it is not known which cell-intrinsic aspects and external factors might play a crucial role in the propagation of a-syn. Therefore, this study aimed to investigate the role of aging as a cell-intrinsic aspect and enriched environment as an external factor in the propagation of a-syn. In addition, the role of these factors on microglia and neuroinflammation as well as neuronal vulnerability was investigated.

2 Material and Methods

2.1 Materials

2.1.1 Compounds, consumables, and commercial kits

All plastic consumables were purchased from BD Falcon (BD Biosciences, Le Pont de Claix, France), Greiner bio-One GmbH (Frickenhausen, Germany), Starlab GmbH (Hamburg, Germany), or Eppendorf AG (Hamburg, Germany). All surgery tools were purchased from World Precision Instruments (WPI, Sarasota, USA), Fine Science tools (FST, Foster City, USA), AgnThos (Lidingö, Sweden), or Hammacher (Solingen, Germany). Mouse toys and wheels for EE were acquired at an online pet store and sterilized with H_20_2 before usage.

Table 2.1: List of consumables and compounds.

Reagent	Manufacturer/Catalog number
BD Microlance 3 Sonderkanülen 26G	Becton Dickinson GmbH (304300)
BD Plastipak Tuberkulinspritzen 1 ml	Becton Dickinson GmbH (300013)
Basal Medium Eagle (BME)	Gibco (21010046)
Bovine Serum albumin (BSA), reagent grade	Hiss Diagnostics (1900-0016)
Buprenorphin-hydrochlorid (Temgesic® 0.3 mg/mL)	GEHE (PZN 00345928)
Carprofen (Rimadyl® Cattle 50 mg/ml)	Pharmacy (PZN P3935116)
cOmplete protease Inhibitor cocktail	Roche Diagnostics (11836153001)
Corning® cell strainer (70 µm)	Merck (CLS431751)
Cresyl violet solution double strength	FD Neurotechnologies (PS102-02)
DPX Mountant for histology	Merck (06522)
Dulbecco's Phosphate Buffered Saline (DPBS) (without Mg^{2+} and Ca^{2+})	Gibco (14190169)
GlycoBlue Coprecipitant (15 mg/mL)	Invitrogen (AM9515)
Hanks' Balanced Salt Solution (HBSS)	Gibco (14025092)
Human Brain Total RNA 1 mg/ml	Invitrogen (AM7962)
Immersol 518 F	Zeiss (10539438)
Isoflurane (Vetflurane® 1000 mg/g)	Pharmacy (PZN 4001404)
MACS LS column	Miltenyi Biotec (140-096-433)
Minimum Essential Medium Eagle (MEM)	Gibco (11090081)
MicroAmp Fast Optical 96-Well Reaction Plate	Applied Biosystems (4346907)
MSD Read Buffer T (4x)	Meso Scale Discovery (R92TD-1)
MVP Total RNA Mouse Brain C57BL6, Male 0.9 µg/µl	Agilent (736501-41)
MULTI-ARRAY® 96 Plate	Meso Scale Discovery (L15XA-6)
Myelin removal beads	Miltenyi Biotec (130-094-060)
Normal horse serum (NHS) blocking solution	Vector Laboratories (S-2000-20)

O.C.T. compound embedding medium	VWR (361603E)
Pentobarbital-natrium (Release ad us. Vet. 300 mg/ml)	Wirtschaftsgenossenschaft deutscher Tierärzte (PZN 21217)
peqGOLD TriFast	VWR (30-2010DE)
Power SYBR Green PCR Master Mix	Thermo Fisher Scientific (4368577)
Precellys® Keramik-Kit (2 ml Tubes with 1.4 mm ceramic beads)	Bertin Instruments (432-3751DE)
SuperFrost Plus slides	Thermo Fisher Scientific (10149870)
Surgical disposable blades (sterile)	B. Braun (BA211)
TaqMan Fast Advanced Master Mix	Applied Biosystems (11380912)
Ultra Mikrotom blade	Thermo Fisher Scientific (3053835)
Zeba Spin Desalting Columns, 40K MWCO	Thermo Fisher Scientific (87768)

Table 2.2: List of commercial kits.

Commercial Kits	Manufacturer/Catalog number
DAB Peroxidase (HRP) Substrate kit	Vector Laboratories (SK-4100)
LDH Assay Kit (Cytotoxicity)	Abcam (ab65393)
LIVE/DEAD Fixable Near-IR Dead Cell stain kit, for 633 or 635 nm excitation	Invitrogen (L10119)
Neural Tissue Dissociation Kit (P)	Miltenyi Biotec (130-092-628)
Pierce BCA protein assay kit	ThermoFisher Scientific (23225)
RecoverALL Total Nucleic Acid Isolation Kit for FFPE	Invitrogen (AM1975)
SuperScript IV Vilo Master Mix with ezDNase enzyme	ThermoFisher Scientific (11766050)
SuperScript Vilo cDNA Synthesis Kit	ThermoFisher Scientific (1754050)
VECTASTAIN Elite ABC-HRP Kit	Vector Laboratories (PK-6100)

2.1.2 Buffers and solutions

2.1.2.1 General buffers

All chemicals were purchased from AppliChem GmbH (Darmstadt, Germany), Merck (Darmstadt, Germany), VWR (Darmstadt, Germany) or Roth (Karlsruhe, Germany). All solutions were prepared with sterile ddH_2O and stored at room temperature (RT) unless described otherwise.

Table 2.3: Summary of general buffers and solutions.

Buffer/Solution	Composition
CHAPS lysis buffer, pH 8.0	1 % [w/v] 3-[(3-cholamidopropyl)dimethylammonio]-1-propanesulfonate 5 mM ethylendiaminetetra acetic acid (EDTA) 50 mM Tris-Hcl at 4° C
flow cytometry (FC) buffer	2.5 % [w/v] BSA 0.5 mM EDTA in PBS at 4° C
maintenance medium	MEM (1x) 0,2 % sodium bicarbonate 0,6 % glucose 1 % sodium pyruvate (100x) 1 % pen-Strep 1 % glutamax 2 % B27 (50x)
0.2 M phosphate buffer, pH 7.4	27.6 g NaH_2PO_4 53.6 of Na_2HPO_4 Add to 1 L with ddH_2O
phosphate buffered saline (PBS), pH 7.4	1 % [w/v] PBS powder
PBST	0.05 [v/v] Tween-20 in PBS
plating medium	BME (1x diluted with Eagle´s BSS) 10 % FBS (filtrated and heat-inactivated) 20 % (w/vol) glucose 1 mM sodium pyruvate 2 mM glutamine 1 % pen-Strep
poly-l lysine (PLL) buffer	0,5 mg/ml poly-l lysine (molecular weight: 30.000-70.000) 94 mM sodium tetrabonate 50 mM boric acid
tris-buffered saline (TBS)	0.05 M TRISMA Base 0.15 M NaCl adjust pH to 7.6 with HCl
TBS-triton	0.25 % [v/v] Triton-X-100 in TBS
TBS-tween	0.1 % [v/v] Tween-20 in TBS

2.1.2.2 Buffers for protein biochemistry

Table 2.4: Buffers for protein biochemistry.

Buffer	Composition
blocking buffer (for ECL)	1 % [w/v] BSA in PBST
homogenization buffer	PBS pH 7.4 1 % [v/v] Triton-X-100 3 µl/ml protease inhibitor mix protease inhibitor was added freshly

2.1.2.3 Buffers for Histology

Table 2.5: Buffers for tissue preparation and histology.

Buffer	Composition
blocking solution (for CIH)	5 % [v/v] NHS in TBS
100 % blocking solution (for IF)	2.5 [v/v] fetal bovine serum (FBS) 2.5 [v/v] BSA 2.5 [v/v] fish gelatin In 1x PBS pH 7.4 Stored at -20° C
mowiol	13.3 % Mowiol 33.3 % Glycerol 133 mM Tris-HCl pH 8.5 24mg/ml DABCO Stored at -20 °C
1x PBS with heparin	1 % [w/v] PBS powder 180 U/ml Heparin
4 % paraformaldehyde (PFA)	4 % [w/v] PFA 400 ml ddH_2O heat up to 55° C 600 ml 0.2 M Phosphate buffer freshly prepared every time, 4° C
quenching solution	10 % [v/v] H_2O_2 10 % [v/v] Methanol in TBS
30 % sucrose	30 % [w/v] Sucrose in 1x PBS at 4° C
Walters antifreeze solution	2.51 g g NaH_2PO_4 8.72 g of Na_2HPO_4 30 % Ethylene glycol 30 % Glycerol Add to 1 L with ddH_2O

2.1.3 Vectors

The rAAV was produced by Sirion Biotech (Munich, Germany) as serotype 2 for the genome and serotype 6 for the capsid. To produce the rAAV a reporter plasmid was used containing the human α-synuclein (ha-syn) sequence, green fluorescent protein (GFP), or no gene sequence insert for an empty rAAV. The gene is under the control of the human synapsin1 promoter to ensure the expression of this gene only in neuronal cells. The plasmids (see Figure 2.1) enclosed additional DNA coding for the woodchuck hepatitis virus post-transcriptional regulatory element (WPRE) and a polyadenylation signal sequence (pA) to enhance gene expression. The rAAVs were purified through a discontinuous iodixanol gradient and the rAAV containing layer further by a heparin affinity chromatography. The stock titer was determined by quantitative PCR against WPRE.

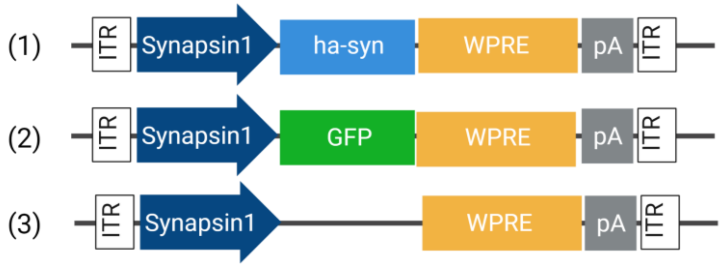

Figure 2.1: Reporter plasmid sequence for rAAVs. The reporter plasmid for a rAAV contained two inverted terminal repeat sequences (ITR) in the beginning and the end of the plasmid. The rAAVs comprised the promoter sequence (human Synapsin 1) followed by the gene for human α-synuclein (ha-syn) (1), the gene for the green fluorescent protein (GFP) (2), or no gene insert at all (3). Additionally, two enhancer sequences the woodchuck hepatitis virus post-transcriptional regulatory element (WPRE) and a polyadenylation signal sequence (pA) were added. Created with Biorender.

2.1.4 Synthetic oligonucleotides

All primers were synthesized by Sigma-Aldrich (Munich, Germany) and purified by high-performance liquid chromatography. Primers were reconstituted with ddH_2O and diluted to a 10 µM working solution and stored at -20° C. All FAM labeled TaqMan probes were ordered from Applied Biosystems (Waltham, USA).

Table 2.6: List of used primers for RT-PCR.

Primer	Sequence [5'-3']
ha-syn forward	AATGAAGAAGGAGCCCCACAG
ha-syn reverse	AAGGCATTTCATAAGCCTCATTGTC

Table 2.7: List of used TaqMan probes for RT-PCR.

Primer	Catalog number
GAPDH	Mm99999915_g1
Iba1	Mm00479862_g1
Il-6	Mm00446190_m1
Il-1β	Mm00434228_m1
TNF-α	Mm00443258_m1
TLR2	Mm00442346_m1
SPP1	Mm00436767_m1

2.1.5 Antibodies

Table 2.8 shows all antibodies used in the electrochemiluminescence (ECL) assay, flow cytometry, and immunohistochemistry (IHC). IHC antibodies are distinguished between immunofluorescence (IF) and chromogenic immunohistochemistry (CIH).

Table 2.8: List of antibodies.

Antibody target [clone]	Fluorophore /tag	Host species	Application /Dilution	Manufacturer /Catalog number
α-synuclein [4B12]		mouse	ECL assay (3 µg/ml)	Biolegend (807801)
α-synuclein [Syn-211]	Sulfotagged	mouse	ECL assay (1 µg/ml)	Invitrogen (32-8100)
goat IgG		goat	ECL assay (1 mg/ml)	Equitech-Bio. Inc (SLG56)
mouse IgG fraction		mouse	ECL assay (1 mg/ml)	Rockland Inc (D609-0200)
CD16/CD32 FcR block [93]		rat	Flow cytometry (1:200)	eBioscience (14-0161-86)
CD45 [30-F11]	BV711	rat	Flow cytometry (1:100)	Biolegend (103147)
CD11b [M1/70]	BUV737	rat	Flow cytometry (1:200)	eBioscience (564443)
CD11c [N418]	BV605	hamster	Flow cytometry (1:100)	Biolegend (117334)
CD68 [FA-11]	AF488	rat	Flow cytometry (1:100)	Biolegend (137011)

CCR2 [SA203G11]	BV510	mouse	Flow cytometry (1:100)	Biolegend (150617)
CLEC7A [bg1fpj]	PE-Cy7	rat	Flow cytometry (1:100)	eBioscience (25-5859-80)
MHC II [M5/114.15.2]	BV421	rat	Flow cytometry (1:100)	Biolegend (107632)
TLR2 [CB225]	PE	rat	Flow cytometry (1:200)	Biolegend (148603)
α-synuclein (MJFR1)		rabbit	CHI primary (1:50000)	Abcam (ab138501)
anti-Rabbit IgG	biotinylated	goat	CHI secondary (1:200)	Vector Laboratories (BA-1000-1.5)
Iba1		goat	IF primary (1:500)	Abcam (ab5076)
anti-Goat IgG	Alexa 555	donkey	IF secondary (1:300)	Thermo Fisher (A21432)

2.1.6 Software

Table 2.9: Overview of used software.

Software	Application	Source
Adobe Illustrator 25.4	Illustration of figures	Adobe Systems Inc
bioRender	Schemes for figures	BioRender.com
Fiji (Imagej.net)	Image processing and analysis	https://imagej.net/software/fiji/
FlowJo	Analysis of flow cytometry data	BD Life Sciences
GraphPad Prism® 9.1	Data and statistical analysis	GraphPad Software Inc.
Ilastik 1.3.3	Automated pixel classification for image analysis	(Berg et al. 2019)
Imaris 9.7.1	Image analysis	Oxford Instruments
MS Office Excel 2016	Data analysis	Microsoft
MS Office Word 2016	Writing and editing	Microsoft
MSD Discovery Workbench 3.0 Data Analysis Toolbox	Analysis of ECL assay	Meso Scale Discovery
Photoshop 22.4.3	Image processing	Adobe Systems Inc
Zen blue 2.3 lite	Image processing	Zeiss

2.2 Methods

2.2.1 Animals

The animal care committee of the State Agency Nature, Environment and Consumer Protection (LANUV) in North Rhine Westphalia approved all animal protocols and procedures. The mice were housed under standard conditions with a 12 h night/12 h day cycle in ventilated cages with free access to food and water. During EE mice were held in rat cages with the addition of several toys and wheels available. Wild-type mice were obtained either from Janvier (C57BL/6JRj) or from Charles River (C57BL/6J). For neuronal cultures, pregnant mice from Charles River (NMRI) were acquired. For experiments with EE, mice were between 9 and 10 months of age. The aging experiments were carried out in three different age groups. Young mice were between 3 and 5 months, mid-aged mice were between 13 and 15 months, and aged mice were between 22 and 23 months old.

2.2.2 Primary neuronal cultures

Neuronal cultures from the cortex of mouse embryos (day 16) were prepared and kindly provided by Dr. Anna Antoniou and Dr. Loic Auderset. The day before 12-well plates were coated with PLL buffer for 1 h at RT and then dried. After dissection 175.000 cortical neurons were seeded per well supplemented with plating medium. Three hours later the medium was changed to 500 µl maintenance medium. Three days after plating the neurons were transfected with rAAV. Here two different multiplicity of infections (MOI) doses were used for rAAVs. The low dose was a MOI of 20.000 equals $3.5x10^9$ Gc and the high dose a MOI of 80.000 equals $1.4x10^{10}$ Gc. Per condition, three technical replicates were prepared.

2.2.3 Enriched environment

The EE protocol was adapted from previously published experiments (Benito et al. 2018). The EE was started two weeks before rAAV injection into the vagus nerve and lasted until six weeks after the injection. In groups of five, the mice were housed in rat cages (1500 cm^2) with two running wheels and seven toys freely accessible. The toys ranged from tunnels in different sizes and materials, seesaws, suspension bridges, houses, walls to climb to little balls in different colors and sizes with bells inside. Every day two toys were

exchanged and the whole EE set up in the cage was altered. At the same time control animals were housed in standard mouse cages (501 cm^2). To expose them to the same stress cages for control mice were every day opened for one min.

2.2.4 Surgical procedure

The rAAV stock titer of $3{,}55x10^{12}$ for ha-syn and $1x10^{13}$ Gc/mL for GFP and empty rAAV was diluted with DPBS to a working concentration of $6x10^{11}$ Gc/mL if not stated otherwise. Mice were intraperitoneally injected with 0.06 mg/kg buprenorphine 30 min before the surgery. Under isoflurane anesthesia supplemented with oxygen and nitrous oxide mice were shaved and a one cm incision was made at the middle line of the neck. Then the left vagus nerve was isolated from the surrounding tissue and placed onto a paraffin plate. A blunt 36-gauge needle, connected by an extension tube to a 10 µl NanoFil syringe, was inserted into the nerve and 800 nl of rAVV were injected with an UltraMicroPump (WPI). While the virus was injected with a flow rate of 350 nl/min the paraffin plate was removed to avoid strong bending of the nerve. After the injection, the needle was kept in place for an additional minute for optimal diffusion of the liquid in the nerve. Then the wound was disinfected and closed with metal clips. The mice were transferred to a new preheated cage and monitored until they recovered from surgery. Mice were treated subcutaneously with 5 mg/kg carprofen for the following three days and wound healing was observed.

2.2.5 Tissue preparation

Depending on the subsequent analysis the brain was prepared and stored differently.

2.2.5.1 Fixed tissue for histology

Mice were injected intraperitoneal with an overdose of pentobarbital (600 mg/kg). When mice were deeply anesthetized (no pedal reflex) the chest was opened and the ascending heart aorta was punctured with a 26G needle. The mouse was perfused with PBS supplemented with Heparin for 2 min and then with ice-cold 4 % PFA for 2.5 min with a 10 rpm/min flow rate (300 series laboratory tube pumps D/E, Watson-Marlow). Next, the brain was removed and post-fixed for 24 h in 4 % PFA and cryopreserved for at least 48 h in 30 % sucrose. To obtain coronal sections the brain was cut with a freezing microtome

Microm HM 458 (Thermo Scientific) in 35 µm sections. The sections were stored at -20° C in Walters antifreeze solution.

2.2.5.2 Fresh tissue for protein and RNA isolation

Mice were sacrificed by cervical dislocation and the brain was removed. After a quick wash in ice-cold PBS, the brain was dried and snap-frozen on dry ice. The brains were stored at -80° C until the dissection. A part of the MO in the brain stem was dissected as this is the region where the injected rAAV transfected the neurons of the DMX. Therefore, brains were thawed for at least 1 h at -20° C and then 80 µm coronal sections were cut on the cryostat 3050S (Leica Microsystems). From the beginning of the brain stem, 12 sections from bregma -7.08 to -8.0 were identified. For that reason, earlier and later sections were stained with cresyl violet to confirm bregma values. From these sections, the cerebellum was discarded and the upper half was dissected. This section containing the DMX and surrounding regions was divided into ipsilateral (ipsi; i.e., injected side) and contralateral (contra; i.e., not-injected side) (see Figure 2.2). For protein isolation 2/3 of the material was used and 1/3 for RNA isolation. All samples were stored at -80° C until further usage.

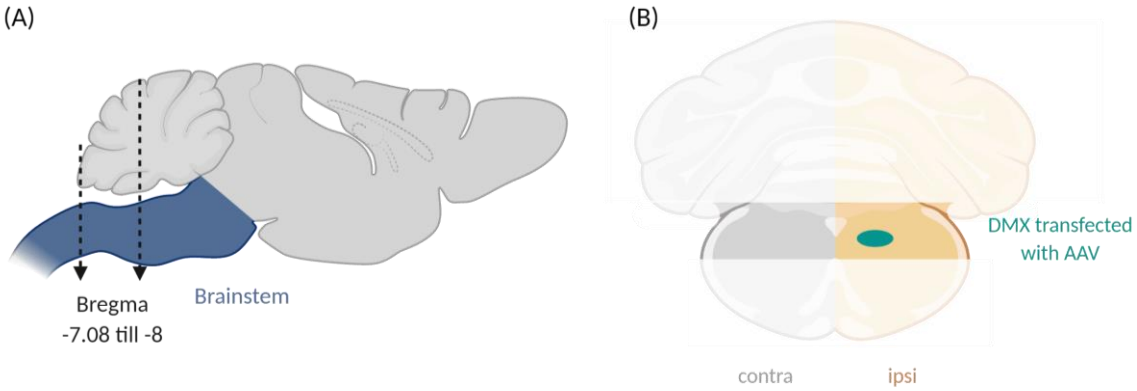

Figure 2.2: Scheme for dissection. (A) Sagittal cut through the mouse brain showing in blue the brain stem. The dotted arrows indicate the region of interest cut coronal for further dissection steps. (B) Coronal view of the region of interest. The contralateral side is gray and the ipsilateral side with DMX transfected by the rAAV is yellow. The shaded area shows the discarded regions. Created with Biorender.

2.2.5.3 Fresh tissue for cell isolation

Mice without injection were processed on the first day. Mice with rAAV injection were processed on the following day. Mice were sacrificed by cervical dislocation and the brain was washed with ice-cold HBSS. The cerebellum was removed and the brain was placed

in a cooled brain matrix. The brain was divided into three regions: MO (bregma from -8.5 to -5.5); Pons and Midbrain (Pons+MB; bregma from -5.5 to -2.5); Forebrain (FB; bregma from -2.5 to +5.0). Each region was put in ice-cold HBSS and immediately processed.

2.2.6 Histology

2.2.6.1 Free-floating chromogenic immunohistochemistry

For ha-syn staining, every 5th section of the brain was used. All free-floating stainings were done in a glass vial or a 24-well-plate depending on the number of sections. All incubations were carried out shaking with a Microplate shaker PMS-1000i (Grant Instruments LTD) at RT. Sections were first washed two times with TBS for 5 min. Then sections were incubated for 30 min with quenching solution to suppress endogenous peroxidase activity. Next, the sections were washed for 10 min three times with TBS-Triton. To block unspecific binding, the samples were incubated with blocking buffer for 1 h and afterwards rinsed three times with TBS-Triton for 10 min. The primary antibody was diluted according to Table 2.8 in TBS-Triton complemented with 1 % BSA and then incubated with sections overnight. Sections were washed three times with TBS-Triton for 10 min and then the appropriate biotinylated secondary antibody (1:200 dilution) in TBS-Triton supplemented with 1 % BSA was added for 1 h. Sections were again washed 10 min three times with TBS-Triton and then treated with the avidin-biotin-peroxidase complex, which was prepared following the kit manual instructions, for 1 h. Sections were washed two times with TBS-Triton and the last time with TBS. For the color reaction following the 3-3'-diaminobenzidine (DAB) peroxidase kit manual, the solution was prepared. Depending on the color reaction the sections were developed for 45 to 60 sec in the solution but always with the same amount of time per experiment. Next, they were washed three times with TBS. Sections were then mounted on coated slides and dried for 2 h at 37° C. Finally, sections were delipidated and dehydrated following the process described in Table 2.10 and then coverslipped with DPX mounting medium.

Table 2.10: Delipidation and dehydration procedure.

Solution	Repetition	Time of incubation
H_2O	1x	2 min
70% ethanol (EtOH)	1x	2 min
95% EtOH	1x	2 min
100% EtOH	3x	2 min
Xylene	3x	2 min

2.2.6.2 On slide chromogenic immunohistochemistry

The nissl staining was done for every 5th section of the brain containing the DMX. Sections were mounted onto coated slides and dried for 2 h at 37° C. Next slides were processed for delipidation and dehydration (see Table 2.10) and stained with cresyl violet following the process described in Table 2.11. Sections were coverslipped using DPX mounting medium.

Table 2.11: Procedure for nissl staining.

Solution	Repetition	Step
100% EtOH	3 x	2 min
95% EtOH	1 x	2 min
70% EtOH	1 x	2 min
H_2O	1 x	2 min
cresyl violet	1 x	between 3 to 5 min
H_2O	1 x	2 min
0.1% acetic acid in 95% EtOH	1 x	between 5 to 30 sec
95% EtOH	1 x	2 min
100% EtOH	3 x	2 min
Xylene	3x	2 min

2.2.6.3 Free-floating immunofluorescence

The staining was carried out in a 24-well plate with maximal three sections per well. All steps were carried out at RT and shaking if not stated otherwise. Sections were washed three times with TBS and then permeabilized with 0.3 % TritonX-100 and 0.6 % H_2O_2 in TBS for 30 min. Sections were washed three times with TBS for 10 min and blocked in 2 % blocking solution in TBS-Tween for 1 h. The primary antibody was diluted according to Table 2.8 in a 2 % blocking solution in TBS-Tween and incubated overnight at 4° C. After washing three times for 10 min the fluorophore-coupled species-specific secondary antibody was used in a 1:300 dilution in 2 % Blocking solution for 1 h. The sections were washed three times with TBS-Tween for 5 min, mounted onto coated slides, and dried for

2 h. Afterwards, they were coverslipped with Mowiol added with 1:1000 4’,6-diamidino-2-phenylindole (DAPI). Sections were stored in the dark and at 4° C.

2.2.7 Histological quantifications

Quantitative analysis was done while blinded to the experimental group. All microscopes used were provided by the light microscope facility of the DZNE (Bonn). The 40x oil objective was used in combination with Immersol 518 F.

2.2.7.1 Counting human α-synuclein (ha-syn) positive fibers

Every 5th section from the brain stained for ha-syn with DAB was used. The section with a predefined bregma value was identified using the 10x magnification objective of the Epi-Scope (Carl-Zeiss). Using a 40x objective with immersion oil the ha-syn positive fibers were counted on the ipsilateral side. A positive fiber was defined as at least two ha-syn dots in the vicinity of each other. Depending on the injection titer and time point the PONS was not counted due to many fibers which could not be separated anymore.

2.2.7.2 Imaging and image processing

Brightfield microscopy

Every 5th section from the brain stained for ha-syn with DAB was used. For an automated evaluation of ha-syn accumulation the section at the bregma value -5.4 and the section before and after was chosen. The whole sections were semi-automatically imaged using the Axioscan Z1 microscope (Carl Zeiss) with the 20x objective and a depth of 24 bit and 1 µm Z-stacks. The tiles were stitched automatically. The ipsilateral side of the sections was exported as Tiff-file and the exact section was cut with Adobe Photoshop.

Fluorescence microscopy

To count Iba1 positive cells two brainstem sections including the DMX were chosen and semi-automatically imaged using the Axioscan Z1 microscope (Carl Zeiss). The DAPI signal was used as a reference channel to find the focus and for automatic stitching. The whole sections were imaged with a 20x objective and a depth of 16 bit and 1 µm Z-stacks. The maximum intensity projection was done with Zen blue 2.3 lite manually and the files were exported as czi-file.

2.2.8 Data analysis

2.2.8.1 Automated fiber counting

For quantification, the pixel classification tool in Ilastik was used. For the training of the program at least five sections per experiment were used. In each section, the background was marked in one color and the brown stained fibers in another color. After successful training, the classification tool was applied to all sections. Next, the exported grayscale masks were imported to Fiji. Here a threshold was set and the area of ha-syn was analyzed.

2.2.8.2 Cell counting

To count the microglia, the czi-files of the Iba1/DAPI images were opened with Fiji. First, the region of interest was defined based on the DAPI and Iba1 signal which contained the DMX, NTS, area postrema, a small part of the hypoglossal nucleus, and the intermediate reticular nucleus. Using the cell counter plugin by Kurt De Vos Iba1 cells that were also positive for DAPI were counted by hand. The number of cells was normalized to the area of the region.

2.2.9 Flow cytometry

2.2.9.1 Cell isolation

All steps were carried out at 4° C and with ice-cooled HBSS. The brain, dissected as described in chapter 2.2.5.3, was homogenized as described in the manual for the neuronal dissociation kit, by enzymatic and mechanical dissociation with the gentleMACS dissociator (Miltenyi biotec). 1 mL of the buffer mix was used for the FB samples and 0.5 mL for the PONS+MB and the MO samples. After the dissociation, each sample was additionally processed through a 70 µm cell strainer to acquire a single cell suspension. The tubes were washed twice and in the end, the samples were topped up to 15 mL with HBSS. After a centrifugation step (400xg, 7 min) samples were washed once more with 15 mL HBSS. The cells were resuspended in 500 µl FC buffer and 120 µl of myelin removal beads for the FB and 60 µl of myelin removal beads for PONS+MB and the MO samples were added to bind the myelin. After 15 min incubation in the dark, the samples were filled up to 10 mL with FC buffer and centrifuged (400xg, 7 min). At the same time, LS columns were placed in a MidiMACS separator magnet (Miltenyi biotec) and were

equilibrated with 3 mL of FC buffer. As the cell suspension was separated by a negative selection the flow-through of the column was collected. Samples were mixed with 1 mL FC buffer and loaded onto a LS column. The tubes were washed with 1 mL of FC buffer and applied onto the respective column. Finally, all columns were washed with 1 mL of FC buffer. The flow-through was centrifuged (400xg, 7 min) and taken up in 1 mL (FB), 500 µl (Pons+MB), or 100 µl (MO) FC buffer.

2.2.9.2 Staining

The antibody mix (see Table 2.8, all antibodies for flow cytometry) was prepared for all staining's in PBS including the Live/dead kit in a 1:1000 dilution. For each region, 100 µl of cell suspension from Section 2.2.9.1 was transferred to a 96-well plate. The plate was spun at 1500 rpm for 5 min. The cells were resuspended in 100 µl of the antibody mix and incubated for 20 min in the dark. This mix contained a dye to visualize dead cells from live cells to exclude them from the flow cytometry analysis. Additionally, a CD16/CD32FcR antibody was present in this solution to block the respective receptors since other antibodies could non-specifically bind to the CD16 or CD32 receptor. Cells were centrifuged (1500 rpm, 5 min) and then fixed with 4 % PFA for 10 min. Samples were measured with a FACSymphony A5 (BD Bioscience).

2.2.10 Biochemical analysis

2.2.10.1 LDH Assay

Supernatant from neuronal cultures from chapter 2.2.2 was taken four days after transduction with rAAVs for the lactate dehydrogenase (LDH) assay. The instructions of the manual were followed and slightly optimized. Non-treated neurons used as high control were lysed for 1 h by adding 20 % of lysis buffer to destroy all cells and get the maximal LDH release. Afterwards, 100 µl of cell supernatant from all samples was taken and centrifuged (600xg, 10 min). Meanwhile, the LDH reaction mix was prepared with WST substrate and LDH assay buffer (1:50). Then 50 µl of the samples and 100 µl of the reaction mix were added into an optically clear 96-well plate. The plate was incubated between 55 and 100 minutes until the high control exceeded an optical density (OD) of 1.6. The plate was measured at 450 nm with the FLUOstar omega plate reader (BMG

Labtech). The cytotoxicity was calculated as a percentage from the OD values. Low control refers to the OD of non-treated cells:

$$cytotoxicity = (Sample - Low\ control)/(High\ control - Low\ control) * 100$$

2.2.10.2 Protein isolation and quantification

Dissected samples from fresh tissue as described in chapter 2.2.5.2 were homogenized mechanically. For that process samples were already dissected and stored at -80° C in 2 mL Precellys tubes. Sterile ceramic beads and 70 µl of homogenization buffer were added to the samples. The tissue was homogenized for 60 sec at 5000 rpm with the Precellys 24-Dual Tissue homogenizer (Bertin Instruments) and transferred to a new tube. Precellys tubes and beads were washed with 30 µl homogenization buffer. Samples were mixed for 10 min at 4° C on a rotator (40 rpm). To break cell membranes, the samples were additionally sonicated (1xcycle, 5 sec, 10 % power) with a Sonicator CL-18 (Thermo Fisher Scientific). Afterwards, lysates were incubated for 10 min at 4° C and centrifuged (3000xg, 30 min). Pellet and supernatant were stored separately at -20° C.

Protein quantification was carried out using the bicinchoninic acid assay (BCA). Following the manual bovine serum albumin standards were prepared using the homogenization buffer. For the samples, 25 µl or 10 µl of the supernatant from protein isolation was diluted (1:6 for 25 µl and 1:4 for 10 µl) with homogenization buffer. All standards and samples were measured as duplicates. Briefly, 10 or 25 µl of standards and samples were added to a 96-well plate. Additionally, 200 µl of the working solution was added and the plate was shaken briefly to mix. After an incubation of 30 minutes in the dark at 37° C the plate was measured at 562 nm with the FLUOstar omega plate reader (BMG Labtech). The data was analyzed using excel.

2.2.10.3 Electrochemiluminescence assay

The electrochemiluminescence (ECL) assay is based on the principle of a sandwich enzyme-linked immunosorbent assay (ELISA) however with a more sensitive detection system that is based on electrochemical stimulation. The detection antibody syn-211 was sulfotagged and kindly provided by Dr. Anne Stündl. A multiarray 96-well plate was coated with 30 µl of the capture antibody 4B12 against ha-syn in PBS overnight at 4° C. The plate

was washed 3 times with PBS-Tween and then blocked by incubation with 150 µl blocking buffer for 1 h at 300 rpm. For the dilution of the standard and samples the buffer, in which the samples were dissolved, was supplemented with 1 % BSA. The recombinant ha-syn standard (kindly provided by Dr. Omar El-Agnaf, Hamad Bin Khalifa University) was diluted in a four-fold series from 25 ng/mL to 6.1 pg/mL. Cell lysates in 1 % CHAPS lysis buffer (kindly provided by Dr. Jing Gong) were used in the following dilutions: 1:2.5, 1:5, 1:10, and 1:100. The mouse tissue samples from chapter 2.2.5.2 in homogenization buffer were used with 7.5 or 2.73 µg of total protein. After blocking the plate was washed 3 times with PBS-Tween and then 25 µl of standard or sample in replicates was applied. The plate was incubated for 1 h at 750 rpm and washed again 3 times with PBS-Tween. 25 µl of the detection antibody in blocking buffer complemented with mouse IgG and goat IgG was added to the plate and mixed at 700 rpm for 1 h. Finally, the plate was washed three times with PBS-Tween and following the read buffer was applied. The plate was measured at 620 nm with the Sector imager 6000 (Meso Scale Discovery) and analyzed with the software by Meso Scale Discovery.

2.2.11 RNA isolation and cDNA synthesis for fresh tissue

RNA isolation

The samples were already dissected as described in chapter 2.2.5.2 and stored at -80° C in 2 mL tubes for the Precellys system. Total RNA extraction was carried out under RNA-free conditions. After thawing the samples on ice 1 mL of Trizol and autoclaved ceramic beads were added. The tissue was then homogenized for 60 sec at 5000 rpm with the Precellys 24-Dual Tissue homogenizer (Bertin Instruments). The solution was transferred to a tube and incubated for 5 min at RT. Then 0.2 mL of chloroform was added and the samples were mixed by turning the tube upside down. After 5 min incubation, the samples were centrifuged for phase separation at 12.000xg for 5 min. The RNA containing aqueous layer at the top was carefully collected without disturbing the other layers and added to a new tube containing 4.7 µl of glycoblue. The blue-colored glycogen was used to precipitate the RNA more efficiently. After precipitating the RNA with the addition of 0.5 mL isopropanol the samples were incubated for 10 min on ice and then centrifuged (10 min, 4° C, 12.000xg). The supernatant was discarded and the pellet was washed two times with 1 mL of 75 % EtOH and centrifuged (10 min, 4° C, 12.000xg). The RNA pellet

was air-dried for 10 to 15 min at RT and then dissolved in 40 µl RNAse free water. The RNA was quantified using the DS-11 Spectrophotometer (DeNovix) and stored at -80° C until further usage.

cDNA synthesis

Following RNA extraction cDNA was synthesized following the manual instruction of the SuperScript IV Vilo kit. Briefly, 100 ng RNA was mixed on ice with 1 µl of ezDNase enzyme and 1 µl of ezDNAse buffer and filled up to 10 µl with RNAse free water. After incubation at 37° C for 2 min in the T3000 Thermocycler Kombi (Biometra) 6 µl of RNAse free water and 4 µl of SuperScript IV Vilo master mix were added. RNA was reverse transcribed with the first incubation at 25° C for 10 min and the next incubation step at 50° C for 10 min. All enzymes were deactivated with an additional step at 85° C for 5 min. Synthesized cDNA was stored at -20° C.

2.2.12 RNA isolation and cDNA synthesis for fixed tissue

Dissection of DMX

The 35 µm sections were dissected as described in chapter 2.2.5.1 but with an additional cut to dissect almost only the DMX. Two sections every 175 µm were pooled from bregma values between -8.0 to -6.8. The dissected sections were stored for a maximum of 3 days in antifreeze solution at -20° C for subsequent RNA isolation.

RNA isolation

Total RNA was extracted using the RevoverAll Total nucleic acid isolation kit under RNAse-free conditions. In brief, sections were centrifuged (13.000 rpm, 5 min) and the cryoprotective medium was discarded. The tissue was treated with 1 mL of xylene and heated to 50° C for 15 min. After centrifugation (13.000 rpm, 5 min) the supernatant was discarded and the pellet was washed twice with 1 mL 100 % EtOH. The pellet was air-dried for 10 minutes and then 100 µl of digestion buffer and 4 µl of protease were added per sample. For digestion, the tube was mixed and then incubated for 15 min at 50° C and then for 15 min at 80° C. To isolate the nucleic acids 120 µl of isolation additive and 275 µl of 100 % EtOH was added and then everything was transferred onto the filter cartridge.

Here all centrifugation steps were carried out at 10.000 rpm for 1 min. After centrifugation, the flow-through was discarded. The filter was washed with 700 µl of wash buffer 1 and then 500 µl of wash buffer 2/3. The filter was centrifuged again to remove buffer residues. For DNA digestion 6 µl of DNase buffer and 4 µl of DNAse were mixed and filled to 60 µl with nuclease-free water. This mixture was pipetted in the center of the filter and incubated at RT for 30 min. Afterwards, 700 µl of wash buffer 1 was incubated for 1 min on the filter, centrifuged, and the flow-through was discarded. Additionally, the filter was washed twice with 500 µl wash buffer 2/3. As the last step, the samples were centrifuged again to remove residual fluid, and then the filter was transferred to a new tube. The extracted RNA was eluted from the filter with 30 µl of nuclease-free water by 1 min incubation and centrifugation. RNA quantity was checked using the DS-11 Spectrophotometer (DeNovix).

cDNA synthesis

Extracted RNA was reverse transcribed into cDNA with the SuperScript Vilo kit. For each sample, 100 ng of RNA was mixed with 4 µl of master mix and filled up to 20 µl with RNAse-free water. All samples were incubated in a T3000 Thermocycler Kombi (Biometra). The reaction was started at 25° C for 10 min, followed by 60 min of 42° C and at 85° C for 5 min. Synthesized cDNA was stored at -20° C.

2.2.13 Reverse transcription polymerase chain reaction (RT-PCR)

RT-PCR was performed using SYBR green reagent and the primers in Table 2.6 or with TaqMan probes listed in Table 2.7 and the TaqMan Fast Advanced Master Mix. The PCR was carried out with a StepOneplus Real-Time PCR machine (Thermo Fisher Scientific). The program included an initial denaturation phase with 10 min 95° C and an amplification phase with 40 cycles including 15 sec at 95° C and 1 min at 60° C. The program ended at 25° C for 15 sec. For SYBR-green the melt curves were generated and checked as quality control.

Quantitative PCR

For quantitative PCR of ha-syn, a reference sample of human RNA was used to generate a standard curve. Hence, 1 µg of this reference human RNA was reverse transcribed into cDNA using the SuperScript Vilo kit. The obtained cDNA was diluted to 6.25 ng/µl and further to 0.39 ng/µl with a two-fold dilution series. The RT-PCR Master mix included 1 µl of forward and reverse primer for ha-syn, 10 µl of SYBR green master mix, and 7 µl of nucleic acid-free water. In the end, 1 µl of sample or reference cDNA was applied to the plate. The generated standard curve was every time incorporated into a master curve of all standard curves of ha-syn.

Relative PCR

For relative quantification, a standard mouse brain RNA was measured on all plates for all genes as an internal calibrator. The RT-PCR mix included 1 µl of TaqMan probe and 10 µl of TaqMan Fast Advanced Master Mix and varying cDNA concentrations depending on the gene of interest. The relative expression of the gene of interest was calculated using the $2^{-\Delta\Delta CT}$ Method.

2.2.14 Statistical analysis

All results were statistically evaluated using GraphPad Prism 9.1. Comparison of means between two groups was analyzed with an unpaired two-tailed *t*-test. Multiple groups were compared with the one-way ANOVA followed by Tukey's multiple comparison test or with two-way ANOVA followed by Tukey's multiple comparison test. All data is represented with the standard error of the mean (SEM) as error bars. All p-values under 0.05 were considered statistically significant and are marked as following: *****p<0.05 ******p<0.01 *******p<0.001 ****p<0.0001. The number of biological samples is indicated by n.

3 Results

3.1 Propagation model of ha-syn

An established mouse model of rAAV-mediated ha-syn overexpression in targeted neurons of the MO was used to study ha-syn propagation to higher brain regions (Helwig et al. 2016, Musgrove et al. 2019). Mice were unilaterally injected with rAAV into the vagus nerve, resulting in a retrograde transfer of rAAV along neural pathways. Subsequently, the rAAV transduces the ganglionic neurons of the inferior ganglion of the vagus (IGX) and the neurons of the DMX and nucleus ambiguous (AMB) confined by the anatomical distribution of the efferent and afferent fibers forming the vagus nerve. In these neurons on the ipsilateral, i.e. the injected side, the overexpressed ha-syn is distributed in the transduced neurons in the soma and in the axons. The axons of the IGX neurons project from the vagus nerve to the nucleus of the tractus solitaire (NTS), to the AP, and to the DMX, and therefore ha-syn accumulations are seen in the neuronal projections in these regions (see Figure 3.1 A). Moreover, these afferent fibers project not only to the injected, i.e., ipsilateral but also to the noninjected, i.e., contralateral, side of the brain. In a time-dependent manner, the overexpressed ha-syn in the transduced regions is transmitted to more rostral brain regions such as the midbrain and forebrain where it accumulates in neuronal projections. This inter-neuronal transmission leads to a progressive propagation and a stereotypic pattern of ha-syn accumulation in distinct higher brain regions as depicted in Figure 3.1 B.

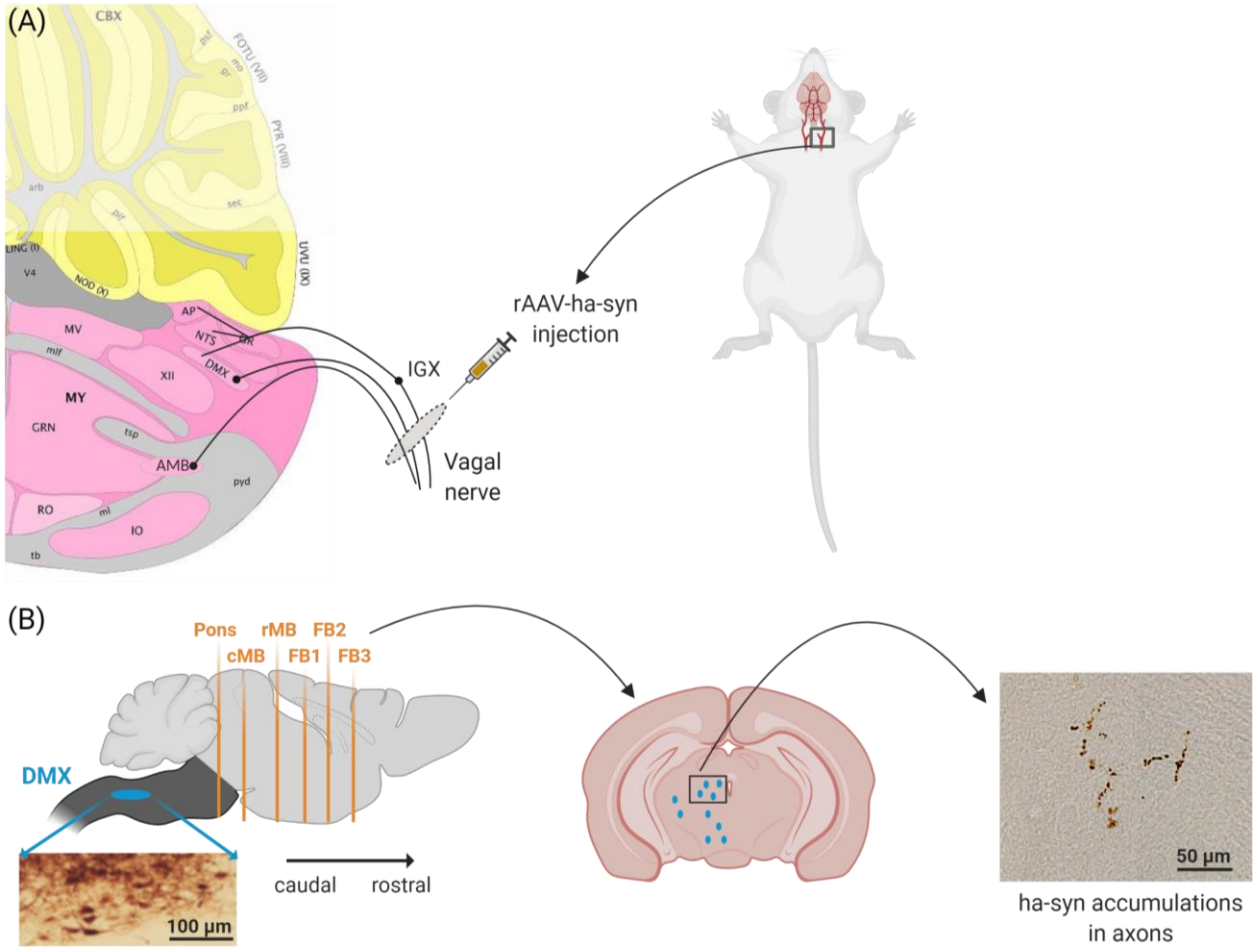

Figure 3.1: Schematic representation of rAAV-mediated and targeted ha-syn overexpression and propagation model. (A) The rAAV is unilaterally injected into the vagus nerve of a mouse. The rAAV transfers retrogradely along the vagus nerve and transduces ganglion neurons in the IGX (black dot) and neurons in the brain stem, which are connected to the vagus nerve tracts, i.e.; in the AMB and the DMX (black dots). These neurons then overexpress the ha-syn protein. The afferent fibers of the IGX neurons project into the AP, NTS, and DMX, so that overexpressed ha-syn in the IGX also accumulates in these neuronal projections. **(B)** Transduced neurons in the DMX are positive for overexpressed ha-syn. This sustained overexpression initiates a time-dependent propagation of the exogenous protein to more rostral brain regions such as the midbrain and forebrain. In these regions, ha-syn accumulates in neuronal projections. To quantify the spreading, the ha-syn immunoreactive fibers are counted at defined Bregma values in the PONS (Bregma -5.4), caudal midbrain (cMB; Bregma -4.6), rostral midbrain (rMB; Bregma -3.4), and forebrain (FB; 1 Bregma -2.18; 2 Bregma -0.94 and 3 Bregma +0.14). Created with Biorender.

3.2 Effect of EE on ha-syn pathology

The EE paradigm is used to enhance the cognitive and motor stimulation of the brain. This is achieved by using toys with different shapes, materials, and sizes, as well as wheels that are freely accessible. To increase the cognitive stimulation the position of the objects and the objects themselves are altered every day to maintain the novelty of the EE model (see Figure 3.2 A). In this experimental setup, only female mice aged 9 to 10 months were

used, as we observed more aggressive behavior in male mice when exposed to EE. Mice were placed in standard housing (SH) or EE two weeks before the rAAV (ha-syn) injection into the vagus nerve. Mice were sacrificed six weeks after injection (see Figure 3.2 B).

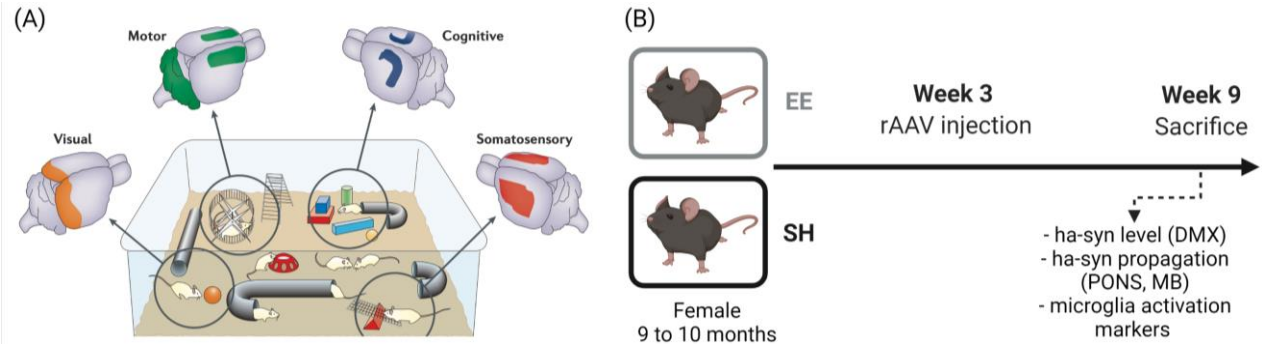

Figure 3.2: Enriched environment model and experimental setup. (A) The EE paradigm is based on providing a multisensory stimulating environment for mice that encompasses a larger space. Access to wheels provides voluntary physical activity and motor stimulation. Cognitive, visual, and somatosensory input is achieved through various toys, dens, and climbing aids that are used in turn. Obtained from (Nithianantharajah & Hannan 2006). **(B)** In this experimental setup, female mice (9 to 10 months) were housed in rat cages with the EE paradigm or in standard housing (SH) in mouse cages for two weeks. Then, the mice were injected with rAAV into the left vagus nerve to induce overexpression of ha-syn in the MO and they were sacrificed six weeks later to analyze ha-syn propagation and microglial activation. Created with Biorender.

3.2.1 Upregulated microglial activation markers in ha-syn overexpressing mice with EE treatment

Wassouf *et al*. reported that microglial gene expression was disturbed by ha-syn pathology and that these changes could be rescued by EE treatment. Therefore, we first wanted to determine whether EE affects microglial activation in our PD model and subsequent neuroinflammation upon ha-syn expression. More specifically, we examined microglial activation markers in wild-type mice and in mice with ha-syn pathology after EE exposure. To characterize the shift of homeostatic and resting microglia to a more reactive phenotype, a series of markers (CD11b, CD45, TLR2, CD11c, MHCII, CD68, and CLEC7A) were examined by flow cytometry. These markers are known to be upregulated in microglia upon activation (Hoogland et al. 2015, Jurga et al. 2020).

To analyze the microglial activation in different brain regions the brain was divided into three main regions based on the ha-syn spreading at six weeks. The MO is the region where the ha-syn is overexpressed and a lot of ha-syn accumulations are found in neuronal projections. In more rostral regions such as the PONS and midbrain (MB), we

see moderate spreading of ha-syn in axons after six weeks of injection. In contrast, in the forebrain (FB), there is little or no spreading of ha-syn at this time after injection (see Figure 3.3 A).

The gating strategy for characterization of microglial markers by flow cytometry is described in Figure 3.3 B. Briefly, the isolated cells from the different brain regions were first gated using the forward (FSC) and sideward scatter (SSC). This allows debris to be excluded as these parameters reflect the granularity and size of cells. Based on the sideward scatter and width doublet cells were then excluded from further analysis as these cells can be a major source of autofluorescence. Next, dead cells were excluded based on a viability stain. Finally, microglia were identified as the CD45^{intermediate} and CD11b^{high} population. For all stained markers, the positive populations were acquired using a fluorescence minus one control and an unstained control.

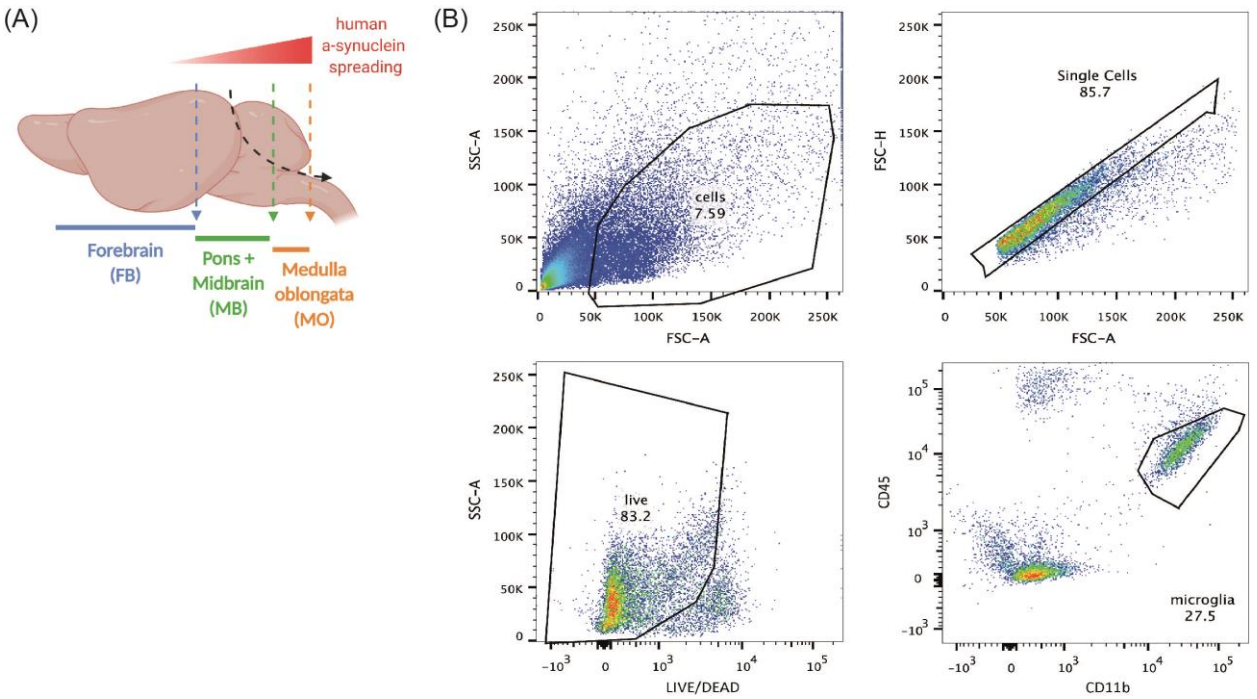

Figure 3.3: Schematic for dissection of brain regions and gating strategy for microglia profiling. Female mice were injected with 6x10^{11} Gc/mL of rAAV (ha-syn) into the left vagus nerve. **(A)** The cerebellum and the olfactory bulbs were discarded. The brain was then divided into three regions, the MO, the PONS with the midbrain (MB), and the forebrain (FB). **(B)** For all regions, cells were isolated and then analyzed by flow cytometry. Cells were gated by the forward and sideward scatter area correlating to their size and granularity. Only individual cells were included and further only live cells were analyzed. Microglia were determined as the CD11b^{high} and CD45^{intermediate} population. Flow cytometry and analysis were performed by Dr. Lily Keane. Created with Biorender.

First, the microglia phenotype of wild-type mice was monitored with and without EE treatment and the expression of CD11b, CD45, TLR2, CD11c, MHC II, CD68, and CLEC7A on microglia was measured. In wild-type mice, we did not detect a difference in the expression of any microglial activation markers between wild-type mice in SH and EE. However, the expression of the markers was different in the different brain regions regardless of EE treatment. In MO, the expression of all activation markers on microglia was higher than in the PONS+MB and in the FB (see Figure 3.4). This suggests a regional difference in the expression of microglial markers in the brain under homeostatic conditions.

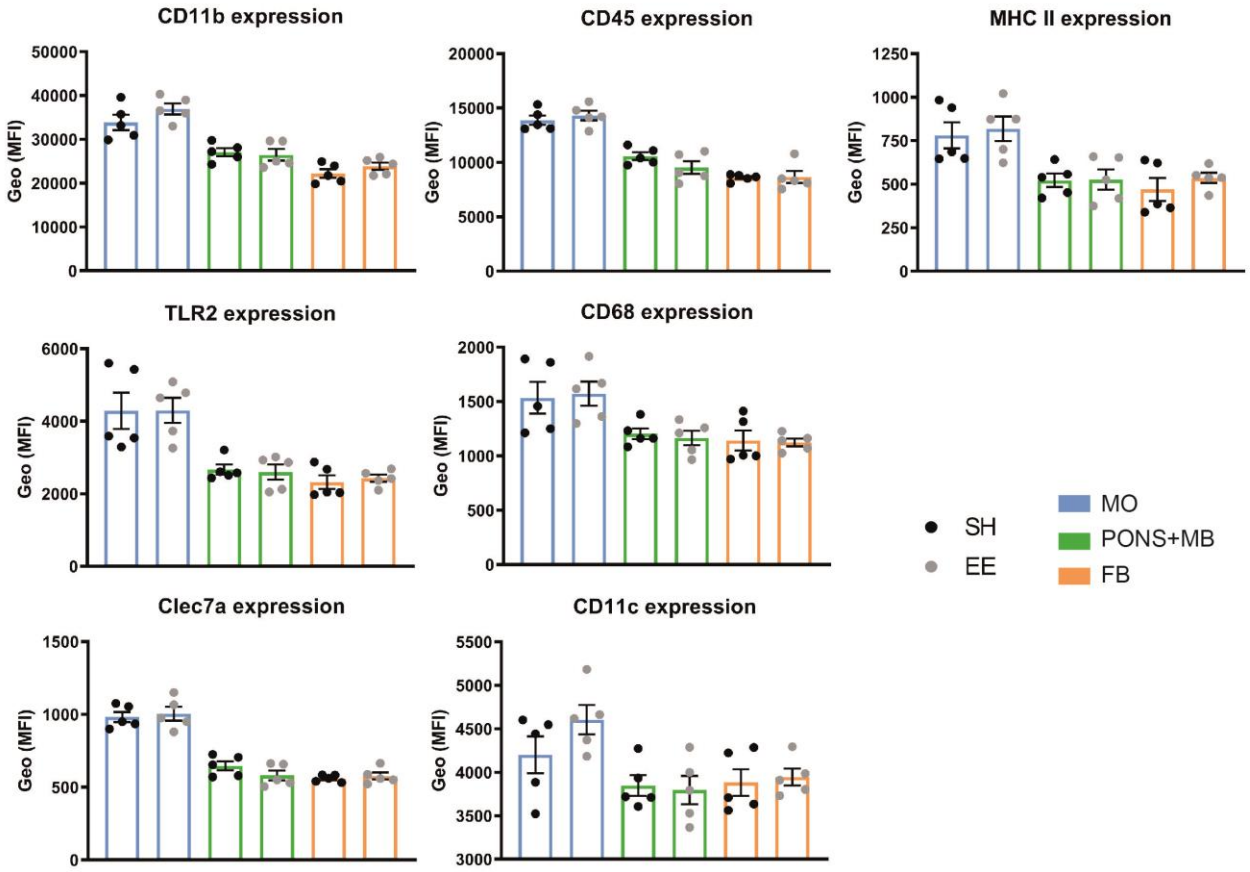

Figure 3.4: Microglia activation markers are not altered by EE in wild-type mice, but exhibit regional differences in expression. The expression of microglial activation markers was assessed for the gated CD11b^{high} and CD45^{intermediate} microglia population by flow cytometry and is given as the geometric mean (GEO) of the mean fluorescence intensity (MFI). Data are represented as mean ± SEM; n=5; Unpaired students t-test for each region.

However, looking at the level of microglial activation markers in mice with ha-syn overexpression in the MO and propagation to more rostral brain regions, a change was seen with EE treatment. Activation markers such as CD11b, CD68, and TLR2 were significantly higher in mice with EE compared to SH mice in the MO, and for CD11b, the change was evident even in the other brain regions. Consistent with this, MHC II and CD45 showed a strong tendency toward upregulated expression after EE treatment in ha-syn affected regions. Only the markers CLEC7A and CD11c showed no change between SH and EE treatment in ha-syn overexpressing mice (see Figure 3.5). These results suggest that in an a-syn pathology challenged surrounding microglia activation is increased upon EE treatment.

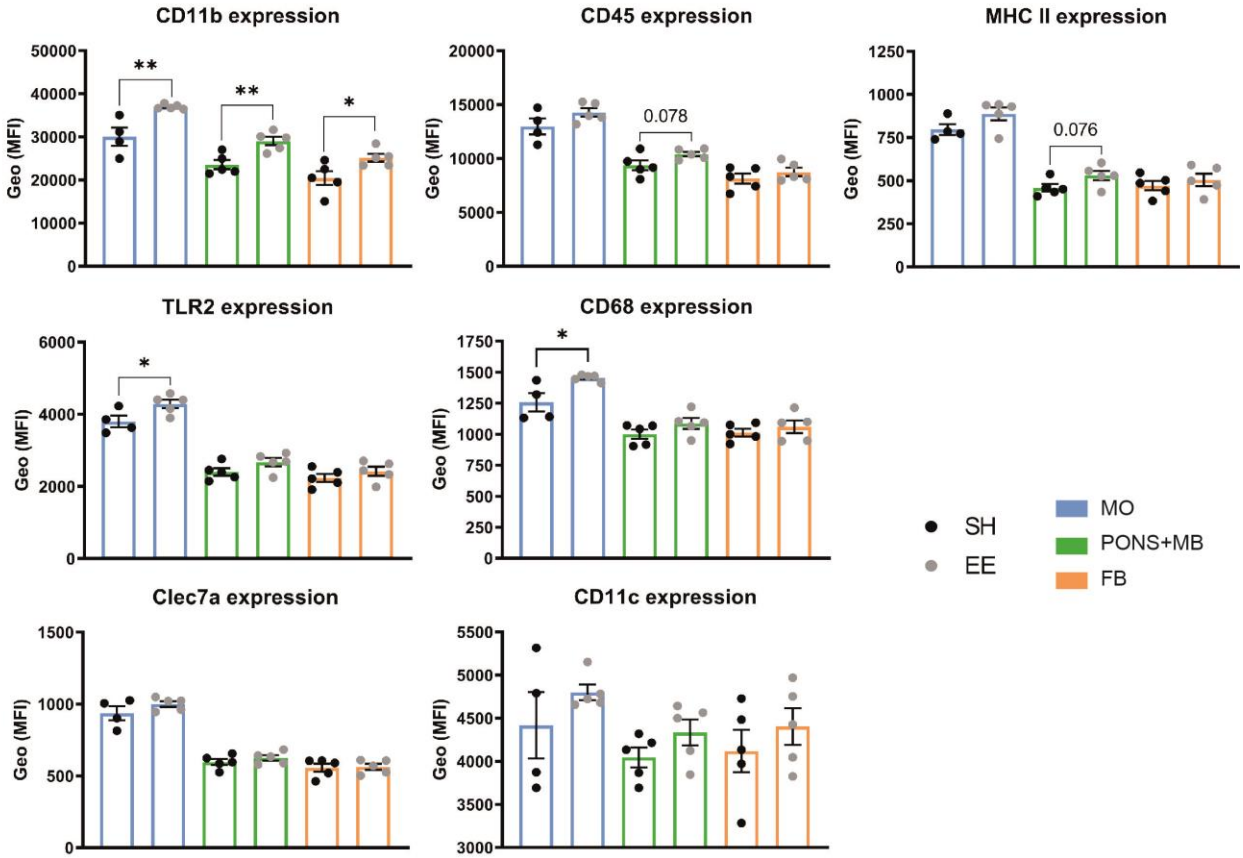

Figure 3.5: Microglia activation markers are partly upregulated by EE in ha-syn overexpressing mice. The expression of microglial activation markers was measured for the gated CD11b^{high} and CD45^{intermediate} microglia population by flow cytometry and is given as the geometric mean (GEO) of the mean fluorescence intensity (MFI). Activation markers like TLR2, CD68, and CD11b are significantly upregulated and CD45 and MHC II show a trend to higher expression in EE-treated mice. This effect is most apparent in the brain stem and midbrain which are the ha-syn affected regions after 6 weeks of rAAV injection. Data is represented as mean ± SEM; * $p<0.05$ and ** $p<0.01$; n=5 except for MO region for EE n=4; Unpaired students t-test for each region.

3.2.2 Ha-syn expression and spreading is not affected by EE treatment

We wanted to know whether this shift in microglial activation in ha-syn overexpressing mice with EE treatment would affect ha-syn propagation from the DMX to higher brain regions. However, we first examined whether EE treatment affected rAAV-mediated ha-syn overexpression in the DMX. For this purpose, the DMX was dissected and ha-syn mRNA was quantified by RT-PCR. The not-injected side, i.e. the contralateral side, was used as a negative control for ha-syn since the rAAV transduces only cells in the DMX on the ipsilateral side (data not shown). The ha-syn mRNA expression levels in the DMX on the ipsilateral side were comparable between the SH and EE groups (see Figure 3.6 A). The level of ha-syn expression was further assessed by semi-quantitative counting of ha-syn positive cells in every 5th DMX containing section. The number of ha-syn-positive cells in the DMX correlated with ha-syn mRNA expression in the DMX in the respective animal (see Figure 3.6 B). In addition, MO sections immunostained for ha-syn showed similar staining of ha-syn in neurons in the DMX and in neuronal projections in the DMX, the NTS, and the AP (see Figure 3.6 C).

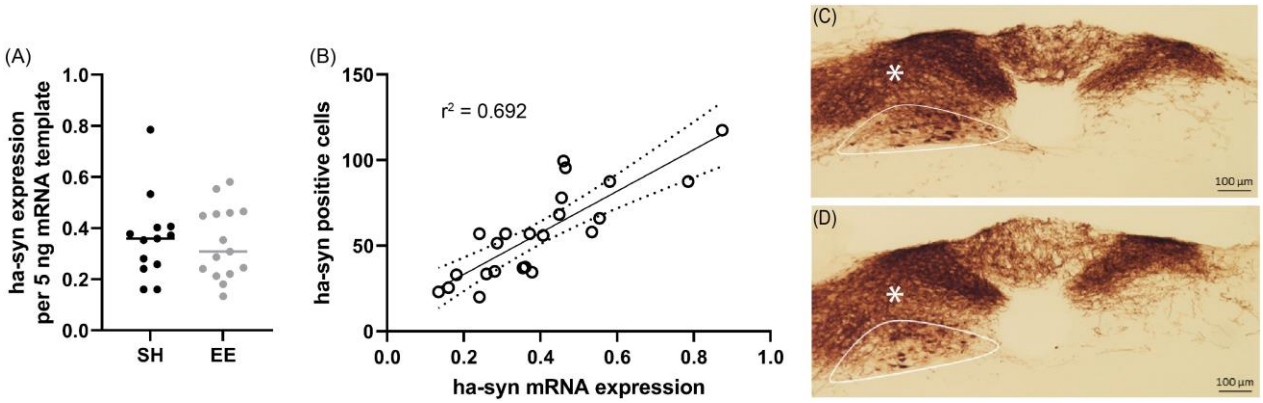

Figure 3.6: Overexpression of ha-syn in DMX is similar in SH and EE mice. Female mice were injected with 6x10^{11} Gc/mL of rAAV (ha-syn) into the left vagus nerve. **(A)** Overexpression of ha-syn mRNA in the DMX was quantified by RT-PCR using a ha-syn standard curve. **(B)** Ha-syn mRNA expression in the DMX determined by RT-PCR correlates with the number of ha-syn positive neurons counted in the DMX of each animal. **(C-D)** Representative images of ha-syn stained MO sections in SH **(C)** and EE **(D)** mice. The DMX with ha-syn expressing neurons on the ipsilateral side is delineated in white and ha-syn immunostained accumulations in neuronal projections of the NTS are indicated by a white asterisk. Data from two independent experiments are presented as mean; Linear regression ± 95% confidence interval and r square value; n=13 for SH and n=15 for EE; Unpaired students t-test.

To evaluate if EE exposure has an impact on the propagation of the overexpressed ha-syn we measured the spreading from the DMX to higher brain regions. The ha-syn accumulations in the neuronal projections were counted as ha-syn positive fibers only on the ipsilateral side of the brain and at specific bregma values, i.e. the PONS (Bregma -5.4) and the caudal midbrain (cMB; Bregma -4.6). The counting revealed no difference in the number of ha-syn positive fibers between the mice with SH and EE (see Figure 3.7). In conclusion, the EE had no effect on ha-syn overexpression in the DMX nor on ha-syn propagation to higher brain regions such as the PONS and the midbrain.

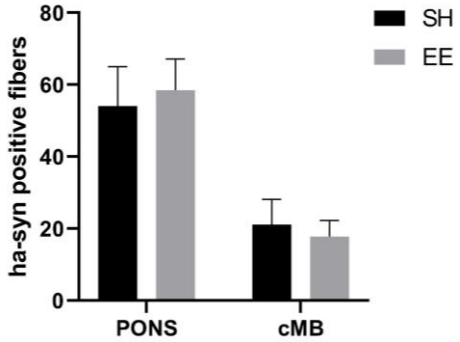

Figure 3.7: No difference in ha-syn propagation in SH and EE mice. Defined sections were counted for ha-syn positive fibers on the ipsilateral side in the PONS (Bregma -5.4) and cMB (Bregma -4.6). Data are represented as mean ± SEM; n=14 for SH and n= 16 for EE; Unpaired students t-test for each region.

3.3 Effect of aging on ha-syn pathology

To investigate the effect of aging on ha-syn propagation, and the phenotype of microglia the ha-syn propagation model was used in three different age groups of mice with 3 to 5 months (young), 13 to 15 months (mid-aged), and 22 to 23 months (aged). The effects were observed at different time points after the rAAV injection inducing the ha-syn overexpression in the MO as depicted in Figure 3.8. Male mice were used for all experiments, except for the experiment at 8 weeks, in which one cohort consisted of male mice and the second independent experiment consisted of female mice. Female and male mice were included as ha-syn propagation was reported to be independent of sex in this model in young mice (Helwig, personal communication).

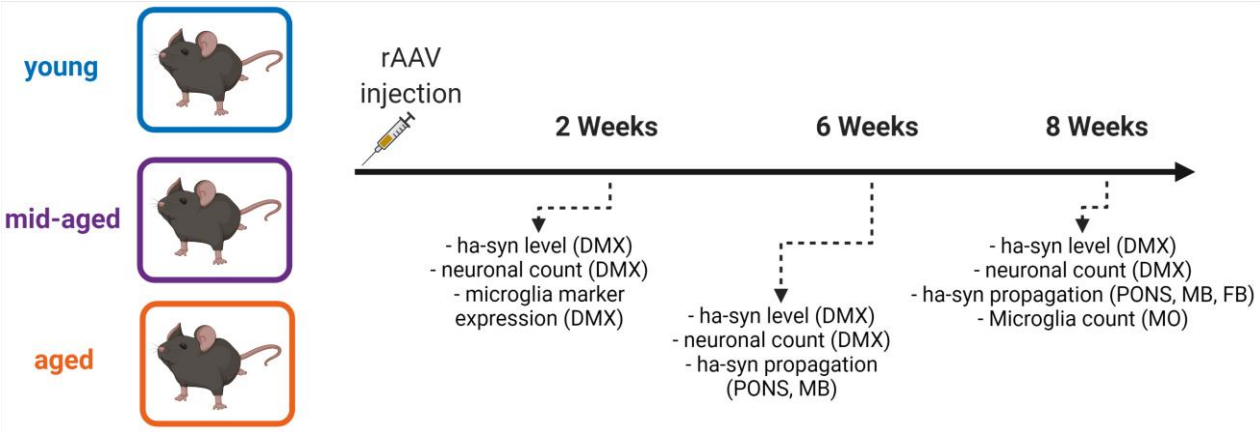

Figure 3.8: Experimental setup for aging study. Young, mid-aged, and aged mice were injected with an rAAV (ha-syn, GFP, or empty) into the vagus nerve and then analyzed two, six, and eight weeks afterward. Created with Biorender.

3.3.1 Specific detection of ha-syn

First, we developed an assay to specifically quantify ha-syn protein expression in mouse tissue with an ECL assay based on the principle of a sandwich ELISA. Only the capture antibody and not the detection of this assay was ha-syn specific. However, only ha-syn was detected, which was demonstrated by measuring cell lysate from a cell line with endogenous mouse a-syn (N2A cells) and a cell line with endogenous ha-syn (HEK cells). While different dilutions of the N2A lysate showed only a low background signal below the detection limit, the HEK lysate showed a signal corresponding to the different dilutions (see Figure 3.9 A). Similarly, naive mouse tissue did not yield a signal in the assay, but when recombinant ha-syn was added, it could be detected (see Figure 3.9 B).

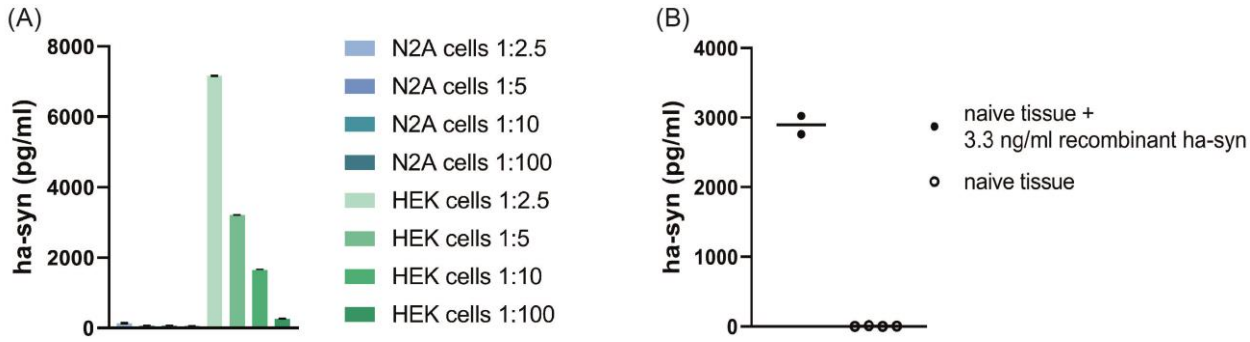

Figure 3.9: Ha-syn can be specifically detected in cell lysates and mouse tissue. Samples were measured by ECL using a ha-syn specific capture antibody and quantified using a recombinant ha-syn standard curve. **(A)** Cell lysates were measured at different dilution levels. The signal from N2A cell lysate was below the detection limit. **(B)** The signal from naive mouse tissue was below the detection limit. However, recombinant ha-syn added to mouse tissue could be measured. Data are represented as mean ± SEM.

3.3.1 Toxicity of rAAV and protein overexpression *in vitro*

The cytotoxicity of rAAV and protein overexpression with rAAV were first examined *in vitro* using cortical neuronal cultures of mouse embryos. Cytotoxicity for empty AAV, GFP, and ha-syn rAAV was measured by LDH release in the supernatant four days after transduction. In addition, two different doses of rAAV, $3.5x10^9$ Gc (low dose) and $1.4x10^{10}$ Gc (high dose) were used for transduction. In empty AAV, cytotoxicity of approximately 5% was measured for both doses of rAAV compared with neurons treated with the solution in which the rAAVs were dissolved (Tween 0.014% or 500 mM in PBS) as a negative control. However, for GFP and ha-syn, there was a dose-dependent cytotoxicity effect that resulted in approximately 15 percent cytotoxicity at a high dose of rAAV (see Figure 3.10). However, it is difficult to conclude from the toxicity of rAAVs *in vitro* to the toxicity of the rAAVs *in vivo*.

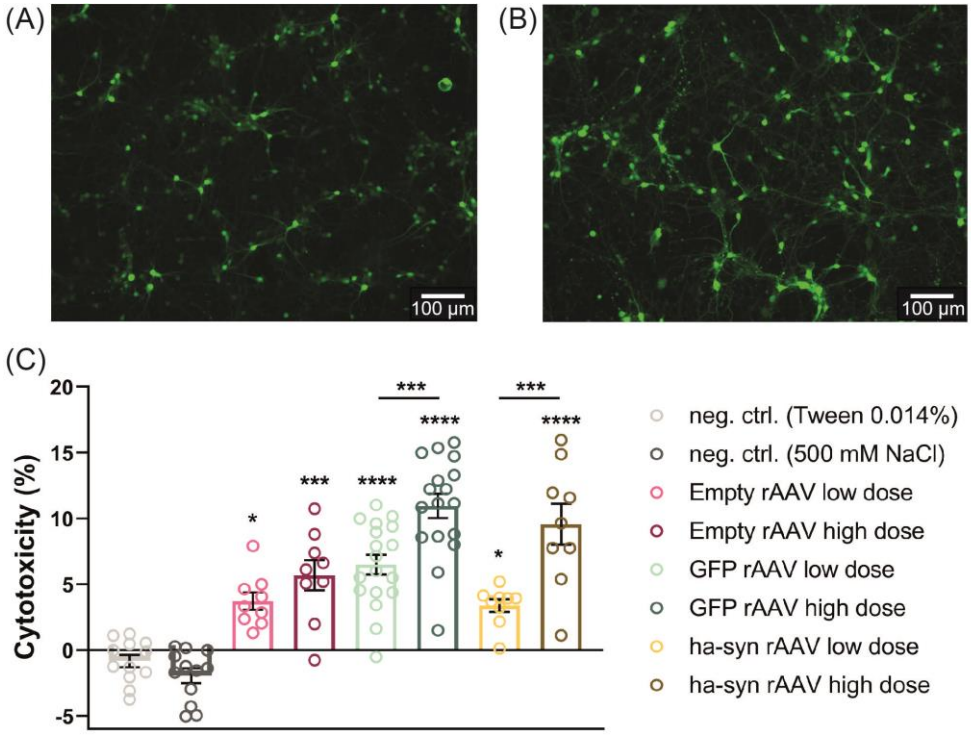

Figure 3.10: Dose-dependent cytotoxicity of protein overexpression and rAAV cytotoxicity in embryonal cortical neurons. Representative images of GFP transduced neurons four days after transduction for low **(A)** and **(B)** high doses of rAAV. **(C)** Cytotoxicity was measured by LDH release in the supernatant of neurons four days after transduction with different rAAVs. Empty AAV showed low cytotoxicity compared to the negative control treated neurons. GFP and ha-syn AAV showed dose-dependent cytotoxicity. The low dose of rAAV was $3.5x10^9$ Gc (MOI 10.000) and the high dose was $1.4x10^{10}$ Gc (MOI 80.000). Neuronal cultures were prepared by Dr. Anna Antoniou and Dr. Loic Auderset. Data are represented as mean ± SEM; * $p<0.05$, ***$p<0.001$ and ****$p<0.0001$; n=3; Two-way ANOVA *posthoc* Tukey's multiple comparison test.

3.3.2 Characterization of ha-syn pathology *in vivo* after two weeks

Two weeks after rAAV injection into the vagus nerve, there is robust transduction of rAAV and ha-syn expression in the MO. Therefore, we wanted to characterize this initial ha-syn expression in the DMX in different age groups.

3.3.2.1 No neuronal loss in the DMX

First, we wanted to investigate whether rAAV transduction and ha-syn overexpression in the DMX could lead to neuronal death in the DMX two weeks after injection. The DMX was delineated in nissl-stained sections, and neurons were stereologically counted on the contralateral side as control (intact side) and on the ipsilateral side (injected side). The number of neurons was counted only in young mice because they showed the highest neuron loss at later time points after rAAV injection. However, in DMX of young mice, no neuronal loss was observed between the ipsilateral and contralateral sides after two weeks of injection (see Figure 3.11).

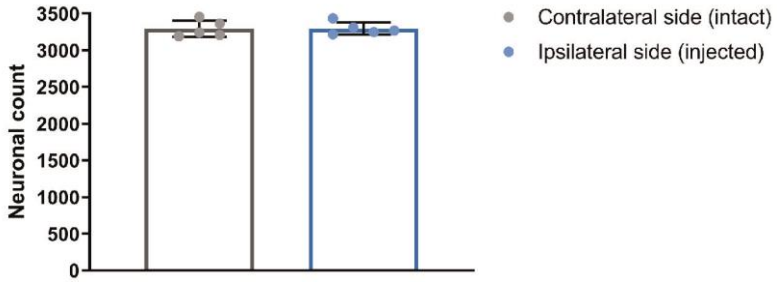

Figure 3.11: Neuronal loss was not observed in young mice after two weeks of rAAV injection and ha-syn overexpression. Male mice were injected with $6x10^{11}$ GC/mL rAAV (ha-syn). Every 5^{th} section of the MO was used for the Nissl staining. The DMX was delineated and the number of neurons on the ipsilateral (injected) and contralateral (intact) sides were counted. Injections were performed by Dr. Michael Helwig. Stereological counting was performed by Dr. Ayse Ulusoy. Data are represented as mean ± SEM; n=5; Unpaired students t-test.

3.3.2.2 Similar ha-syn expression in the DMX

It was important to determine whether aging affected ha-syn mRNA and protein levels in the MO two weeks post-injection. All age groups were injected with the same amount of rAAV for ha-syn overexpression in the MO. RNA and protein levels were measured for the ipsilateral and contralateral side, respectively. For mRNA expression, the contralateral side was used as a negative control, because the neurons here were not rAAV-transduced and therefore do not express ha-syn mRNA. On the ipsilateral side, ha-syn mRNA expression quantified by RT-PCR was comparable in young, mid-aged, and aged mice

(see Figure 3.12 A). At the protein level, four times more ha-syn was measured on the ipsilateral side than on the contralateral side in all mice (data not shown), because more ha-syn protein accumulates in neuronal projections on the ipsilateral side. Overall, ha-syn protein accumulations in MOs analyzed with ha-syn-specific ECL showed the same amount of ha-syn protein expression in young, mid-aged, and aged mice (see Figure 3.12 B). Interestingly, ha-syn mRNA expression in DMX and ha-syn protein levels in DMX, NTS, and AP of the same animal correlated well in all age groups, except for one outlier in the aged group (see Figure 3.12 C).

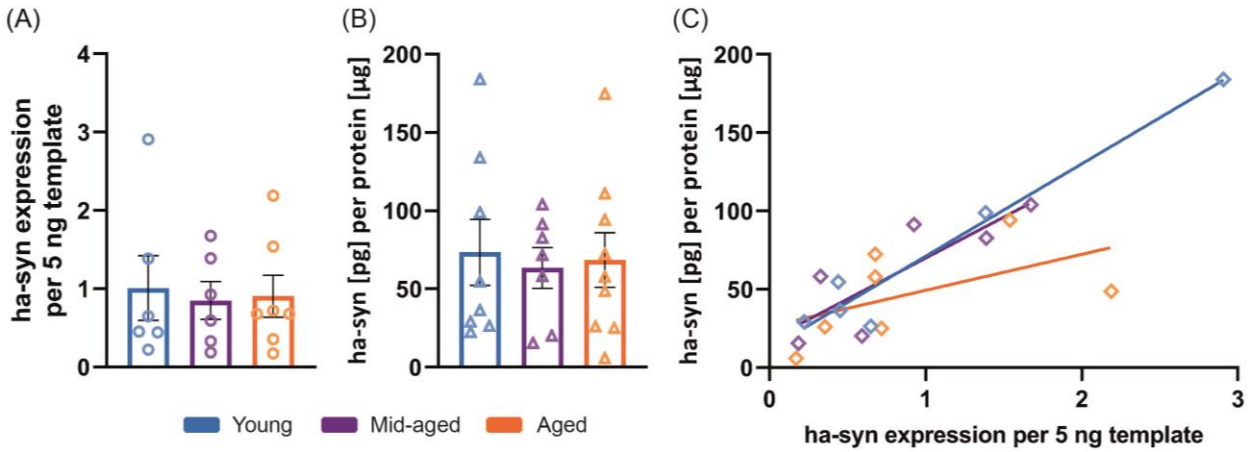

Figure 3.12: Ha-syn protein and mRNA expression is comparable in young, mid-aged, and aged mice two weeks after injection. Male mice were injected with $6x10^{11}$ GC/mL rAAV (ha-syn). The MO was dissected from the brain, and RNA was isolated from one-third of the alternating sections and protein from two-thirds of the alternating sections. **(A)** The mRNA expression of ha-syn was determined by RT-PCR and quantified using a ha-syn standard curve. **(B)** Ha-syn protein levels were quantified by ECL and normalized to total tissue protein levels measured by BCA. **(C)** Correlation of ha-syn mRNA and protein concentrations in MO of the same animals. Injections were performed by Angela Rollar and Dr. Michael Helwig. Data are represented as mean ± SEM; For (A) n=9 for young, 7 for mid-aged, 9 for aged; For (B+C) n=6 for young and mid-aged, 7 for aged. One-way ANOVA *posthoc* Tukey's multiple comparison test.

3.3.2.3 Age-related changes in activation of microglia with ha-syn overexpression

It is known that a-syn can bind to receptors on the microglia surface leading to their activation, resulting in a reactive phenotype that creates a pro-inflammatory environment, as described in chapter 1.4.3. Therefore, we wanted to investigate whether overexpression of ha-syn differentially alters microglia expression patterns in young, mid-aged, and aged mice. To this end, we examined the mRNA expression of pro-inflammatory cytokines TNF-α, IL-6, and IL-1β and the microglial activation markers Iba1,

TLR2, and SPP1 in the MO. The mRNA expression levels were normalized to the housekeeping gene GAPDH. In general, for each cytokine and activation marker, we found similar expression on the ipsilateral and contralateral sides in all age groups.

The cytokines TNF-α, lL-6, and IL-1β are mainly produced by activated microglia and are the major mediators of a pro-inflammatory environment (DiSabato et al. 2016). TNF-α showed an age-dependent increase in mRNA expression and mRNA levels were significantly altered between young and aged mice. IL-6 mRNA expression also showed a trend toward higher expression in mid-aged and aged mice compared with young mice, whereas IL-1β mRNA levels did not differ between age groups (see Figure 3.13).

Microglia exhibit constitutive expression of Iba1. However, the protein is known to be upregulated by microglial activation and associated with phagocytosis (Ohsawa et al. 2000, Sasaki et al. 2001). TLR2 is a toll like receptor expressed on microglia and neurons. It is known that a-syn binds to TLR2 leading to the activation of microglia (Dzamko et al., 2017; Kim et al., 2013). SPP1, also known as osteopontin, is elevated in numerous CNS pathologies, modulates inflammatory processes, and is mainly expressed by activated microglia (Shin et al. 2011, Riew et al. 2019). Iba1 mRNA levels were slightly elevated in mid-aged mice and significantly increased in aged mice compared to young mice. TLR2 mRNA expression was significantly increased in the mid-aged and even more in the aged than in young mice. However, SPP1 mRNA was not altered between young, mid-aged, and aged mice (see Figure 3.13). In conclusion, in mice overexpressing ha-syn, the mRNA expression of microglial activation markers and pro-inflammatory cytokines are differentially expressed with age.

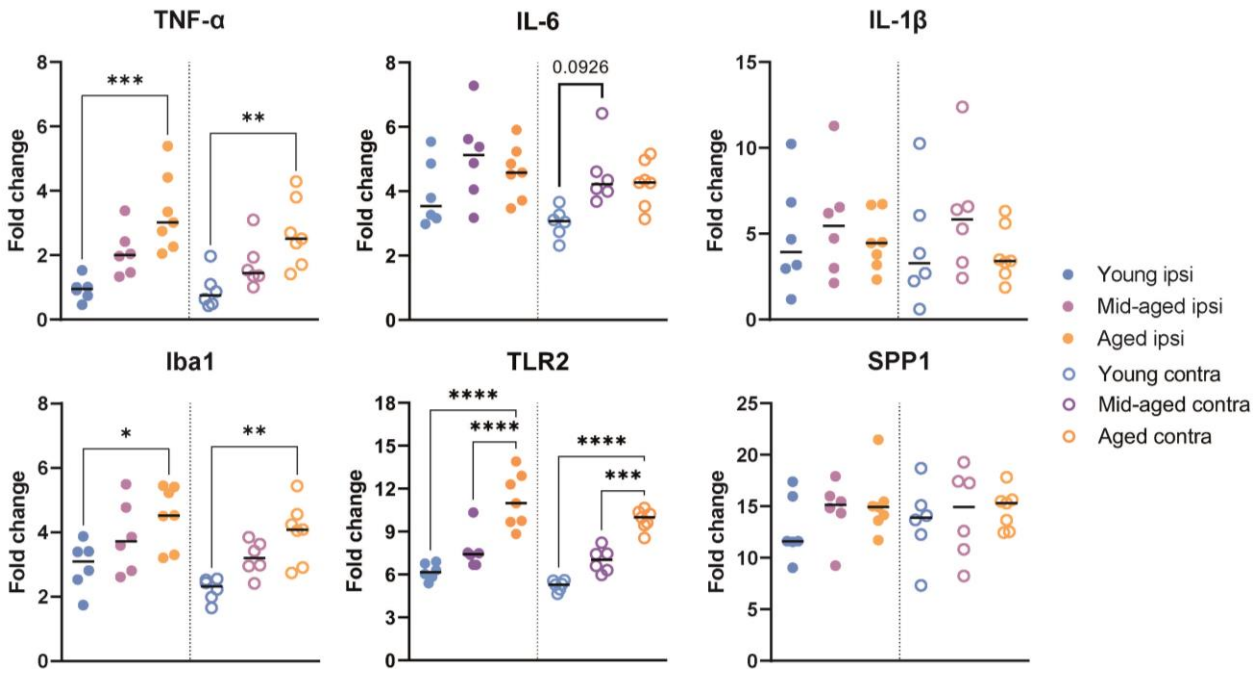

Figure 3.13: Age-dependent increase in some pro-inflammatory cytokines and microglial activation markers associated with ha-syn overexpression. Pro-inflammatory markers and microglia activation markers were assessed by relative RT-PCR normalized to the expression of GAPDH on the ipsilateral (injected) and contralateral (intact) sides after two weeks of injection. All markers showed comparable results between the ipsi- and contralateral sides. The pro-inflammatory marker TNF-α was significantly increased in aged mice compared with young mice. In addition, microglial activation markers Iba1 and TRL-2 were significantly higher in aged mice than in young. Data are represented as mean; * p<0.05, ** p<0.01, ***p<0.001 and ****p<0.0001; n=6 for young and mid-aged, 7 for aged; One-way ANOVA *posthoc* Tukey's multiple comparison test.

3.3.3 Characterization of ha-syn pathology *in vivo* after six weeks

As the ha-syn propagation that is induced by ha-syn overexpression in the MO is time-dependent we analyzed young, mid-aged, and aged mice six weeks after rAAV treatment. The ha-syn positive fibers were counted in more rostral brain areas such as the PONS and midbrain. In addition, we characterized the neuronal number and the ha-syn expression in the DMX at that time point.

3.3.3.1 Changes in ha-syn expression and neuronal numbers in the DMX

Ha-syn expression was evaluated by mRNA isolation from PFA-perfused brain sections. Detected ha-syn mRNA levels in the DMX changed slightly between the age groups compared to the evaluation at two weeks. Ha-syn levels in young and aged mice were comparable, but ha-syn levels of mid-aged mice were almost significantly increased (see Figure 3.14 A). Analysis of neuronal numbers in the DMX showed that there was a slight

neuronal loss in young and aged mice, but it was highly variable in both groups. However, the percentage of neurons in the DMX was not significantly different between young, mid-aged, and aged mice, with neuronal counts normalized to the respective contralateral (intact) side (see Figure 3.14 B).

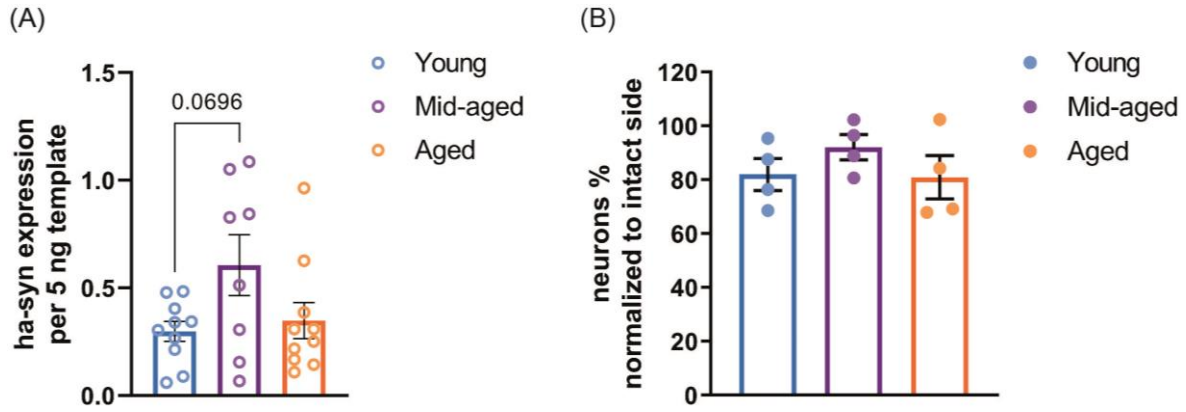

Figure 3.14: Ha-syn expression is altered after six weeks of injection but no significant neuronal loss is observed in the DMX. Male mice were injected with $6x10^{11}$ GC/mL rAAV (ha-syn). **(A)** Ha-syn mRNA expression in the DMX was measured by quantitative RT-PCR after six weeks of injection. In the mid-aged group, ha-syn expression was almost significantly increased compared with the young and aged animals. **(B)** In nissl stained sections, the neurons in the delineated DMX were counted and the ipsilateral (injected) counts were normalized to the counts of the contralateral (intact) side. Injections were performed by Angela Rollar. Stereological counting was performed by Dr. Ayse Ulusoy. Data are represented as mean ± SEM; for (A) n=9 for young, 8 for mid-aged, 10 for aged; For (B) n=4; One-way ANOVA *posthoc* Tukey's multiple comparison test.

3.3.3.2 No difference in ha-syn propagation

Considering the increased ha-syn load in mid-aged mice in the DMX, we wondered if there was also a difference in ha-syn propagation from the MO to more rostral brain regions. However, the graph depicted in Figure 3.15 A shows no difference in ha-syn positive fibers counted in the PONS or the caudal midbrain (cMB) between young, mid-aged, and aged mice. Automatic analysis of the area of ha-syn accumulations in three consecutive PONS brain sections also showed no significant change in the extent of ha-syn accumulations between young, mid-aged, and aged mice (see Figure 3.15 B).

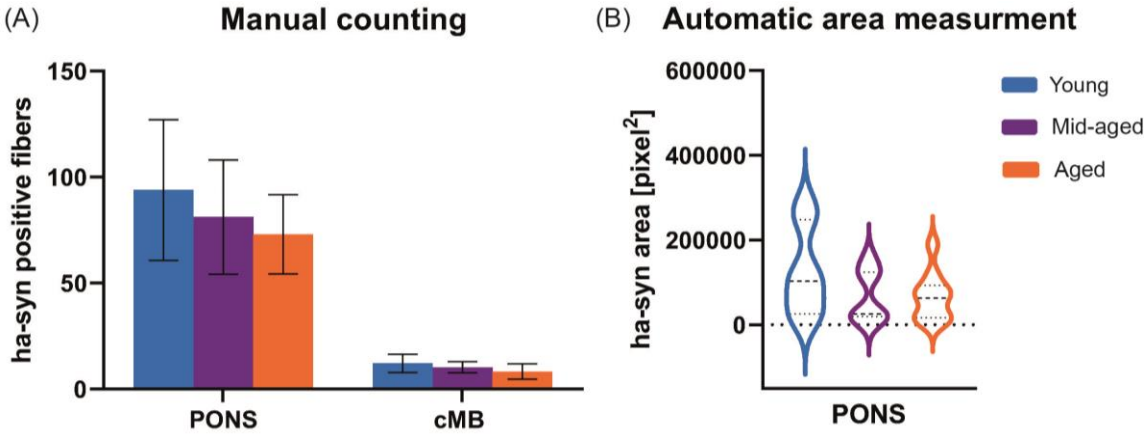

Figure 3.15: No difference in ha-syn spreading to higher brain regions after six weeks of injection. (A) Defined sections rostral to the MO were manually counted for ha-syn positive fibers on the ipsilateral side in the PONS (Bregma -5.4) and cMB (Bregma -4.6). **(B)** For the same samples, three consecutive sections in the PONS (middle section with Bregma -5.4) were automatically measured for ha-syn accumulation by area. Data are represented as mean ± SEM (A) or as median with first and third quartile (B); n=8 for young, 7 for mid-aged,9 for aged; One-way ANOVA *posthoc* Tukey's multiple comparison test.

3.3.4 Characterization of ha-syn pathology *in vivo* after eight weeks

Next, we characterized young, mid-aged, and aged mice eight weeks post AAV injection to see whether ha-syn levels continued to change in the DMX and whether this had a delayed effect on ha-syn propagation and accumulation in more rostral brain regions.

3.3.4.1 Altered ha-syn levels in DMX and propagation to higher brain regions

DMX mRNA was isolated from PFA-perfused brain sections. Analysis of two independent experiments showed the same results, independent of sex and a slightly different rAAV stock titer. It revealed that ha-syn mRNA expression in DMX was significantly higher after eight weeks not only in mid-aged mice but also in aged mice compared with young mice (see Figure 3.16 A). Consistent with this result, ha-syn staining showed more ha-syn positive cells in the DMX of mid-aged and aged mice compared to young mice (see Figure 3.16 B).

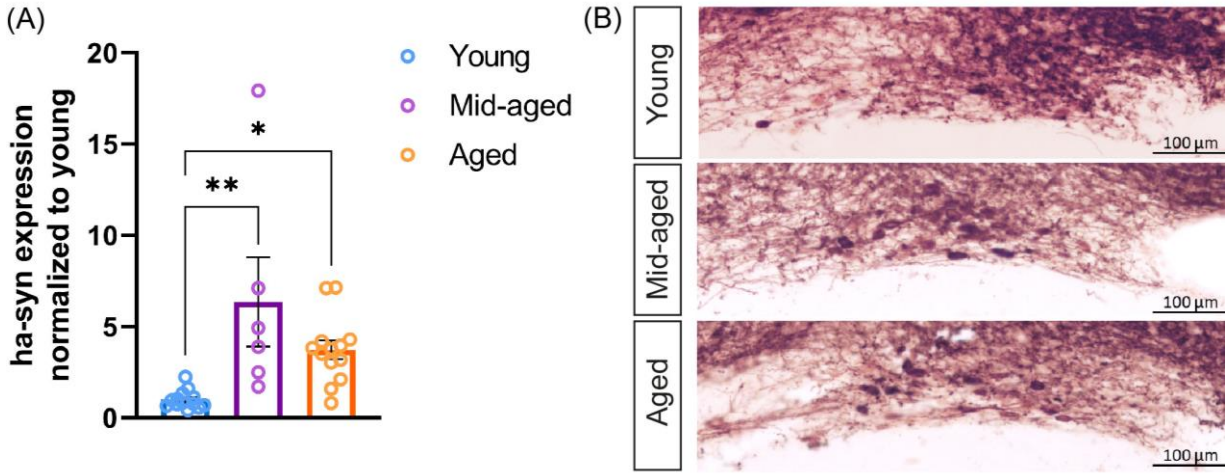

Figure 3.16: Ha-syn expression is augmented in mid-aged and aged mice eight weeks post-injection. Female mice were injected with a virus titer of $5x10^{11}$ Gc/mL and male mice were injected with a virus titer of $6x10^{11}$ Gc/mL. **(A)** Ha-syn mRNA in the DMX was evaluated by quantitative RT-PCR and expression levels were normalized to those of young mice. Aged and mid-aged mice showed significantly elevated ha-syn levels compared to young mice after eight weeks post rAAV injection. **(B)** Representative images of ha-syn positive neurons in DMX for young, mid-aged, and aged mice. Injections were done by Angela Rollar and Dr. Michael Helwig. Data are represented as mean ± SEM; * $p<0.05$ and ** $p<0.01$; n=13 for young, 7 for mid-aged,13 for aged; One-way ANOVA *posthoc* Tukey's multiple comparison test.

After eight weeks, the propagation of ha-syn was observed in neuronal projections up to the forebrain to Bregma values of -0.94 for one experiment (young and aged mice) and +0.14 for the second experiment (young, mid-aged, and aged mice). Unfortunately, ha-syn accumulations in the PONS were so high in the second experiment that ha-syn positive fibers could not be counted manually. The observed propagation was consistent with previous results showing progressive rostral propagation of ha-syn over time and higher ha-syn accumulation. The spreading pattern of ha-syn at six and eight weeks was consistent with the anatomical connection of neuronal projections of the MO to higher brain regions. Moreover, all mice showed the same topographic distribution in the affected regions.

Eight weeks after rAAV injection, aged and mid-aged mice showed increased ha-syn-positive fibers in the PONS, midbrain, and forebrain compared with young mice. This trend was not evident only in the rostral midbrain (rMB), but the general number of ha-syn fibers was very low in this region at all ages. The increase of ha-syn fibers was significant in the Forebrain 1 and caudal midbrain for the mid-aged mice compared to young mice (see Figure 3.17 A). In line with that, we observed a 2-fold increase in ha-syn accumulations in

three consecutive PONS sections in mid-aged and aged mice compared with young mice (see Figure 3.17 B). This effect is also observed in the parabrachial area which is a stereotypic region for ha-syn accumulation in the PONS (see Figure 3.17 C and D). Here, mid-aged and aged mice have enhanced ha-syn accumulation compared to young mice. Briefly, these results show that after eight weeks of AAV injection, there is an age-dependent shift to higher ha-syn levels in the DMX and augmented ha-syn propagation to more rostral brain regions.

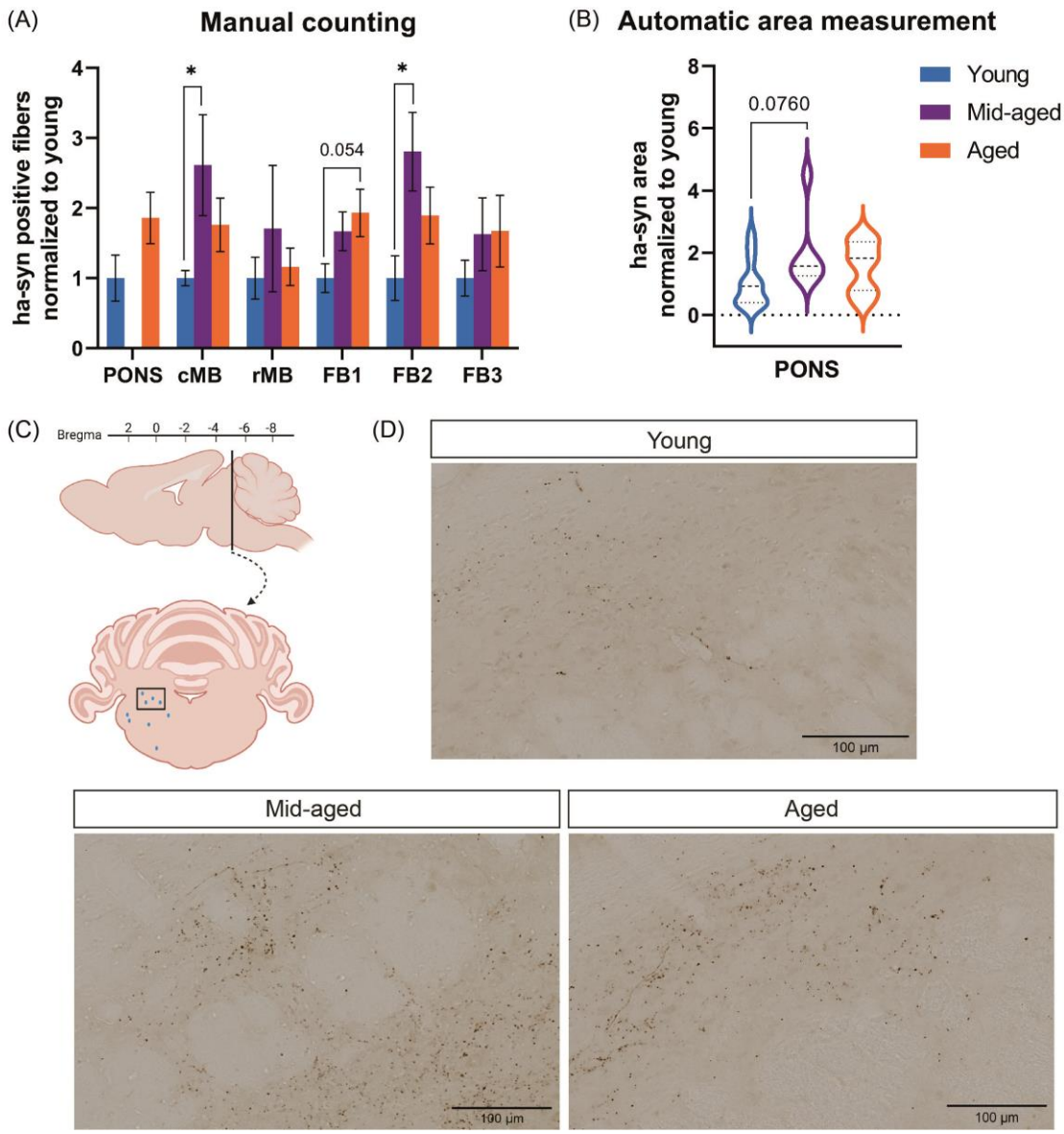

Figure 3.17: Increased ha-syn propagation and accumulation in mid-aged and aged mice. **(A)** Spreading of ha-syn positive fibers was determined on the ipsilateral side of the brain. Regions were counted up to the FB2 or FB3 for the respective experiment. The counted fibers on the ipsilateral side were increased in aged and mid-aged mice compared with young mice. **(B)** The same trend was observed by automatic measurement of ha-syn accumulation in three consecutive

PONS sections. **(C)** The whole PONS section at Bregma -5.4 was counted manually for ha-syn fibers and measured automatically for the ha-syn area. Representative images were acquired in the parabrachial region indicated by the black box. **(D)** Representative images of ha-syn positive accumulations in neuronal projections. Data from two independent experiments are presented as mean ± SEM (A) and as median with first and third quartile (B); * $p<0.05$; n=13 for young, 6 for mid-aged,13 for aged except for (A) PONS n=5 for young and aged and for FB3 n=8 for young and aged; One-way ANOVA *posthoc* Tukey's multiple comparison test per region. Created with Biorender.

3.3.4.2 Neuronal loss in DMX by protein overexpression

Ha-syn overexpression in the DMX was significantly altered in mid-aged and aged mice after eight weeks of injection compared to young mice, leading to the question of whether this difference was due to the loss of ha-syn overexpressing cells in the DMX of young mice. Therefore, neurons in the DMX were counted by stereology for all age groups in the injected (ipsilateral side) and intact side (contralateral side). Surprisingly, the percentage of neuronal loss normalized to the intact side showed that age inversely correlated with neuronal loss. Neuron loss was about 50 percent in young mice, but only 35 percent in mid-aged mice and 25 percent in aged mice (see Figure 3.18 A and B). Subsequently, we investigated whether this neuronal vulnerability was ha-syn specific or due to general protein overexpression or AAV transduction. For that, mice were injected into the vagus nerve with empty rAAV, rAAV overexpressing GFP or ha-syn for eight weeks. The neurons in the DMX were counted by stereology. The empty AAV control showed almost no neuronal loss in the DMX, suggesting that the AAV transduction has no effect on neuronal viability. However, for GFP and ha-syn, we observed a comparable inverse correlation between age and neuronal loss in the DMX (see Figure 3.18 C). Young mice displayed significantly fewer neurons, approximately 30 percent, in the DMX compared with aged mice, suggesting an age-dependent neuronal susceptibility to overexpression toxicity of GFP and ha-syn in the DMX.

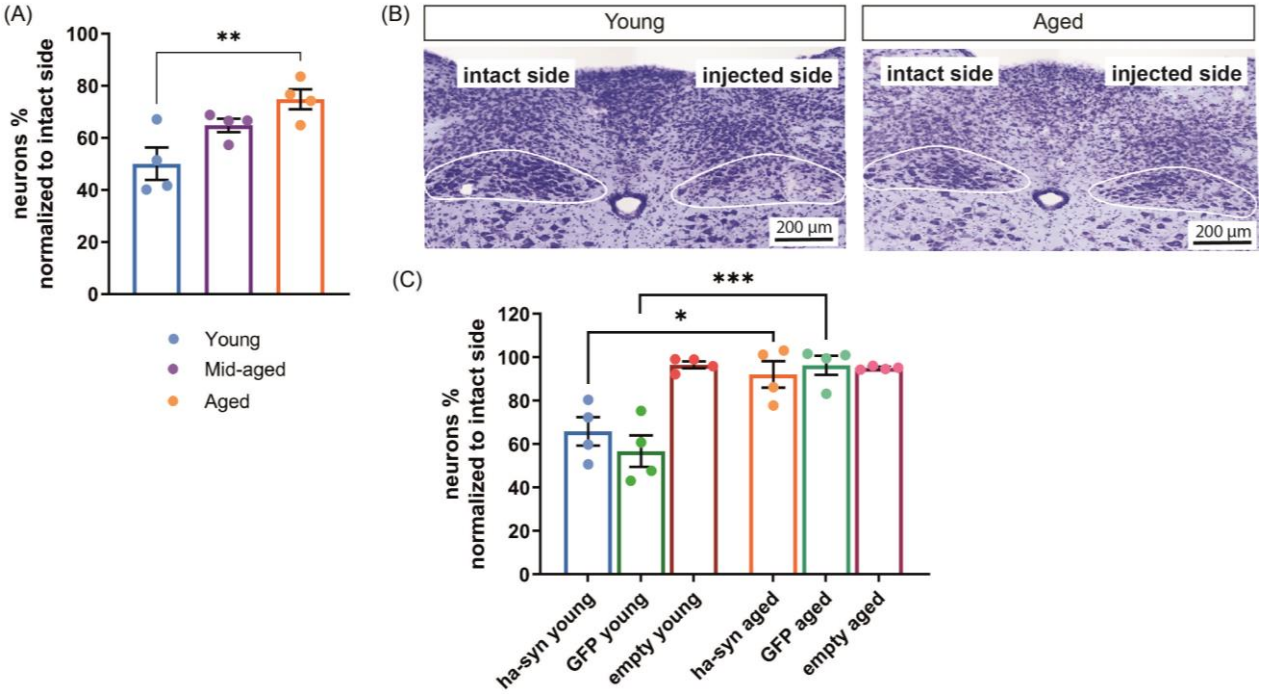

Figure 3.18: Neuronal loss correlates inversely with age in ha-syn and GFP overexpressing mice. (A) Female mice were injected with rAAV into the vagus nerve (titer $5x10^{11}$ Gc/mL). Neurons in the DMX were stereologically counted in every 5th section containing the DMX. The number of neurons was normalized to the contralateral, i.e., intact, side for each animal. In young mice, neuron loss in the DMX was significantly higher than in aged mice. **(B)** Representative images of nissl stained sections with the DMX delineated in white. The neuronal loss on the injected side is visible in young mice compared to the intact side. However, in aged mice, the neuronal numbers in the DMX are comparable to those on the intact side. **(C)** Male mice were injected with an rAAV titer of $6x10^{11}$ Gc/mL into the vagus nerve. Young mice injected with GFP or ha-syn show a significantly reduced number of neurons compared to the intact side in the DMX after eight weeks of injection. In aged mice, there is no significant difference in neuronal numbers in the DMX for ha-syn or GFP injection and overexpression. Stereological counting was performed by Dr. Ayse Ulusoy. Data are presented as mean ± SEM; * $p<0.05$ and ** $p<0.01$; ****$p<0.0001$; n=4; One-way ANOVA (A) and two-way ANOVA (D) *posthoc* Tukey's multiple comparison test.

3.3.4.3 Microglia numbers are affected by age and ha-syn overexpression

To investigate the mechanism of neuronal loss in the DMX and the reason for the inversely correlated neuronal vulnerability, we characterized microglia at eight weeks after ha-syn overexpression. For this purpose, sections containing the DMX eight weeks after rAAV injection were stained for Iba1 and DAPI. Microglia were counted as Iba1 and DAPI double-positive cells in the DMX and surrounding areas such as the NTS and AP in control (naive) and ha-syn overexpressing mice (see Figure 3.19 A). Consistent with published data, the number of microglia was increased in aged naive mice compared with young naive mice. Interestingly, with ha-syn overexpression, the number of microglia was increased in young mice compared with young naive mice. However, the number of

microglia in aged mice was similar between the naive mice and ha-syn overexpressing mice (see Figure 3.19 B). Furthermore, in ha-syn mice, we did not detect any difference in the number of microglia between the ipsilateral and contralateral side (see Figure 3.19 C). In short, overexpression of ha-syn in DMX leads to increased numbers of microglia in young mice but not in aged mice.

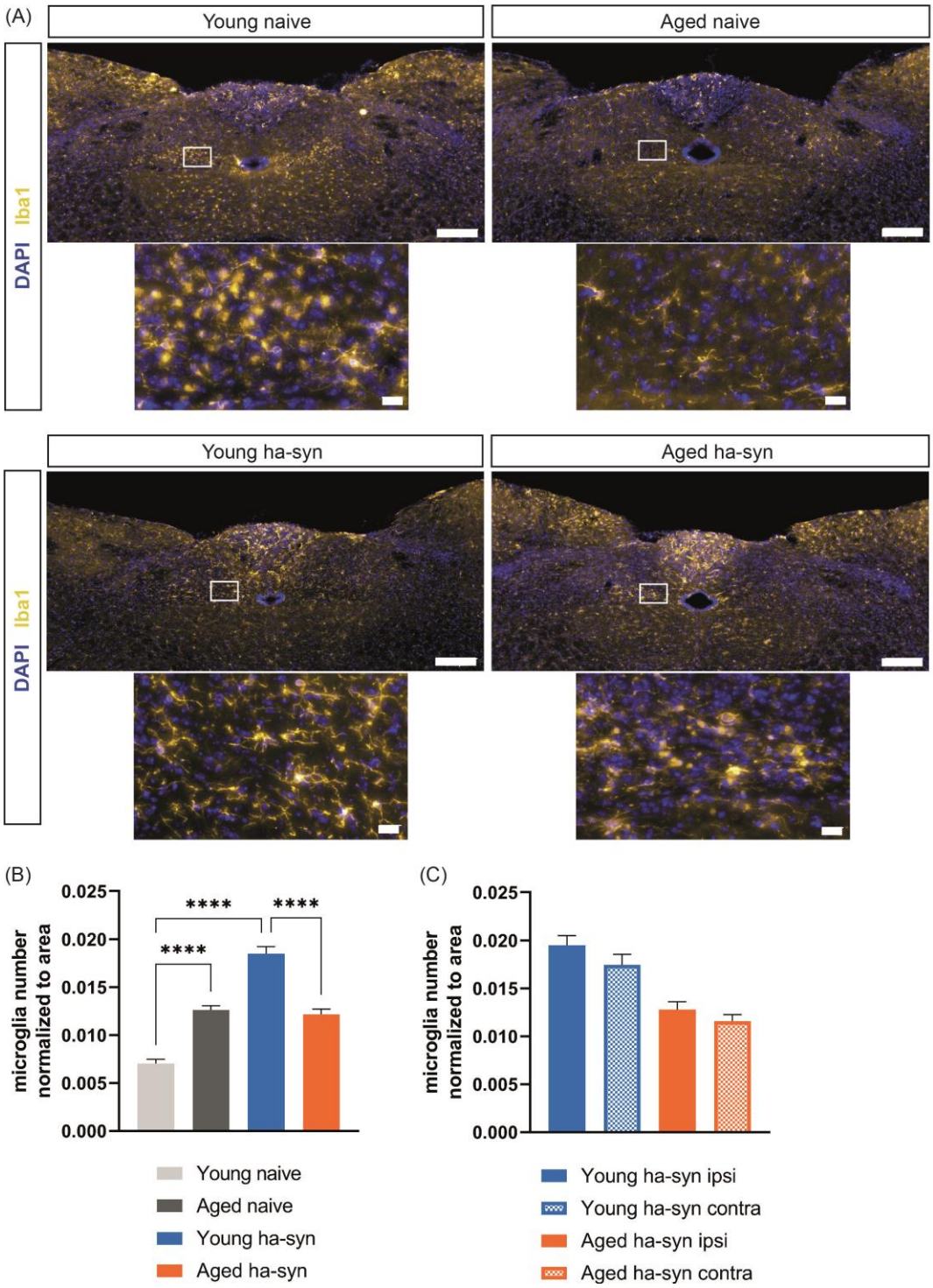

Figure 3.19: Number of microglia is elevated in young but not in aged mice upon ha-syn expression. (A) Representative images of Iba1 and DAPI stained MO sections. Microglia were counted in this region in wild-type (naive) and 8 weeks rAAV (ha-syn) injected mice in young and aged groups. The white box shows the DMX in higher magnification. Scale bar 200 µm for the whole section and 20 µm for higher magnification. **(B)** Iba1 and DAPI double-positive cells were counted and normalized to the area of the counted region. Microglia were increased in aged compared with young naive mice but also upregulated in young ha-syn expressing mice in contrast to young naive mice. **(C)** The number of microglia counted did not differ between the ipsilateral (injected) and contralateral (not injected) sides in ha-syn overexpressing mice. Data are presented as mean ± SEM; ****p<0.0001; n=3 for naive mice, 4 for ha-syn injected mice; two MO sections were analyzed per animal; Two-way ANOVA *posthoc* Tukey's multiple comparison test.

4 Discussion

4.1 Propagation model of ha-syn

The stereotypical distribution of LBs containing high amounts of aggregated a-syn in the brain is an important hallmark in PD. *In vitro,* it was shown that soluble a-syn possesses the capability to transfer from cell to cell (Sung et al. 2001, Ahn et al. 2006, Domert et al. 2016). Furthermore, the transmission of a-syn to grafted neurons in the SN or striatum has been reported in mice (Desplats et al. 2009a, Hansen et al. 2011) and PD patients (Chu & Kordower, 2010; Li et al., 2008). This intercellular spread of a-syn in the brain is thought to occur through neuronal transsynaptic transmission (Kiechle et al. 2019).

To better understand the propagation of a-syn and the factors that influence it, a mouse model was used in which rAAVs were injected into the vagus nerve to induce a targeted overexpression of ha-syn (see Figure 3.1 A). It has been already shown that injection of rAAV into the vagus nerve leads to a retrograde transfer of the rAAV and the targeted transduction of neurons in the MO such as the DMX and the AP. The restricted transduction of the rAAV only in the neurons of these regions was confirmed by measuring the WPRE expression of the rAAV. More rostral brain regions are devoid of this WPRE expression but are affected by the ha-syn spreading excluding AAV diffusion and proving ha-syn propagation (Helwig et al. 2016). Using a control protein such as GFP it was also demonstrated that the propagation is a specific feature of ha-syn since GFP could not be detected in higher brain regions after overexpression in the MO (Helwig et al. 2016). The stereotypical pattern of ha-syn propagation in this model showed affected areas known to have no direct anatomical connections to the vagus nerve. Therefore, this model demonstrates the neuronal transmission of ha-syn from the MO to the neurons, which project from higher brain regions such as the coeruleus–subcoeruleus complex (pons), dorsal raphae (midbrain), amygdala (medial temporal lobe) to the MO (own observation) (Ulusoy et al. 2013, Helwig et al. 2016, Rusconi et al. 2018).

This consistent a-syn spreading pattern to distinct brain regions, however, did not reach the SN. Normally this region is affected by LB pathology in PD patients as shown in chapter 1.4.1. An additional limitation in this model is that the transferred a-syn was only

detected in neuronal projections but did not accumulate in the soma of the neurons. LB pathology in PD patients is observed in axons as well as in neuronal somas.

In summary, we and others showed, that this model displays *in vivo* transmission of the overexpressed ha-syn from neuron to neuron from the MO to higher brain regions.

4.2 Effect of Enriched environment

A study by Wassouf *et al.* demonstrated that gene expression changes in neurons and microglia caused by ha-syn overexpression in the hippocampus could be reversed by long-term EE treatment (Wassouf et al. 2018). However, it has not yet been investigated whether this change in gene expression upon EE treatment leads to a change in microglial activation based on the expression of activation markers. In addition, we wanted to assess if EE already modifies the microglial activation markers under homeostatic conditions in wild-type mice. In this context, we also wanted to know whether the changes in microglia after EE treatment could have a direct effect on the propagation of a-syn to higher brain regions.

4.2.1 EE effect on microglial activation in wild-type mice

EE exposure to wild-type mice did not change the expression of microglial activation markers as depicted in Figure 3.4. However, all markers were generally higher expressed in the MO compared to the PONS and midbrain, and the forebrain. In mice overexpressing ha-syn in the MO and with ha-syn propagation to higher brain regions, we could observe an increase of most activation markers on microglia (see Figure 3.5). This impact was most pronounced in the ha-syn affected brain regions such as the MO, Pons, and midbrain.

Only a few studies examined changes in microglia activation upon EE exposure in wild-type mice. Previous studies indicated that pro-inflammatory genes were reduced and microglia morphology was altered upon long-term EE treatment in aged mice (McMurphy et al. 2018, Ali et al. 2019). However, the change in inflammation gene expression was observable in the hypothalamus but was not present in the amygdala. Another study investigated the gene expression in the hippocampus of wild-type mice upon EE exposure compared to control mice and this revealed only a small number of differentially regulated

genes in all cell types (Wassouf et al. 2018). Overall based on literature, the changes of EE exposure in healthy conditions on cells in the brain seem to be subtle if present at all. Our data indicate no change in microglial activation markers upon EE in wild-type mice. Therefore, it would be important to analyze individual brain regions such as the hippocampus or the hypothalamus to capture these subtle changes in the activation state of microglia in other brain regions.

Surprisingly, we could demonstrate higher expression levels of microglial activation markers in the MO compared to the other measured regions independent of EE treatment. The regional heterogeneity of microglia based on mRNA, protein expression patterns, or morphology was already described in many studies (de Haas et al., 2008; Grabert et al., 2016; Li et al., 2019; Masuda et al., 2019; Orit et al., 2016; Sharma et al., 2015). They also revealed that the microglia mRNA pattern of the brainstem cluster with the cerebellum and, based on proteomic studies, these regions share a similar microenvironment in contrast to other brain regions (Sharma et al. 2015, Masuda et al. 2019). Assuming that brainstem microglia are similar to the cerebellum based on their gene and protein expression pattern, our data are consistent with studies showing that microglia in the cerebellum are in a so-called "immune-vigilant" state, in which microglial activation markers are elevated compared with other brain regions such as the cortex or midbrain (Grabert et al. 2016).

4.2.2 EE effect on microglial activation in ha-syn overexpressing mice

The microglial activation markers are mostly involved in immune signaling or phagocytosis and they are increased when microglia are shifted to a reactive state. (Boche et al. 2013, Ransohoff & El Khoury 2015). It is also known from literature that ha-syn overexpression and accumulation activates microglia (Hirsch & Hunot, 2009). Therefore, it was unexpected to detect an increase in microglial activation markers in ha-syn overexpressing and propagating mice after EE exposure compared to mice in SH (see Figure 3.5). However, the higher level of activation upon EE exposure of microglia had no positive or negative effect on ha-syn propagation.

In brain diseases such as stroke, depression, or glioma it was shown that microglia are shifted to a reactive and pro-inflammatory state in the disease model and rescued upon

EE exposure to an anti-inflammatory or homeostatic state resulting in the improvement of the disease's phenotype or progression (Chabry et al., 2015; Garofalo et al., 2015; Quattromani et al., 2014). AD models are more deeply studied with EE exposure and they exhibit contradicting results. Two studies showed that EE can prevent a shift of microglia to a more pro-inflammatory state upon Aβ or tau pathology (Lahiani-Cohen et al., 2011; Xu et al., 2016). These mice were young (one or four months) when exposed to eight weeks or nine months of EE. However, another study revealed that mid-aged mice treated six months with EE had no difference in Aβ load and less microglia but microglia were shifted to a more reactive state (Stuart et al. 2019). In PD there is only one study examining microglia and EE exposure. It showed in the hippocampus that microglia gene expression patterns upon a-syn overexpression were more reactive but were rescued to a more homeostatic microglia state upon EE (Wassouf et al. 2018).

The results of the microglial activation phenotype upon EE in ha-syn overexpressing and propagating mice are partly contradicting to what is reported in the literature for microglia activation in other brain disease models. However, studies in AD models suggest that EE exposure may have differential effects on microglia at different ages, as microglia in young mice transition to a less reactive state, whereas they adopt a more reactive state in mid-aged mice. This fits with our results showing more activation in eleven to twelve months old mice. Compared with the study performed in a PD model, some differences should be considered. In our study, we examined the expression of microglial activation markers on protein level compared to mRNA levels in the literature, which may indicate differential regulation of these markers at the protein level. Moreover, our study was performed in different brain regions and not well-specified regions, which means that different microenvironments and heterogeneity of microglia may play a role and the EE effect in single brain regions can get lost. Another important step is to verify that our EE protocol is working successfully. Benito and colleagues have shown that the EE protocol used in this study successfully increased synaptic plasticity, a known factor modulated by EE, by increasing long-term potentiation in the hippocampus (Benito et al. 2018). Nevertheless, it would be valuable to verify whether EE treatment was successful in our experimental setup. This could be done by validating a known EE effect, such as increased adult neurogenesis in the dentate gyrus by staining of doublecortin for neuronal precursor cells

and a proliferation marker such as Ki67 (Couillard-Despres et al. 2005) or increased BDNF levels in the hippocampus by RT-PCR (Jha et al. 2016).

In conclusion, microglia are more activated after EE exposure at six weeks with ha-syn pathology. Nevertheless, it remains a question whether this is an increase in activation compared with microglia activation with ha-syn pathology or whether it is a rescue of microglia activation disrupted by ha-syn pathology. To answer this question, the next step must be to stain and analyze wild-type and ha-syn overexpression mice with and without EE on the same day to directly compare microglia activation levels between wild-type and ha-syn overexpressing mice. Considering that upregulated microglial activation upon EE exposure could be a rescue of microglial activation disrupted by ha-syn, this would suggest that microglial activation might be helpful at elevated a-syn levels. It is possible that microglial activation is beneficial in the early stages of PD, represented by our PD mouse model since microglia are able to clear a-syn and a-syn-burdened neurons. Only later in the course of PD could microglial activation become detrimental after long-term activation and neuroinflammation. Therefore, it would be interesting to investigate whether increased microglia activation with EE treatment leads to greater a-syn clearance in ha-syn overexpressing mice than in control mice.

4.2.3 EE effect on ha-syn propagation

Interestingly, the ha-syn overexpression in the DMX and ha-syn propagation to higher brain regions showed no difference when mice were exposed to EE treatment compared to standard housed mice (see Figure 3.6 and Figure 3.7). It might be that the consequences of EE exposure do not modulate a-syn propagation due to several reasons. In AD models, the most common neurodegenerative disease, controversial reports were described on how or if EE affects Aβ levels and depositions, as Aβ is aggregating and forming plaques in AD (Jankowsky et al. 2003, Arendash et al. 2004, Lazarov et al. 2005). Foremost, it could be that molecular and cellular changes seen in other studies upon EE (see chapter 1.6.2) do not necessarily translate into functional changes altering a-syn propagation to other brain regions. Especially as most studies show the beneficial effect of EE on the brain or in neurodegenerative disease in brain regions such as the hippocampus, the cortex, or the SN (Kempermann 2019).

However, it might be that EE could modulate a-syn propagation and there are limitations by the experimental setup. The effect of EE could depend on the age at which enrichment starts since EE tends to have a higher beneficial impact at a younger age and during brain development (Baroncelli et al. 2010, Fischer 2016). In our study, the mice were already mid-aged at nine to ten months, so EE may affect ha-syn propagation in younger mice. In addition, the duration of exposure to enriched environments is critical to the outcome as demonstrated by many studies (Rampon et al. 2000, Nithianantharajah & Hannan 2006, Garofalo et al. 2015, Hase et al. 2017). It could be that EE treatment affects ha-syn spread after longer time points following exposure. Another important factor in interpreting these results is to confirm that the EE protocol was successful, as described earlier in the section on the effects of EE on microglial activation markers.

4.3 Effect of aging

Aging is a major risk factor in PD and the protein a-syn is the most central player in PD disease. We wanted to investigate if and how aging could have a direct effect on ha-syn propagation.

4.3.1 Age-dependent ha-syn overexpression in DMX and propagation to higher brain regions

In our model of rAAV induced ha-syn overexpression in the MO and propagation to more rostral brain regions, we found a time-dependent effect of aging on ha-syn propagation. After eight weeks but not after six weeks post-injection, we detected a more pronounced propagation of ha-syn to more rostral brain regions in the mid-aged and aged mice compared with young mice (see Figure 3.15 and Figure 3.17). This alteration of ha-syn propagation was accompanied by a change of ha-syn overexpression levels in the DMX over time. After two weeks, the level of ha-syn overexpression by rAAV injection was similar in all age groups. However, after six weeks there was an increase in ha-syn overexpression in mid-aged mice and at eight weeks a similar rise in mid-aged and aged mice compared to young (see Figure 3.14 and Figure 3.16).

There are not many studies published on the a-syn propagation in animal models of PD that address the effects of aging on a-syn pathology and spreading. However, our data fit with previously published results based on the PFF model, which also concluded that age

enhances the spread of a-syn fibrils and pathology (Challis et al. 2020, Van Den Berge et al. 2021). In addition, in an animal model of AD, it has been reported that the spread of tau is enhanced in aged mice (Susanne et al. 2021).

We have shown that there is a correlation between ha-syn mRNA expression and ha-syn positive cells in the DMX and between ha-syn mRNA and protein quantity (see Figure 3.6 and Figure 3.12). In addition, in previous work using this ha-syn propagation mouse model, it has been shown that there is a relationship between the level of ha-syn overexpression in the DMX and the extent of ha-syn propagation. It was demonstrated that the concentration of the injected rAAV and consequently the level of ha-syn overexpression in the DMX directly correlates with the amount of ha-syn propagation and how far rostrally ha-syn spreads (Helwig et al. 2016). In another study, the toxicity of different purified rAAV stocks revealed that fewer ha-syn containing neurons in the DMX cause less prominent ha-syn spreading. This suggests that α-syn is not spread by dying neurons but by interneuronal transmission across living neurons (Ulusoy et al. 2015). Interestingly, this can also be observed with long-term ha-syn overexpression in the DMX for several months. Specifically, it was reported that ha-syn-containing neurons in the DMX and ha-syn overexpression decline three months after injection compared with six weeks and continued to decline after six months and one year. At the same time, the ha-syn spreading to higher regions increased at three months compared to six weeks but then decreased dramatically at six months and one year. This shows a delayed effect between the amount of ha-syn overexpression in DMX and the resulting ha-syn propagation (Rusconi et al. 2018). Ultimately, this suggests that the propagation of a-syn depends on its continued overexpression in DMX. However, when these neurons die, this leads to a disruption of propagation.

Overall, our data indicate that aging affects a-syn pathology in our model. However, it does not seem to directly affect the ha-syn transmission and the resulting propagation, but the level of ha-syn overexpression in the DMX.

4.3.2 Inverse age-dependent neuronal vulnerability in DMX by protein overexpression

We reported that overexpression of ha-syn was increased in older mice and that this resulted in enhanced ha-syn propagation and accumulation in more rostral brain regions such as the midbrain and forebrain. We wondered whether this difference was due to loss of ha-syn expressing neurons in the DMX in young but not in aged mice. Could aging be responsible for differential susceptibility of DMX neurons to overexpression of ha-syn?

In cortical embryonal neurons *in vitro*, we observed that empty rAAV induced some neuronal death. However, GFP and ha-syn overexpression by rAAV transduction revealed a dose-dependent increase in cell death (see Figure 3.10). Nevertheless, it is difficult to conclude about rAAV or protein toxicity from *in vitro* results to *in vivo* processes (Royo et al. 2008). *In vivo,* we observed some cell death in DMX at six weeks, which was significant at eight weeks (see Figure 3.14 and Figure 3.18). The most striking observation in the DMX eight weeks post-injection was that there is an inverse correlation of neuronal loss and aging, with young mice showing 30 percent more neuronal loss than aged mice. This effect was evident for GFP and ha-syn overexpression, while the empty rAAV caused no significant neuronal loss.

In vivo, rAAVs are commonly used for protein overexpression because they are known to have a low chance of integrating into the host genome and are not very immunogenic (Albert et al. 2017). Therefore, it is consistent with the literature that the empty rAAV does not cause significant neuronal death in DMX eight weeks after transduction. However, rAAV-induced GFP overexpression is already known to result in considerable loss of neurons, e.g., dopaminergic neurons in the SN (Klein et al., 2006; Koprich et al., 2011; Landeck et al., 2017; Ortinski et al., 2010). This potential toxicity of GFP by overexpression, which is also known in other paradigms and *in vitro*, leads to the suggestion that GFP is not an optimal protein control (Ulusoy et al. 2010). It has been suggested that proteins such as actin, collagen, or β-Galactosidase, which are unlikely to become toxic by overexpression, may serve as better controls (Albert et al. 2017). Assuming that GFP and ha-syn have this intrinsic property and are more susceptible to toxicity by overexpression, the next step should be to overexpress other proteins to examine neuronal vulnerability in DMX in young and aged mice. These control proteins

should not be susceptible to toxicity by overexpression and should be also relevant *in vivo*, e.g., another endogenous expressed neuronal protein.

We are the first to describe an inverse age-dependent sensitivity in neurons by a distinctive insult such as protein overexpression in young and aged mice in the DMX. There is only one other study addressing age-related neuronal vulnerability, in which huntingtin protein was overexpressed in the striatum of young and old rats. However, this showed that older animals had a greater loss of neurons compared to young animals (Diguet et al. 2009). These contradictory results raise the question of whether this effect might be region-specific (DMX vs. striatum), which could be answered by overexpression of ha-syn in other brain regions. Furthermore, this effect could be dependent on the protein and its toxicity when overexpressed.

4.3.3 Age and ha-syn dependent changes in microglia

This neuronal vulnerability may not only be mediated by general protein overexpression but may be related to the response of microglia to this challenge. Indeed, a recent study has shown that microglia overexpressing a-syn and thus activated can trigger neuronal death in the SN. However, these neurons showed almost no a-syn depositions and die due to the toxic environment generated by the microglia (Bido et al. 2021).

Therefore, we hypothesized that the inverse age-dependent neuronal vulnerability we see in the DMX might be caused by a differential response of microglia in young and aged mice to ha-syn pathology. Many reasons suggest the involvement of microglia in this context as it is known that overexpression of ha-syn by rAAV causes activation of microglia (Theodore et al. 2008). In addition, as discussed in chapter 1.4.3, the activation of microglia can lead to neuronal death or phagocytosis of dysfunctional neurons. However, this phagocytic ability of microglia is known to decrease with aging (Bliederhaeuser et al. 2016).

Two weeks after rAAV injection and ha-syn overexpression, the pro-inflammatory cytokine IL-6 was augmented and TNF-α was significantly increased in aged mice compared with young counterparts. In addition, microglial activation markers Iba1 and TLR2 were also significantly increased in aged mice compared with young mice (see Figure 3.13).

Moreover, eight weeks after injection, the number of microglia identified as Iba1-positive and DAPI-positive was increased in young mice compared with naive controls. However, there was no difference in the number of microglia in aged mice with ha-syn overexpression compared with naive aged mice. In general, the number of microglia increased with age in wild-type mice (see Figure 3.19).

Consistent with the literature, aged microglia in the ha-syn propagation model showed increased TNF-α and Il-6 production in the DMX compared with young mice. It is well described that a more reactive phenotype is established in aging microglia, leading to an exaggerated pro-inflammatory state (Perry & Holmes 2014, Michell-Robinson et al. 2015) and a stronger pro-inflammatory response to insults (Rawji et al. 2016). For example, aged microglia in mice produce higher levels of TNF-α and IL-6 in the CNS upon stimulation and *ex vivo* compared with young microglia (Godbout et al. 2005, Njie et al. 2012, Bliederhaeuser et al. 2016). Consistent with the observed effects on microglia activation markers, Iba1 and TLR2 are known to be upregulated by a-syn and with aging (Kim et al., 2015; Letiembre et al., 2007; Ogura et al., 1994; Watson et al., 2012).

However, there are certain limitations in the interpretation of our data based on the experimental design used to characterize microglial activation and pro-inflammatory markers two weeks after overexpression of ha-syn. We did not measure the expression levels of the activation and pro-inflammatory markers in young and aged wild-type mice. Therefore, we cannot distinguish the extent to which the increase of these markers is due to the age effect or the ha-syn pathology insult. This is an important experiment that should be performed in the future. In addition, the marker Iba1 is also expressed by peripheral macrophages (Sasaki et al. 2001), so the signal of Iba1 expression might not only originate from microglia but also partly from macrophages infiltrating the brain. Another limitation is that the receptor TLR2 is expressed on microglia as well as on neurons and plays a role in a-syn pathology in both cell types (Kwon et al. 2019). It has been reported that the expression of TLR2 is upregulated by the a-syn interaction on microglia and neurons and triggers a pro-inflammatory response. However, this activation leads to upregulation of phagocytosis of a-syn in microglia, whereas in neurons it reduces uptake and degradation of a-syn (Dzamko et al., 2017; Kim et al., 2015).

Our finding that microglia numbers increase with age in naive mice is consistent with the literature (Tremblay et al., 2012; Wong, 2013). It is difficult to compare the number of microglia in the MO with ha-syn overexpression with other studies as microglia were counted in other brain regions, at different ages, and/or at different time points after a-syn expression. One study showed in the SN that one month-old mice overexpressing a-syn had higher microglia counts compared with age-matched control mice. However, after twelve months a-syn expressing mice had a lower number of microglia than age-matched mice (Su et al. 2009). The majority of a-syn transgenic mice as in this study, express a-syn from the developmental stage onwards, and therefore the effects in old mice are accumulated by lifelong a-syn expression.

We observed an interesting age-dependent difference between the numbers of young and aged microglia eight weeks after rAAV injection when ha-syn is overexpressed in the DMX. The increase of microglia numbers is known to be a part of the normal activation process (Davis et al. 2017). It appears that in aged mice the process of microglial activation is impaired with ha-syn pathology. Therefore, we want to further characterize the phenotype and activation of microglia to better understand how young and old microglia are differentially affected by ha-syn pathology. Using Iba1 microglia staining, we could recognize that the morphology of young and aged microglia looks different in ha-syn overexpressing mice (see Figure 3.19 A). For this reason, we plan to characterize microglial morphology and pro-inflammatory cytokine expression in young and aged mice at eight weeks. In a next step, we aim to characterize the number of microglia in young and old mice two weeks after rAAV injection in the absence of neuronal loss in DMX. This should determine if microglia reaction upon ha-syn early on is already different in young and aged mice.

4.4 Conclusion and outlook

In this study, we investigated the influence of aging as a cell-intrinsic factor and EE as an external factor on a-syn propagation, neuronal susceptibility, and the impact on microglia. We conclude that EE has no effect on ha-syn propagation in this mouse model but modulates microglial activation in ha-syn challenged regions. However, aging increased the propagation of ha-syn to more rostral brain regions. These increased ha-syn accumulations in mid-aged and aged mice compared to young could be explained by the higher ha-syn overexpression in the mice in the DMX eight weeks after rAAV injection. Furthermore, we reported that a possible cause for this age-dependent shift in ha-syn overexpression in the DMX was due to differential loss of these neurons. In summary, our results show an increased loss of neurons and a decrease in ha-syn levels in young mice in DMX, whereas the opposite is observed in aged mice. This inverse age-dependent neuronal vulnerability was observed not only in mice overexpressing ha-syn in the DMX but also in GFP-overexpressing mice. We also detected age-dependent differences in the response of microglia to ha-syn in DMX, which may be related to the neuronal vulnerability in the DMX.

Surprisingly, the results suggest that age-related changes contribute to decreased neuronal susceptibility of DMX in aged mice. This neuronal vulnerability is caused by high expression of ha-syn and GFP, which are known to have toxic properties when present in excessive amounts in the cell. However, the consequence of age-related differences in protein concentrations in our mouse model is a-syn specific, as only ha-syn shows propagation to higher brain regions. Considering that a-syn is endogenously expressed and known to increase with age in the brain (Végh et al. 2014), we hypothesize that this may be a relevant mechanism in PD, where neurons with high a-syn levels in aged neurons do not die and are not cleared by microglia but continue to secrete a-syn.

It would be interesting to decipher the exact mechanism of how neurons die in this paradigm and why this mechanism fails with aging. Concurrently, the mechanism which fails with age could be the clearance of the dysfunctional or dead neurons by microglia.

5 Abstract

Parkinson´s disease (PD) is the second most common neurodegenerative disease. The prevalence of sporadic PD results from a complex interaction of demographic, genetic, and environmental factors. Age is one of the strongest risk factors, while on the other hand, physical activity is considered a protective factor. PD is characterized by three pathological hallmarks (i) α-synuclein-rich inclusions found in neurons known as Lewy bodies, (ii) loss of dopaminergic neurons in the Substantia nigra pars compacta, and (iii) chronic neuroinflammation. The α-synuclein depositions show a spatiotemporal distribution pattern in PD patients during disease progression suggesting that α-synuclein may propagate to distinct neuronal populations throughout the brain by neuronal connectivity.

However, it is unclear how aging as a cell-intrinsic factor and an enriched environment (EE) combining physical exercise and cognitive stimulation as an external factor influence α-synuclein pathology. To investigate how these factors may modulate the propagation of α-synuclein, we have chosen a PD mouse model with unilateral injection of recombinant adeno-associated viral vectors into the vagus nerve which leads to overexpression of human α-synuclein (ha-syn) in the neurons of its dorsal motor nucleus. This model shows selective spreading of the overexpressed ha-syn from the medulla oblongata to the pons, midbrain, and forebrain by neuron-to-neuron transmission. Our results show in the affected regions of ha-syn expression (DMX) and spreading (e.g. pons and midbrain) an increase in microglial activation with EE treatment compared to standard housed mice. However, EE does not influence the ha-syn propagation to more rostral brain regions. We demonstrate that aging accelerates the propagation of ha-syn, as mid-aged (13-15 months) and aged mice (22-23 months) showed increased accumulations in higher brain regions compared with young mice (3-5 months). Interestingly, this propagation was related to increased ha-syn levels in the DMX over time in mid-aged and aged mice. We showed that these higher levels resulted from inverse neuronal loss in the DMX, with young mice exhibiting more neuronal loss than older mice. This inverse age-dependent susceptibility was also observed in GFP overexpression, indicating a general susceptibility to overexpression of toxic proteins. Moreover, these results might be related to the different number and activation of microglia in young and aged animals.

These findings suggest an inverse age-specific vulnerability of neurons in the DMX, which then specifically drives ha-syn propagation in aged animals in our ha-syn overexpression and propagation model. This may be an important process in PD that neurons with high levels of α-synuclein cannot be degraded and continue to propagate and accumulate α-synuclein to other brain regions.

6 List of Figures

7 List of Tables

8 References

Abeliovich A, Schmitz Y, Fariñas I, Choi-Lundberg D, Ho WH, Castillo PE, Shinsky N, Garcia Verdugo JM, Armanini M, Ryan A, Hynes M, Phillips H, Sulzer D, Rosenthal A. Mice lacking α-synuclein display functional deficits in the nigrostriatal dopamine system. Neuron 2000; 25:239–252

Abounit S, Bousset L, Loria F, Zhu S, de Chaumont F, Pieri L, Olivo-Marin J-C, Melki R, Zurzolo C. Tunneling nanotubes spread fibrillar α-synuclein by intercellular trafficking of lysosomes. EMBO J 2016; 35:2120–2138

Ahn KJ, Paik SR, Chung KC, Kim J. Amino acid sequence motifs and mechanistic features of the membrane translocation of alpha-synuclein. J Neurochem 2006; 97:265–279

Albert K, Voutilainen MH, Domanskyi A, Airavaara M. AAV Vector-Mediated Gene Delivery to Substantia Nigra Dopamine Neurons: Implications for Gene Therapy and Disease Models. Genes (Basel) 2017; 8:63

Ali S, Liu X, Queen NJ, Patel RS, Wilkins RK, Mo X, Cao L. Long-term environmental enrichment affects microglial morphology in middle age mice. Aging (Albany NY) 2019; 11:2388–2402

Anastasía A, Torre L, de Erausquin GA, Mascó DH. Enriched environment protects the nigrostriatal dopaminergic system and induces astroglial reaction in the 6-OHDA rat model of Parkinson's disease. J Neurochem 2009; 109:755–765

Arendash GW, Garcia MF, Costa DA, Cracchiolo JR, Wefes IM, Potter H. Environmental enrichment improves cognition in aged Alzheimer's transgenic mice despite stable beta-amyloid deposition. Neuroreport 2004; 15:1751–1754

Ascherio A, Schwarzschild MA. The epidemiology of Parkinson's disease: risk factors and prevention. Lancet Neurol 2016; 15:1257–1272

Baba Y, Markopoulou K, Putzke JD, Whaley NR, Farrer MJ, Wszolek ZK, Uitti RJ. Phenotypic commonalities in familial and sporadic Parkinson disease. Arch Neurol 2006; 63:579–583

Ball N, Teo WP, Chandra S, Chapman J. Parkinson's disease and the environment. Front Neurol 2019; 10:218

Baroncelli L, Braschi C, Spolidoro M, Begenisic T, Sale A, Maffei L. Nurturing brain plasticity: impact of environmental enrichment. Cell Death Differ 2010; 17:1092–1103

Beach TG, Adler CH, Lue LF, Sue LI, Bachalakuri J, Henry-Watson J, Sasse J, Boyer S, Shirohi S, Brooks R, Eschbacher J, White CL, Akiyama H, Caviness J, Shill HA, Connor DJ, Sabbagh MN, Walker DG. Unified staging system for Lewy body disorders: Correlation with nigrostriatal degeneration, cognitive impairment and motor dysfunction. Acta Neuropathol 2009; 117:613–634

Bellou V, Belbasis L, Tzoulaki I, Evangelou E, A Ioannidis JP, Ioannidis JP, Wiley J. Environmental risk factors and Parkinson's disease: an umbrella review of meta-analyses. Parkinsonism Relat Disord 2016; 23:1–9

Belvisi D, Pellicciari R, Fabbrini G, Tinazzi M, Berardelli A, Defazio G. Modifiable risk and protective factors in disease development, progression and clinical subtypes of Parkinson's disease: What do prospective studies suggest? Neurobiol Dis 2020; 134

Benito E, Kerimoglu C, Ramachandran B, Pena-Centeno T, Jain G, Stilling RM, Islam MR, Capece V, Zhou Q, Edbauer D, Dean C, Fischer A. RNA-Dependent Intergenerational Inheritance of Enhanced Synaptic Plasticity after Environmental Enrichment. Cell Rep 2018; 23:546–554

Bennett DA, Beckett LA, Murray AM, Shannon KM, Goetz CG, Pilgrim DM, Evans DA. Prevalence of Parkinsonian Signs and Associated Mortality in a Community Population of Older People. N Engl J Med 1996; 334:71–76

Benskey MJ, Perez RG, Manfredsson FP. The contribution of alpha synuclein to neuronal survival and function - Implications for Parkinson's disease. J Neurochem 2016; 137:331–359

Berg S, Kutra D, Kroeger T, Straehle CN, Kausler BX, Haubold C, Schiegg M, Ales J, Beier T, Rudy M, Eren K, Cervantes JI, Xu B, Beuttenmueller F, Wolny A, Zhang C, Koethe U, Hamprecht FA, Kreshuk A. Ilastik: interactive machine learning for (bio)image analysis. Nat Methods 2019; 16:1226–1232

Van Den Berge N, Ferreira N, Mikkelsen TW, Alstrup AKO, Tamgüney G, Karlsson P, Terkelsen AJ, Nyengaard JR, Jensen PH, Borghammer P. Ageing promotes pathological alpha-synuclein propagation and autonomic dysfunction in wild-type rats. Brain 2021; 144:1853–1868

Bertini I, Gupta YK, Luchinat C, Parigi G, Peana M, Sgheri L, Yuan J. Paramagnetism-based NMR restraints provide maximum allowed probabilities for the different conformations of partially independent protein domains. J Am Chem Soc 2007; 129:12786–12794

Bertoncini CW, Jung YS, Fernandez CO, Hoyer W, Griesinger C, Jovin TM, Zweckstetter M. Release of long-range tertiary interactions potentiates aggregation of natively unstructured α-synuclein. Proc Natl Acad Sci U S A 2005; 102:1430–1435

Betarbet R, Sherer TB, MacKenzie G, Garcia-Osuna M, Panov A V, Greenamyre JT. Chronic systemic pesticide exposure reproduces features of Parkinson's disease. Nat Neurosci 2000; 3:1301–1306

Bezard E, Dovero S, Belin D, Duconger S, Jackson-Lewis V, Przedborski S, Piazza PV, Gross CE, Jaber M. Enriched Environment Confers Resistance to 1-Methyl-4-Phenyl-1,2,3,6-Tetrahydropyridine and Cocaine: Involvement of Dopamine Transporter and Trophic Factors. J Neurosci 2003; 23:10999 LP – 11007

Bido S, Muggeo S, Massimino L, Marzi MJ, Giannelli SG, Melacini E, Nannoni M, Gambarè D, Bellini E, Ordazzo G, Rossi G, Maffezzini C, Iannelli A, Luoni M, Bagicaluppi M, Gregori S, Nicassio F, Broccoli V. Microglia-specific overexpression of α-synuclein leads to severe dopaminergic neurodegeneration by phagocytic exhaustion and oxidative toxicity. Nat Commun 2021; 12:6237

Blandini F, Armentero M-T. Animal models of Parkinson's disease. FEBS J 2012; 279:1156–1166

Bliederhaeuser C, Grozdanov V, Speidel A, Zondler L, Ruf WP, Bayer H, Kiechle M, Feiler MS, Freischmidt A, Brenner D, Witting A, Hengerer B, Fändrich M, Ludolph AC, Weishaupt JH, Gillardon F, Danzer KM. Age-dependent defects of alpha-synuclein oligomer uptake in microglia and monocytes. Acta Neuropathol 2016; 131:379–391

Boche D, Perry VH, Nicoll JAR. Review: activation patterns of microglia and their identification in the human brain. Neuropathol Appl Neurobiol 2013; 39:3–18

de Boer A, Storm A, Gomez-Soler M, Smolders S, Rué L, Poppe L, B Pasquale E, Robberecht W, Lemmens R. Environmental enrichment during the chronic phase after experimental stroke promotes functional recovery without synergistic effects of EphA4 targeted therapy. Hum Mol Genet 2020; 29:605–617

Bohingamu Mudiyanselage S, Watts JJ, Abimanyi-Ochom J, Lane L, Murphy AT, Morris ME, Iansek R. Cost of Living with Parkinson's Disease over 12 Months in Australia: A Prospective Cohort Study. Parkinsons Dis 2017; 5932675

Braak H, Ghebremedhin E, Rüb U, Bratzke H, Del Tredici K. Stages in the development of Parkinson's disease-related pathology. Cell Tissue Res 2004; 318:121–134

Braak H, Del Tredici K. Neuroanatomy and Pathology of Sporadic Parkinson's Disease. Adv Anatomy, Embryol Cell Biol 2009; 201:1–119

Braak H, Del Tredici K. Neuropathological Staging of Brain Pathology in Sporadic Parkinson's disease: Separating the Wheat from the Chaff. J Parkinsons Dis 2017; 7:73–87

Braak H, Del Tredici K, Rüb U, de Vos RAI, Jansen Steur ENH, Braak E. Staging of brain pathology related to sporadic Parkinson's disease. Neurobiol Aging 2003; 24:197–211

Breid S, Bernis ME, Babila JT, Garza MC, Wille H, Tamgüney G. Neuroinvasion of α-Synuclein Prionoids after Intraperitoneal and Intraglossal Inoculation. J Virol 2016; 90:9182–9193

Brettschneider J, Del Tredici K, Lee VMY, Trojanowski JQ. Spreading of pathology in neurodegenerative diseases: A focus on human studies. Nat Rev Neurosci 2015; 16:109–120

Brown BM, Peiffer JJ, Martins RN. Multiple effects of physical activity on molecular and cognitive signs of brain aging: can exercise slow neurodegeneration and delay Alzheimer's disease? Mol Psychiatry 2013; 18:864–874

Bruel-Jungerman E, Laroche S, Rampon C. New neurons in the dentate gyrus are involved in the expression of enhanced long-term memory following environmental enrichment. Eur J Neurosci 2005; 21:513–521

Brundin P, Melki R. Prying into the prion hypothesis for parkinson's disease. J Neurosci 2017; 37:9808–9818

Buchman AS, Shulman JM, Nag S, Leurgans SE, Arnold SE, Morris MC, Schneider JA, Bennett DA. Nigral pathology and parkinsonian signs in elders without Parkinson disease. Ann Neurol 2012; 71:258–266

Burré J. The synaptic function of α-synuclein. J Parkinsons Dis 2015; 5:699–713

Burré J, Sharma M, Tsetsenis T, Buchman V, Etherton MR, Südhof TC. α-Synuclein promotes SNARE-complex assembly in vivo and in vitro. Science 2010; 329:1663–1667

Bussell R, Eliezer D. A structural and functional role for 11-mer repeats in α-synuclein and other exchangeable lipid binding proteins. J Mol Biol 2003; 329:763–778

Cabin DE, Shimazu K, Murphy D, Cole NB, Gottschalk W, McIlwain KL, Orrison B, Chen A, Ellis CE, Paylor R, Lu B, Nussbaum RL. Synaptic vesicle depletion correlates with attenuated synaptic responses to prolonged repetitive stimulation in mice lacking α-synuclein. J Neurosci 2002; 22:8797–8807

Cardinale A, Calabrese V, de Iure A, Picconi B. Alpha-Synuclein as a Prominent Actor in the Inflammatory Synaptopathy of Parkinson's Disease. Int J Mol Sci 2021; 22

Carr J, de la Fuente-Fernández R, Schulzer M, Mak E, Calne SM, Calne DB. Familial and sporadic Parkinson's disease usually display the same clinical features. Parkinsonism Relat Disord 2003; 9:201–204

Chabry J, Nicolas S, Cazareth J, Murris E, Guyon A, Glaichenhaus N, Heurteaux C, Petit-Paitel A. Enriched environment decreases microglia and brain macrophages inflammatory phenotypes through adiponectin-dependent mechanisms: Relevance to depressive-like behavior. Brain Behav Immun 2015; 50:275–287

Chahine LM, Weintraub D, Hawkins KA, Siderowf A, Eberly S, Oakes D, Seibyl J, Stern MB, Marek K, Jennings D, Russell D, Fiocco A, Sethi K, Jackson P, Frank S, Thomas

CA, James RC, Simuni T, Borushko E, Stern M, Rick J, Hauser R, Khavarian L, Richard I, Deeley C, Liang GS, Infeld L, Adler CH, Duffy AK, Saunders-Pullman R, Evatt ML, McMurray B, Lai E, Johnson S, DeBakey ME, Subramanian I, Gratiano A, Chung K, Lobb B, O'Conner S. Cognition in individuals at risk for Parkinson's: Parkinson associated risk syndrome (PARS) study findings. Mov Disord 2016; 31:86–94

Challis C, Hori A, Sampson TR, Yoo BB, Challis RC, Hamilton AM, Mazmanian SK, Volpicelli-Daley LA, Gradinaru V. Gut-seeded α-synuclein fibrils promote gut dysfunction and brain pathology specifically in aged mice. Nat Neurosci 2020; 23:327–336

Chartier-Harlin M-C, Kachergus J, Roumier C, Mouroux V, Douay X, Lincoln S, Levecque C, Larvor L, Andrieux J, Hulihan M, Waucquier N, Defebvre L, Amouyel P, Farrer M, Destée A. Alpha-synuclein locus duplication as a cause of familial Parkinson's disease. Lancet (London, England) 2004; 364:1167–1169

Chen EY, Kallwitz E, Leff SE, Cochran EJ, Mufson EJ, Kordower JH, Mandel RJ. Age-related decreases in GTP-cyclohydrolase-I immunoreactive neurons in the monkey and human substantia nigra. J Comp Neurol 2000; 426:534–548

Cherubini M, Wade-Martins R. Convergent pathways in Parkinson's disease. Cell Tissue Res 2018; 373:79–90

Chia SJ, Tan E-K, Chao Y-X. Historical Perspective: Models of Parkinson's Disease. Int J Mol Sci 2020; 21

Choi B-K, Choi M-G, Kim J-Y, Yang Y, Lai Y, Kweon D-H, Lee NK, Shin Y-K. Large α-synuclein oligomers inhibit neuronal SNARE-mediated vesicle docking. Proc Natl Acad Sci U S A 2013; 110:4087–4092

Choi I, Zhang Y, Seegobin SP, Pruvost M, Wang Q, Purtell K, Zhang B, Yue Z. Microglia clear neuron-released α-synuclein via selective autophagy and prevent neurodegeneration. Nat Commun 2020; 11:1386

Choi YR, Kang S-J, Kim J-M, Lee S-J, Jou I, Joe E-H, Park SM. FcγRIIB mediates the inhibitory effect of aggregated α-synuclein on microglial phagocytosis. Neurobiol Dis 2015; 83:90–99

Choubey V, Safiulina D, Vaarmann A, Cagalinec M, Wareski P, Kuum M, Zharkovsky A, Kaasik A. Mutant A53T alpha-synuclein induces neuronal death by increasing mitochondrial autophagy. J Biol Chem 2011; 286:10814–10824

Chu Y, Kordower JH. Age-associated increases of alpha-synuclein in monkeys and humans are associated with nigrostriatal dopamine depletion: Is this the target for Parkinson's disease? Neurobiol Dis 2007; 25:134–149

Chu Y, Kordower JH. Lewy body pathology in fetal grafts. Ann N Y Acad Sci 2010; 1184:55–67

Cohen AD, Tillerson JL, Smith AD, Schallert T, Zigmond MJ. Neuroprotective effects of prior limb use in 6-hydroxydopamine-treated rats: possible role of GDNF. J Neurochem 2003; 85:299–305

Colla E, Coune P, Liu Y, Pletnikova O, Troncoso JC, Iwatsubo T, Schneider BL, Lee MK. Endoplasmic reticulum stress is important for the manifestations of α-synucleinopathy in vivo. J Neurosci 2012; 32:3306–3320

Collier TJ, Kanaan NM, Kordower JH. Aging and Parkinson's disease: Different sides of the same coin? Mov Disord 2017; 32:983–990

Combs-Miller SA, Moore ES. Predictors of outcomes in exercisers with Parkinson disease: A two-year longitudinal cohort study. NeuroRehabilitation 2019; 44:425–432

Conway KA, Lee SJ, Rochet JC, Ding TT, Williamson RE, Lansbury PTJ. Acceleration of oligomerization, not fibrillization, is a shared property of both alpha-synuclein mutations linked to early-onset Parkinson's disease: implications for pathogenesis and therapy. Proc Natl Acad Sci U S A 2000; 97:571–576

Cooper AA, Gitler AD, Cashikar A, Haynes CM, Hill KJ, Bhullar B, Liu K, Xu K, Strathearn KE, Liu F, Cao S, Caldwell KA, Caldwell GA, Marsischky G, Kolodner RD, Labaer J, Rochet J-C, Bonini NM, Lindquist S. Alpha-synuclein blocks ER-Golgi traffic and Rab1 rescues neuron loss in Parkinson's models. Science 2006; 313:324–328

Couch Y, Alvarez-Erviti L, Sibson NR, Wood MJA, Anthony DC. The acute inflammatory response to intranigral α-synuclein differs significantly from intranigral lipopolysaccharide and is exacerbated by peripheral inflammation. J Neuroinflammation 2011; 8:166

Couillard-Despres S, Winner B, Schaubeck S, Aigner R, Vroemen M, Weidner N, Bogdahn U, Winkler J, Kuhn H-G, Aigner L. Doublecortin expression levels in adult brain reflect neurogenesis. Eur J Neurosci 2005; 21:1–14

Croisier E, Moran LB, Dexter DT, Pearce RKB, Graeber MB. Microglial inflammation in the parkinsonian substantia nigra: relationship to alpha-synuclein deposition. J Neuroinflammation 2005; 2:14

Danzer KM, Kranich LR, Ruf WP, Cagsal-Getkin O, Winslow AR, Zhu L, Vanderburg CR, McLean PJ. Exosomal cell-to-cell transmission of alpha synuclein oligomers. Mol Neurodegener 2012; 7:42

Danzer KM, Krebs SK, Wolff M, Birk G, Hengerer B. Seeding induced by α-synuclein oligomers provides evidence for spreading of α-synuclein pathology. J Neurochem 2009; 111:192–203

Davidson WS, Jonas A, Clayton DF, George JM. Stabilization of α-Synuclein secondary structure upon binding to synthetic membranes. J Biol Chem 1998; 273:9443–9449

Davis BM, Salinas-Navarro M, Cordeiro MF, Moons L, De Groef L. Characterizing microglia activation: a spatial statistics approach to maximize information extraction. Sci Rep 2017; 7:1576

van Dellen A, Blakemore C, Deacon R, York D, Hannan AJ. Delaying the onset of Huntington's in mice. Nature 2000; 404:721–722

Deng H, Wang P, Jankovic J. The genetics of Parkinson disease. Ageing Res Rev 2018; 42:72–85

Desplats P, Lee H-J, Bae E-J, Patrick C, Rockenstein E, Crews L, Spencer B, Masliah E, Lee S-J. Inclusion formation and neuronal cell death through neuron-to-neuron transmission of alpha-synuclein. Proc Natl Acad Sci U S A 2009a; 106:13010–13015

Desplats P, Lee H-J, Bae E-J, Patrick C, Rockenstein E, Crews L, Spencer B, Masliah E, Lee S-J. Inclusion formation and neuronal cell death through neuron-to-neuron transmission of α-synuclein. Proc Natl Acad Sci 2009b; 106:13010 LP – 13015

Dieriks BV, Park TI-H, Fourie C, Faull RLM, Dragunow M, Curtis MA. α-synuclein transfer through tunneling nanotubes occurs in SH-SY5Y cells and primary brain pericytes from Parkinson's disease patients. Sci Rep 2017; 7:42984

Diguet E, Petit F, Escartin C, Cambon K, Bizat N, Dufour N, Hantraye P, Déglon N, Brouillet E. Normal aging modulates the neurotoxicity of mutant huntingtin. PLoS One 2009; 4:e4637

DiSabato DJ, Quan N, Godbout JP. Neuroinflammation: the devil is in the details. J Neurochem 2016; 139 Suppl:136–153

Domert J, Sackmann C, Severinsson E, Agholme L, Bergström J, Ingelsson M, Hallbeck

M. Aggregated Alpha-Synuclein Transfer Efficiently between Cultured Human Neuron-Like Cells and Localize to Lysosomes. PLoS One 2016; 11:e0168700

Doorn KJ, Moors T, Drukarch B, van de Berg WD, Lucassen PJ, van Dam A-M. Microglial phenotypes and toll-like receptor 2 in the substantia nigra and hippocampus of incidental Lewy body disease cases and Parkinson's disease patients. Acta Neuropathol Commun 2014; 2:90

Dorsey RE, Elbaz A, Nichols E, Abd-Allah F, Abdelalim A, Adsuar JC, Ansha MG, Brayne C, Choi JYJ, Collado-Mateo D, Dahodwala N, Do HP, Edessa D, Endres M, Fereshtehnejad SM, Foreman KJ, Gankpe FG, Gupta R, Hankey GJ, Hay SI, Hegazy MI, Hibstu DT, Kasaeian A, Khader Y, Khalil I, Khang YH, Kim YJ, Kokubo Y, Logroscino G, Massano J, Ibrahim NM, Mohammed MA, Mohammadi A, Moradi-Lakeh M, Naghavi M, Nguyen BT, Nirayo YL, Ogbo FA, Owolabi MO, Pereira DM, Postma MJ, Qorbani M, Rahman MA, Roba KT, Safari H, Safiri S, Satpathy M, Sawhney M, Shafieesabet A, Shiferaw MS, Smith M, Szoeke CEI, Tabarés-Seisdedos R, Truong NT, Ukwaja KN, Venketasubramanian N, Villafaina S, Weldegwergs KG, Westerman R, Wijeratne T, Winkler AS, Xuan BT, Yonemoto N, Feigin VL, Vos T, Murray CJL. Global, regional, and national burden of Parkinson's disease, 1990–2016: a systematic analysis for the Global Burden of Disease Study 2016. Lancet Neurol 2018; 17:939–953

Duffy MF, Collier TJ, Patterson JR, Kemp CJ, Luk KC, Tansey MG, Paumier KL, Kanaan NM, Fischer DL, Polinski NK, Barth OL, Howe JW, Vaikath NN, Majbour NK, El-Agnaf OMA, Sortwell CE. Lewy body-like alpha-synuclein inclusions trigger reactive microgliosis prior to nigral degeneration. J Neuroinflammation 2018; 15:129

Duffy PE, Tennyson VM. Phase and Electron Microscopic Observations of Lewy Bodies and Melanin Granules in the Substantia Nigra and Locus Caeruleus in Parkinson's Disease*†. J Neuropathol Exp Neurol 1965; 24:398–414

Dzamko N, Geczy CL, Halliday GM. Inflammation is genetically implicated in Parkinson's disease. Neuroscience 2015; 302:89–102

Dzamko N, Gysbers A, Perera G, Bahar A, Shankar A, Gao J, Fu YH, Halliday GM. Toll-like receptor 2 is increased in neurons in Parkinson's disease brain and may contribute to alpha-synuclein pathology. Acta Neuropathol 2017; 133:303–319

Ehninger D, Kempermann G. Regional effects of wheel running and environmental enrichment on cell genesis and microglia proliferation in the adult murine neocortex. Cereb Cortex 2003; 13:845–851

Ejlerskov P, Rasmussen I, Nielsen TT, Bergström AL, Tohyama Y, Jensen PH, Vilhardt F. Tubulin polymerization-promoting protein (TPPP/p25α) promotes unconventional secretion of α-synuclein through exophagy by impairing autophagosome-lysosome fusion. J Biol Chem 2013; 288:17313–17335

El-Agnaf OMA, Salem SA, Paleologou KE, Cooper LJ, Fullwood NJ, Gibson MJ, Curran MD, Court JA, Mann DMA, Ikeda S-I, Cookson MR, Hardy J, Allsop D. A-Synuclein implicated in Parkinson's disease is present in extracellular biological fluids, including human plasma. FASEB J 2003a; 17:1–16

El-Agnaf OMA, Salem SA, Paleologou KE, Cooper LJ, Fullwood NJ, Gibson MJ, Curran MD, Court JA, Mann DMA, Ikeda S, Cookson MR, Hardy J, Allsop D. Alpha-synuclein implicated in Parkinson's disease is present in extracellular biological fluids, including human plasma. FASEB J Off Publ Fed Am Soc Exp Biol 2003b; 17:1945–1947

Emmanouilidou E, Melachroinou K, Roumeliotis T, Garbis SD, Ntzouni M, Margaritis LH, Stefanis L, Vekrellis K. Cell-produced α-synuclein is secreted in a calcium-dependent

manner by exosomes and impacts neuronal survival. J Neurosci 2010; 30:6838–6851
Emmer KL, Waxman EA, Covy JP, Giasson BI. E46K human alpha-synuclein transgenic mice develop Lewy-like and tau pathology associated with age-dependent, detrimental motor impairment. J Biol Chem 2011; 286:35104–35118
Erwig L-P, Henson PM. Immunological consequences of apoptotic cell phagocytosis. Am J Pathol 2007; 171:2–8
Faherty CJ, Kerley D, Smeyne RJ. A Golgi-Cox morphological analysis of neuronal changes induced by environmental enrichment. Brain Res Dev Brain Res 2003; 141:55–61
Faherty CJ, Raviie Shepherd K, Herasimtschuk A, Smeyne RJ. Environmental enrichment in adulthood eliminates neuronal death in experimental Parkinsonism. Brain Res Mol Brain Res 2005; 134:170–179
Fellner L, Irschick R, Schanda K, Reindl M, Klimaschewski L, Poewe W, Wenning GK, Stefanova N. Toll-like receptor 4 is required for α-synuclein dependent activation of microglia and astroglia. Glia 2013; 61:349–360
Ferreira SA, Romero-Ramos M. Microglia response during Parkinson's disease: Alpha-synuclein intervention. Front Cell Neurosci 2018; 12:1–17
Fischer A. Environmental enrichment as a method to improve cognitive function. What can we learn from animal models? Neuroimage 2016; 131:42–47
Franceschi C, Bonafè M, Valensin S, Olivieri F, De Luca M, Ottaviani E, De Benedictis G. Inflamm-aging. An evolutionary perspective on immunosenescence. Ann N Y Acad Sci 2000; 908:244–254
Franceschi C, Capri M, Monti D, Giunta S, Olivieri F, Sevini F, Panourgia MP, Invidia L, Celani L, Scurti M, Cevenini E, Castellani GC, Salvioli S. Inflammaging and anti-inflammaging: a systemic perspective on aging and longevity emerged from studies in humans. Mech Ageing Dev 2007; 128:92–105
Frost B, Diamond MI. Prion-like mechanisms in neurodegenerative diseases. Nat Rev Neurosci 2010; 11:155–159
Gao H-M, Zhang F, Zhou H, Kam W, Wilson B, Hong J-S. Neuroinflammation and α-synuclein dysfunction potentiate each other, driving chronic progression of neurodegeneration in a mouse model of Parkinson's disease. Environ Health Perspect 2011; 119:807–814
Garcia-Reitböck P, Anichtchik O, Bellucci A, Iovino M, Ballini C, Fineberg E, Ghetti B, Della Corte L, Spano P, Tofaris GK, Goedert M, Spillantini MG. SNARE protein redistribution and synaptic failure in a transgenic mouse model of Parkinson's disease. Brain 2010; 133:2032–2044
Garofalo S, D'Alessandro G, Chece G, Brau F, Maggi L, Rosa A, Porzia A, Mainiero F, Esposito V, Lauro C, Benigni G, Bernardini G, Santoni A, Limatola C. Enriched environment reduces glioma growth through immune and non-immune mechanisms in mice. Nat Commun 2015; 6:6623
Gerhard A, Pavese N, Hotton G, Turkheimer F, Es M, Hammers A, Eggert K, Oertel W, Banati RB, Brooks DJ. In vivo imaging of microglial activation with [11C](R)-PK11195 PET in idiopathic Parkinson's disease. Neurobiol Dis 2006; 21:404–412
Giasson BI, Duda JE, Murray I V, Chen Q, Souza JM, Hurtig HI, Ischiropoulos H, Trojanowski JQ, Lee VM. Oxidative damage linked to neurodegeneration by selective alpha-synuclein nitration in synucleinopathy lesions. Science 2000; 290:985–989
Giasson BI, Murray IVJ, Trojanowski JQ, Lee VMY. A Hydrophobic Stretch of 12 Amino Acid Residues in the Middle of α-Synuclein Is Essential for Filament Assembly. J Biol

Chem 2001; 276:2380–2386
Giguère N, Nanni SB, Trudeau LE. On cell loss and selective vulnerability of neuronal populations in Parkinson's disease. Front Neurol 2018; 9
Glizer D, MacDonald PA. Cognitive Training in Parkinson's Disease: A Review of Studies from 2000 to 2014. Park Dis 2016; 2016:9291713
Godbout JP, Chen J, Abraham J, Richwine AF, Berg BM, Kelley KW, Johnson RW. Exaggerated neuroinflammation and sickness behavior in aged mice following activation of the peripheral innate immune system. FASEB J Off Publ Fed Am Soc Exp Biol 2005; 19:1329–1331
Goedert M. Alpha-synuclein and neurodegenerative diseases. Nat Rev Neurosci 2001; 2:492–501
Goedert M, Spillantini MG, Del Tredici K, Braak H. 100 years of Lewy pathology. Nat Rev Neurol 2013; 9:13–24
Goldberg NRS, Haack AK, Meshul CK. Enriched environment promotes similar neuronal and behavioral recovery in a young and aged mouse model of Parkinson's disease. Neuroscience 2011; 172:443–452
Gómez-Benito M, Granado N, García-Sanz P, Michel A, Dumoulin M, Moratalla R. Modeling Parkinson's Disease With the Alpha-Synuclein Protein. Front Pharmacol 2020; 11:356
González Fleitas MF, Devouassoux JD, Aranda ML, Calanni JS, Chianelli MS, Dorfman D, Rosenstein RE. Enriched environment provides neuroprotection against experimental glaucoma. J Neurochem 2020; 152:103–121
Gordon R, Albornoz EA, Christie DC, Langley MR, Kumar V, Mantovani S, Robertson AAB, Butler MS, Rowe DB, O'Neill LA, Kanthasamy AG, Schroder K, Cooper MA, Woodruff TM. Inflammasome inhibition prevents α-synuclein pathology and dopaminergic neurodegeneration in mice. Sci Transl Med 2018; 10:eaah4066
Grabert K, Michoel T, Karavolos MH, Clohisey S, Baillie JK, Stevens MP, Freeman TC, Summers KM, McColl BW. Microglial brain region−dependent diversity and selective regional sensitivities to aging. Nat Neurosci 2016; 19:504–516
Grozdanov V, Danzer KM. Release and uptake of pathologic alpha-synuclein. Cell Tissue Res 2018; 373:175–182
Gualtieri F, Brégère C, Laws GC, Armstrong EA, Wylie NJ, Moxham TT, Guzman R, Boswell T, Smulders T V. Effects of Environmental Enrichment on Doublecortin and BDNF Expression along the Dorso-Ventral Axis of the Dentate Gyrus. Front Neurosci 2017; 11:488
Guo M, Wang J, Zhao Y, Feng Y, Han S, Dong Q, Cui M, Tieu K. Microglial exosomes facilitate α-synuclein transmission in Parkinson's disease. Brain 2020; 143:1476–1497
de Haas AH, Boddeke HWGM, Biber K. Region-specific expression of immunoregulatory proteins on microglia in the healthy CNS. Glia 2008; 56:888–894
Haehner A, Hummel T, Hummel C, Sommer U, Junghanns S, Reichmann H. Olfactory loss may be a first sign of idiopathic Parkinson's disease. Mov Disord 2007; 22:839–842
Haenseler W, Zambon F, Lee H, Vowles J, Rinaldi F, Duggal G, Houlden H, Gwinn K, Wray S, Luk KC, Wade-Martins R, James WS, Cowley SA. Excess α-synuclein compromises phagocytosis in iPSC-derived macrophages. Sci Rep 2017; 7:9003
Halliday GM, Li YW, Blumbergs PC, Joh TH, Cotton RGH, Howe PRC, Blessing WW, Geffen LB. Neuropathology of immunohistochemically identified brainstem neurons

in Parkinson’s disease. Ann Neurol 1990; 27:373–385
Hansen C, Angot E, Bergström A-L, Steiner JA, Pieri L, Paul G, Outeiro TF, Melki R, Kallunki P, Fog K, Li J-Y, Brundin P. α-Synuclein propagates from mouse brain to grafted dopaminergic neurons and seeds aggregation in cultured human cells. J Clin Invest 2011; 121:715–725
Hase Y, Craggs L, Hase M, Stevenson W, Slade J, Lopez D, Mehta R, Chen A, Liang D, Oakley A, Ihara M, Horsburgh K, Kalaria RN. Effects of environmental enrichment on white matter glial responses in a mouse model of chronic cerebral hypoperfusion. J Neuroinflammation 2017; 14:81
Helwig M, Klinkenberg M, Rusconi R, Musgrove RE, Majbour NK, El-Agnaf OMA, Ulusoy A, Di Monte DA. Brain propagation of transduced α-synuclein involves non-fibrillar protein species and is enhanced in α-synuclein null mice. Brain 2016; 139:856–870
Hely MA, Reid WGJ, Adena MA, Halliday GM, Morris JGL. The Sydney Multicenter Study of Parkinson’s disease: The inevitability of dementia at 20 years. Mov Disord 2008; 23:837–844
Herman T, Giladi N, Gruendlinger L, Hausdorff JM. Six weeks of intensive treadmill training improves gait and quality of life in patients with Parkinson’s disease: a pilot study. Arch Phys Med Rehabil 2007; 88:1154–1158
Hernandez DG, Reed X, Singleton AB. Genetics in Parkinson disease: Mendelian versus non-Mendelian inheritance. J Neurochem 2016; 139:59–74
Hickman S, Izzy S, Sen P, Morsett L, El Khoury J. Microglia in neurodegeneration. Nat Neurosci 2018; 21:1359–1369
Hicks AU, Hewlett K, Windle V, Chernenko G, Ploughman M, Jolkkonen J, Weiss S, Corbett D. Enriched environment enhances transplanted subventricular zone stem cell migration and functional recovery after stroke. Neuroscience 2007; 146:31–40
Hirsch EC, Hunot S. Neuroinflammation in Parkinson’s disease: a target for neuroprotection? Lancet Neurol 2009; 8:382–397
Hirsch L, Jette N, Frolkis A, Steeves T, Pringsheim T. The Incidence of Parkinson’s Disease: A Systematic Review and Meta-Analysis. Neuroepidemiology 2016; 46:292–300
Hoogland ICM, Houbolt C, van Westerloo DJ, van Gool WA, van de Beek D. Systemic inflammation and microglial activation: systematic review of animal experiments. J Neuroinflammation 2015; 12:114
Imamura K, Hishikawa N, Sawada M, Nagatsu T, Yoshida M, Hashizume Y. Distribution of major histocompatibility complex class II-positive microglia and cytokine profile of Parkinson’s disease brains. Acta Neuropathol 2003; 106:518–526
Iwai A, Masliah E, Yoshimoto M, Ge N, Flanagan L, Rohan de Silva HA, Kittel A, Saitoh T. The precursor protein of non-Aβ component of Alzheimer’s disease amyloid is a presynaptic protein of the central nervous system. Neuron 1995; 14:467–475
Janda E, Boi L, Carta AR. Microglial phagocytosis and its regulation: A therapeutic target in parkinson’s disease? Front Mol Neurosci 2018; 11:1–8
Jang A, Lee HJ, Suk JE, Jung JW, Kim KP, Lee SJ. Non-classical exocytosis of α-synuclein is sensitive to folding states and promoted under stress conditions. J Neurochem 2010; 113:1263–1274
Janković M, Svetel M, Kostić V. Frequency of REM sleep behavior disorders in patients with Parkinson’s disease. Vojnosanit Pregl 2015; 72:442–446
Jankowsky JL, Xu G, Fromholt D, Gonzales V, Borchelt DR. Environmental Enrichment Exacerbates Amyloid Plaque Formation in a Transgenic Mouse Model of Alzheimer

Disease. J Neuropathol Exp Neurol 2003; 62:1220–1227
Jellinger KA. A critical evaluation of current staging of α-synuclein pathology in Lewy body disorders. Biochim Biophys Acta - Mol Basis Dis 2009; 1792:730–740
Jellinger KA. Lewy body-related alpha-synucleinopathy in the aged human brain. J Neural Transm 2004; 111:1219–1235
Jha S, Dong BE, Xue Y, Delotterie DF, Vail MG, Sakata K. Antidepressive and BDNF effects of enriched environment treatment across ages in mice lacking BDNF expression through promoter IV. Transl Psychiatry 2016; 6:e896–e896
Jurga AM, Paleczna M, Kuter KZ. Overview of General and Discriminating Markers of Differential Microglia Phenotypes. Front Cell Neurosci 2020; 14:198
Kalaitzakis ME, Graeber MB, Gentleman SM, Pearce RKB. The dorsal motor nucleus of the vagus is not an obligatory trigger site of Parkinson's disease: A critical analysis of α-synuclein staging. Neuropathol Appl Neurobiol 2008; 34:284–295
Kalia L V., Kalia SK, McLean PJ, Lozano AM, Lang AE. α-synuclein oligomers and clinical implications for parkinson disease. Ann Neurol 2013; 73:155–169
Kalia L V., Lang AE. Parkinson's disease. Lancet 2015; 386:896–912
Kam T-I, Hinkle JT, Dawson TM, Dawson VL. Microglia and astrocyte dysfunction in parkinson's disease. Neurobiol Dis 2020; 144:105028
Keane L, Antignano I, Riechers S-P, Zollinger R, Dumas AA, Offermann N, Bernis ME, Russ J, Graelmann F, McCormick PN, Esser J, Tejera D, Nagano A, Wang J, Chelala C, Biederbick Y, Halle A, Salomoni P, Heneka MT, Capasso M. MTOR-dependent translation amplifies microglia priming in aging mice. J Clin Invest 2021; 131
Kempermann G. Environmental enrichment, new neurons and the neurobiology of individuality. Nat Rev Neurosci 2019; 20:235–245
Kempermann G, Gast D, Gage FH. Neuroplasticity in old age: sustained fivefold induction of hippocampal neurogenesis by long-term environmental enrichment. Ann Neurol 2002; 52:135–143
Kiechle M, von Einem B, Höfs L, Voehringer P, Grozdanov V, Markx D, Parlato R, Wiesner D, Mayer B, Sakk O, Baumann B, Lukassen S, Liss B, Ekici AB, Ludolph AC, Walther P, Ferger B, McLean PJ, Falkenburger BH, Weishaupt JH, Danzer KM. In Vivo Protein Complementation Demonstrates Presynaptic α-Synuclein Oligomerization and Age-Dependent Accumulation of 8-16-mer Oligomer Species. Cell Rep 2019; 29:2862-2874.e9
Killinger BA, Kordower JH. Spreading of alpha-synuclein – relevant or epiphenomenon? J Neurochem 2019; 150:605–611
Kim C, Ho D-H, Suk J-E, You S, Michael S, Kang J, Joong Lee S, Masliah E, Hwang D, Lee H-J, Lee S-J. Neuron-released oligomeric α-synuclein is an endogenous agonist of TLR2 for paracrine activation of microglia. Nat Commun 2013; 4:1562
Kim C, Rockenstein E, Spencer B, Kim H-K, Adame A, Trejo M, Stafa K, Lee H-J, Lee S-J, Masliah E. Antagonizing Neuronal Toll-like Receptor 2 Prevents Synucleinopathy by Activating Autophagy. Cell Rep 2015; 13:771–782
Kim KS, Choi YR, Park JY, Lee JH, Kim DK, Lee SJ, Paik SR, Jou I, Park SM. Proteolytic cleavage of extracellular α-synuclein by plasmin: Implications for Parkinson disease. J Biol Chem 2012; 287:24862–24872
Klegeris A, Pelech S, Giasson BI, Maguire J, Zhang H, McGeer EG, McGeer PL. Alpha-synuclein activates stress signaling protein kinases in THP-1 cells and microglia. Neurobiol Aging 2008; 29:739–752
Klein RL, Dayton RD, Leidenheimer NJ, Jansen K, Golde TE, Zweig RM. Efficient

neuronal gene transfer with AAV8 leads to neurotoxic levels of tau or green fluorescent proteins. Mol Ther 2006; 13:517–527

Koprich JB, Johnston TH, Huot P, Reyes MG, Espinosa M, Brotchie JM. Progressive neurodegeneration or endogenous compensation in an animal model of Parkinson's disease produced by decreasing doses of alpha-synuclein. PLoS One 2011; 6:e17698

Koprich JB, Johnston TH, Reyes MG, Sun X, Brotchie JM. Expression of human A53T alpha-synuclein in the rat substantia nigra using a novel AAV1/2 vector produces a rapidly evolving pathology with protein aggregation, dystrophic neurite architecture and nigrostriatal degeneration with potential to model the pa. Mol Neurodegener 2010; 5:43

Kordower JH, Dodiya HB, Kordower AM, Terpstra B, Paumier K, Madhavan L, Sortwell C, Steece-Collier K, Collier TJ. Transfer of host-derived alpha synuclein to grafted dopaminergic neurons in rat. Neurobiol Dis 2011; 43:552–557

Kordower JH, Olanow CW, Dodiya HB, Chu Y, Beach TG, Adler CH, Halliday GM, Bartus RT. Disease duration and the integrity of the nigrostriatal system in Parkinson's disease. Brain 2013; 136:2419–2431

Kovesdi E, Gyorgy AB, Kwon S-KC, Wingo DL, Kamnaksh A, Long JB, Kasper CE, Agoston D V. The effect of enriched environment on the outcome of traumatic brain injury; a behavioral, proteomics, and histological study. Front Neurosci 2011; 5:42

Kowal SL, Dall TM, Chakrabarti R, Storm M V, Jain A. The current and projected economic burden of Parkinson's disease in the United States. Mov Disord 2013; 28:311–318

Kraemmer J, Kovacs GG, Perju-Dumbrava L, Pirker S, Traub-Weidinger T, Pirker W. Correlation of striatal dopamine transporter imaging with post mortem substantia nigra cell counts. Mov Disord 2014; 29:1767–1773

Kronenberg G, Wang L-P, Geraerts M, Babu H, Synowitz M, Vicens P, Lutsch G, Glass R, Yamaguchi M, Baekelandt V, Debyser Z, Kettenmann H, Kempermann G. Local origin and activity-dependent generation of nestin-expressing protoplasmic astrocytes in CA1. Brain Struct Funct 2007; 212:19–35

Krüger R, Kuhn W, Müller T, Woitalla D, Graeber M, Kösel S, Przuntek H, Epplen JT, Schöls L, Riess O. Ala30Pro mutation in the gene encoding alpha-synuclein in Parkinson's disease. Nat Genet 1998; 18:106–108

Kwon S, Iba M, Masliah E, Kim C. Targeting Microglial and Neuronal Toll-like Receptor 2 in Synucleinopathies. Exp Neurobiol 2019; 28:547–553

Lahiani-Cohen I, Lourbopoulos A, Haber E, Rozenstein-Tsalkovich L, Abramsky O, Grigoriadis N, Rosenmann H. Moderate environmental enrichment mitigates tauopathy in a neurofibrillary tangle mouse model. J Neuropathol Exp Neurol 2011; 70:610–621

Landeck N, Buck K, Kirik D. Toxic effects of human and rodent variants of alpha-synuclein in vivo. Eur J Neurosci 2017; 45:536–547

Lashuel HA, Overk CR, Oueslati A, Masliah E. The many faces of α-synuclein: From structure and toxicity to therapeutic target. Nat Rev Neurosci 2013; 14:38–48

Lashuel HA, Petre BM, Wall J, Simon M, Nowak RJ, Walz T, Lansbury PT. A-Synuclein, Especially the Parkinson'S Disease-Associated Mutants, Forms Pore-Like Annular and Tubular Protofibrils. J Mol Biol 2002; 322:1089–1102

de Lau LML, Breteler MMB. Epidemiology of Parkinson's disease. Lancet Neurol 2006; 5:525–535

Lavedan C. The synuclein family. Genome Res 1998; 8:871–880

Lazarov O, Robinson J, Tang Y-P, Hairston IS, Korade-Mirnics Z, Lee VM-Y, Hersh LB, Sapolsky RM, Mirnics K, Sisodia SS. Environmental enrichment reduces Abeta levels and amyloid deposition in transgenic mice. Cell 2005; 120:701–713

Lee H-J, Khoshaghideh F, Patel S, Lee S-J. Clearance of alpha-synuclein oligomeric intermediates via the lysosomal degradation pathway. J Neurosci 2004; 24:1888–1896

Lee H-J, Suk J-E, Bae E-J, Lee J-H, Paik SR, Lee S-J. Assembly-dependent endocytosis and clearance of extracellular alpha-synuclein. Int J Biochem Cell Biol 2008a; 40:1835–1849

Lee HJ, Patel S, Lee SJ. Intravesicular localization and exocytosis of α-synuclein and its aggregates. J Neurosci 2005; 25:6016–6024

Lee HJ, Suk JE, Bae EJ, Lee SJ. Clearance and deposition of extracellular α-synuclein aggregates in microglia. Biochem Biophys Res Commun 2008b; 372:423–428

Leggio MG, Mandolesi L, Federico F, Spirito F, Ricci B, Gelfo F, Petrosini L. Environmental enrichment promotes improved spatial abilities and enhanced dendritic growth in the rat. Behav Brain Res 2005; 163:78–90

Letiembre M, Hao W, Liu Y, Walter S, Mihaljevic I, Rivest S, Hartmann T, Fassbender K. Innate immune receptor expression in normal brain aging. Neuroscience 2007; 146:248–254

Leung IHK, Walton CC, Hallock H, Lewis SJG, Valenzuela M, Lampit A. Cognitive training in Parkinson disease: A systematic review and meta-analysis. Neurology 2015; 85:1843–1851

Lewy F. Paralysis agitans. I. Pathologische Anatomie. In: Lewandowsky M, Abelsdorff G. eds. Handbuch der Neurologie. Springer Verlag, 1912: 920-930

Li JY, Englund E, Holton JL, Soulet D, Hagell P, Lees AJ, Lashley T, Quinn NP, Rehncrona S, Björklund A, Widner H, Revesz T, Lindvall O, Brundin P. Lewy bodies in grafted neurons in subjects with Parkinson's disease suggest host-to-graft disease propagation. Nat Med 2008; 14:501–503

Li Q, Cheng Z, Zhou L, Darmanis S, Neff NF, Okamoto J, Gulati G, Bennett ML, Sun LO, Clarke LE, Marschallinger J, Yu G, Quake SR, Wyss-Coray T, Barres BA. Developmental Heterogeneity of Microglia and Brain Myeloid Cells Revealed by Deep Single-Cell RNA Sequencing. Neuron 2019; 101:207-223.e10

Li W, Lesuisse C, Xu Y, Troncoso JC, Price DL, Lee MK. Stabilization of alpha-synuclein protein with aging and familial parkinson's disease-linked A53T mutation. J Neurosci 2004; 24:7400–7409

Li X, Patel JC, Wang J, Avshalumov M V, Nicholson C, Buxbaum JD, Elder GA, Rice ME, Yue Z. Enhanced striatal dopamine transmission and motor performance with LRRK2 overexpression in mice is eliminated by familial Parkinson's disease mutation G2019S. J Neurosci 2010; 30:1788–1797

Li Y, Liu W, Oo TF, Wang L, Tang Y, Jackson-Lewis V, Zhou C, Geghman K, Bogdanov M, Przedborski S, Beal MF, Burke RE, Li C. Mutant LRRK2R1441G BAC transgenic mice recapitulate cardinal features of Parkinson's disease. Nat Neurosci 2009; 12:826–828

Llorens F, Schmitz M, Varges D, Kruse N, Gotzmann N, Gmitterová K, Mollenhauer B, Zerr I. Cerebrospinal α-synuclein in α-synuclein aggregation disorders: tau/α-synuclein ratio as potential biomarker for dementia with Lewy bodies. J Neurol 2016; 263:2271–2277

Logroscino G, Sesso HD, Paffenbarger RSJ, Lee I-M. Physical activity and risk of

Parkinson’s disease: a prospective cohort study. J Neurol Neurosurg Psychiatry 2006; 77:1318–1322

López-Otín C, Blasco MA, Partridge L, Serrano M, Kroemer G. The Hallmarks of Aging. Cell 2013; 153:1194–1217

Luk KC, Kehm VM, Zhang B, O’Brien P, Trojanowski JQ, Lee VMY. Intracerebral inoculation of pathological α-synuclein initiates a rapidly progressive neurodegenerative α-synucleinopathy in mice. J Exp Med 2012; 209:975–986

Ma SY, Röytt M, Collan Y, Rinne JO. Unbiased morphometrical measurements show loss of pigmented nigral neurones with ageing. Neuropathol Appl Neurobiol 1999; 25:394–399

Mao X, Ou MT, Karuppagounder SS, Kam T-I, Yin X, Xiong Y, Ge P, Umanah GE, Brahmachari S, Shin J-H, Kang HC, Zhang J, Xu J, Chen R, Park H, Andrabi SA, Kang SU, Gonçalves RA, Liang Y, Zhang S, Qi C, Lam S, Keiler JA, Tyson J, Kim D, Panicker N, Yun SP, Workman CJ, Vignali DAA, Dawson VL, Ko HS, Dawson TM. Pathological α-synuclein transmission initiated by binding lymphocyte-activation gene 3. Science 2016; 353

Marín-Teva JL, Cuadros MA, Martín-Oliva D, Navascués J. Microglia and neuronal cell death. Neuron Glia Biol 2011; 7:25–40

Maroteaux L, Scheller RH. The rat brain synucleins; family of proteins transiently associated with neuronal membrane. Brain Res Mol Brain Res 1991; 11:335–343

Marras C, Canning CG, Goldman SM. Environment, lifestyle, and Parkinson’s disease: Implications for prevention in the next decade. Mov Disord 2019; 34:801–811

Martí MJ, Tolosa E, Campdelacreu J. Clinical overview of the synucleinopathies. Mov Disord 2003; 6:21-27

Martin LJ, Pan Y, Price AC, Sterling W, Copeland NG, Jenkins NA, Price DL, Lee MK. Parkinson’s disease alpha-synuclein transgenic mice develop neuronal mitochondrial degeneration and cell death. J Neurosci 2006; 26:41–50

Martinez-Vicente M, Talloczy Z, Kaushik S, Massey AC, Mazzulli J, Mosharov E V, Hodara R, Fredenburg R, Wu D-C, Follenzi A, Dauer W, Przedborski S, Ischiropoulos H, Lansbury PT, Sulzer D, Cuervo AM. Dopamine-modified alpha-synuclein blocks chaperone-mediated autophagy. J Clin Invest 2008; 118:777–788

Masliah E, Rockenstein E, Veinbergs I, Mallory M, Hashimoto M, Takeda A, Sagara Y, Sisk A, Mucke L. Dopaminergic Loss and Inclusion Body Formation in α-Synuclein Mice: Implications for Neurodegenerative Disorders. Science 2000; 287:1265–1269

Masuda T, Sankowski R, Staszewski O, Böttcher C, Amann L, Sagar, Scheiwe C, Nessler S, Kunz P, van Loo G, Coenen VA, Reinacher PC, Michel A, Sure U, Gold R, Grün D, Priller J, Stadelmann C, Prinz M. Spatial and temporal heterogeneity of mouse and human microglia at single-cell resolution. Nature 2019; 566:388–392

Mazzulli JR, Zunke F, Isacson O, Studer L, Krainc D. α-Synuclein-induced lysosomal dysfunction occurs through disruptions in protein trafficking in human midbrain synucleinopathy models. Proc Natl Acad Sci U S A 2016; 113:1931–1936

McGeer PL, Itagaki S, Boyes BE, McGeer EG. Reactive microglia are positive for HLA-DR in the substantia nigra of Parkinson’s and Alzheimer’s disease brains. Neurology 1988; 38:1285–1291

McMurphy T, Huang W, Queen NJ, Ali S, Widstrom KJ, Liu X, Xiao R, Siu JJ, Cao L. Implementation of environmental enrichment after middle age promotes healthy aging. Aging (Albany NY) 2018; 10:1698–1721

Michell-Robinson MA, Touil H, Healy LM, Owen DR, Durafourt BA, Bar-Or A, Antel JP,

Moore CS. Roles of microglia in brain development, tissue maintenance and repair. Brain 2015; 138:1138–1159

Milber JM, Noorigian J V, Morley JF, Petrovitch H, White L, Ross GW, Duda JE. Lewy pathology is not the first sign of degeneration in vulnerable neurons in Parkinson disease. Neurology 2012; 79:2307–2314

Murphy DD, Rueter SM, Trojanowski JQ, Lee VM. Synucleins are developmentally expressed, and alpha-synuclein regulates the size of the presynaptic vesicular pool in primary hippocampal neurons. J Neurosci 2000; 20:3214–3220

Musgrove RE, Helwig M, Bae E-J, Aboutalebi H, Lee S-J, Ulusoy A, Di Monte DA. Oxidative stress in vagal neurons promotes parkinsonian pathology and intercellular α-synuclein transfer. J Clin Invest 2019; 129:3738–3753

Nakai M, Fujita M, Waragai M, Sugama S, Wei J, Akatsu H, Ohtaka-Maruyama C, Okado H, Hashimoto M. Expression of α-synuclein, a presynaptic protein implicated in Parkinson's disease, in erythropoietic lineage. Biochem Biophys Res Commun 2007; 358:104–110

Nakamura K, Nemani VM, Azarbal F, Skibinski G, Levy JM, Egami K, Munishkina L, Zhang J, Gardner B, Wakabayashi J, Sesaki H, Cheng Y, Finkbeiner S, Nussbaum RL, Masliah E, Edwards RH. Direct membrane association drives mitochondrial fission by the Parkinson disease-associated protein alpha-synuclein. J Biol Chem 2011; 286:20710–20726

Napoli I, Neumann H. Microglial clearance function in health and disease. Neuroscience 2009; 158:1030–1038

Nemani VM, Lu W, Berge V, Nakamura K, Onoa B, Lee MK, Chaudhry FA, Nicoll RA, Edwards RH. Increased expression of alpha-synuclein reduces neurotransmitter release by inhibiting synaptic vesicle reclustering after endocytosis. Neuron 2010; 65:66–79

Neumann M, Kahle PJ, Giasson BI, Ozmen L, Borroni E, Spooren W, Müller V, Odoy S, Fujiwara H, Hasegawa M, Iwatsubo T, Trojanowski JQ, Kretzschmar HA, Haass C. Misfolded proteinase K-resistant hyperphosphorylated alpha-synuclein in aged transgenic mice with locomotor deterioration and in human alpha-synucleinopathies. J Clin Invest 2002; 110:1429–1439

Nimmerjahn A, Kirchhoff F, Helmchen F. Resting microglial cells are highly dynamic surveillants of brain parenchyma in vivo. Science 2005; 308:1314–1318

Nithianantharajah J, Hannan AJ. Enriched environments, experience-dependent plasticity and disorders of the nervous system. Nat Rev Neurosci 2006; 7:697–709

Njie EG, Boelen E, Stassen FR, Steinbusch HWM, Borchelt DR, Streit WJ. Ex vivo cultures of microglia from young and aged rodent brain reveal age-related changes in microglial function. Neurobiol Aging 2012; 33:195.e1–12

Oguh O, Eisenstein A, Kwasny M, Simuni T. Back to the basics: regular exercise matters in parkinson's disease: results from the National Parkinson Foundation QII registry study. Parkinsonism Relat Disord 2014; 20:1221–1225

Ogura K, Ogawa M, Yoshida M. Effects of ageing on microglia in the normal rat brain: immunohistochemical observations. Neuroreport 1994; 5:1224–1226

Ohsawa K, Imai Y, Kanazawa H, Sasaki Y, Kohsaka S. Involvement of Iba1 in membrane ruffling and phagocytosis of macrophages/microglia. J Cell Sci 2000; 113:3073–3084

Oliveras-Salvá M, Van der Perren A, Casadei N, Stroobants S, Nuber S, D'Hooge R, Van den Haute C, Baekelandt V. RAAV2/7 vector-mediated overexpression of alpha-synuclein in mouse substantia nigra induces protein aggregation and progressive

dose-dependent neurodegeneration. Mol Neurodegener 2013; 8:44

Orit M-N, R. WD, Amir G, Stephanie VA, Amit S, Sandrine S, Hila B-Y, Eyal D, Fabiola ZG, Pierre P, Hadas K-S, Meital G, David L-A, A. TC, Merav C, Keren BH, Kuti B, Aleksandra D, Erika L-V, Shalev I, Eran E, H. SM, Michal S, Ido A. Microglia development follows a stepwise program to regulate brain homeostasis. Science 2016; 353:aad8670

Ortinski PI, Dong J, Mungenast A, Yue C, Takano H, Watson DJ, Haydon PG, Coulter DA. Selective induction of astrocytic gliosis generates deficits in neuronal inhibition. Nat Neurosci 2010; 13:584–591

Outeiro TF, Lindquist S. Yeast cells provide insight into alpha-synuclein biology and pathobiology. Science 2003; 302:1772–1775

Paiva I, Jain G, Lázaro DF, Jerčić KG, Hentrich T, Kerimoglu C, Pinho R, Szegő ÈM, Burkhardt S, Capece V, Halder R, Islam R, Xylaki M, Caldi Gomes LA, Roser A-E, Lingor P, Schulze-Hentrich JM, Borovečki F, Fischer A, Outeiro TF. Alpha-synuclein deregulates the expression of COL4A2 and impairs ER-Golgi function. Neurobiol Dis 2018; 119:121–135

Pang SY-Y, Ho PW-L, Liu H-F, Leung C-T, Li L, Chang EES, Ramsden DB, Ho S-L. The interplay of aging, genetics and environmental factors in the pathogenesis of Parkinson's disease. Transl Neurodegener 2019; 8:23

Parkinson J. An essay on the shaking palsy. 1817. J Neuropsychiatry Clin Neurosci 2002; 14:223–36

Patterson SL. Immune dysregulation and cognitive vulnerability in the aging brain: Interactions of microglia, IL-1β, BDNF and synaptic plasticity. Neuropharmacology 2015; 96:11–18

Paul KC, Chuang Y-H, Shih I-F, Keener A, Bordelon Y, Bronstein JM, Ritz B. The association between lifestyle factors and Parkinson's disease progression and mortality. Mov Disord 2019; 34:58–66

Peelaerts W, Bousset L, Van der Perren A, Moskalyuk A, Pulizzi R, Giugliano M, Van den Haute C, Melki R, Baekelandt V. α-Synuclein strains cause distinct synucleinopathies after local and systemic administration. Nature 2015; 522:340–344

Perry VH, Holmes C. Microglial priming in neurodegenerative disease. Nat Rev Neurol 2014; 10:217–224

Pieri L, Madiona K, Bousset L, Melki R. Fibrillar α-synuclein and huntingtin exon 1 assemblies are toxic to the cells. Biophys J 2012; 102:2894–2905

Polymeropoulos MH, Lavedan C, Leroy E, Ide SE, Dehejia A, Dutra A, Pike B, Root H, Rubenstein J, Boyer R, Stenroos ES, Chandrasekharappa S, Athanassiadou A, Papapetropoulos T, Johnson WG, Lazzarini AM, Duvoisin RC, Di Iorio G, Golbe LI, Nussbaum RL. Mutation in the α-synuclein gene identified in families with Parkinson's disease. Science 1997; 276:2045–2047

Postuma RB, Berg D, Stern M, Poewe W, Olanow CW, Oertel W, Obeso J, Marek K, Litvan I, Lang AE, Halliday G, Goetz CG, Gasser T, Dubois B, Chan P, Bloem BR, Adler CH, Deuschl G. MDS clinical diagnostic criteria for Parkinson's disease. Mov Disord 2015; 30:1591–1601

van Praag H, Kempermann G, Gage FH. Neural consequences of environmental enrichment. Nat Rev Neurosci 2000; 1:191–198

Pringsheim T, Jette N, Frolkis A, Steeves TDL. The prevalence of Parkinson's disease: A systematic review and meta-analysis. Mov Disord 2014; 29:1583–1590

Proukakis C, Dudzik CG, Brier T, MacKay DS, Cooper JM, Millhauser GL, Houlden H,

Schapira AH. A novel α-synuclein missense mutation in Parkinson disease. Neurology 2013; 80:1062–1064

Quattromani MJ, Cordeau P, Ruscher K, Kriz J, Wieloch T. Enriched housing down-regulates the Toll-like receptor 2 response in the mouse brain after experimental stroke. Neurobiol Dis 2014; 66:66–73

Ragu Varman D, Rajan KE. Environmental Enrichment Reduces Anxiety by Differentially Activating Serotonergic and Neuropeptide Y (NPY)-Ergic System in Indian Field Mouse (Mus booduga): An Animal Model of Post-Traumatic Stress Disorder. PLoS One 2015; 10:e0127945

Rampon C, Jiang CH, Dong H, Tang Y-P, Lockhart DJ, Schultz PG, Tsien JZ, Hu Y. Effects of environmental enrichment on gene expression in the brain. Proc Natl Acad Sci 2000; 97:12880 LP – 12884

Ransohoff RM. How neuroinflammation contributes to neurodegeneration. Science 2016; 353:777–783

Ransohoff RM, El Khoury J. Microglia in Health and Disease. Cold Spring Harb Perspect Biol 2015; 8:a020560–a020560

Rawji KS, Mishra MK, Michaels NJ, Rivest S, Stys PK, Yong VW. Immunosenescence of microglia and macrophages: impact on the ageing central nervous system. Brain 2016; 139:653–661

Recasens A, Dehay B, Bové J, Carballo-Carbajal I, Dovero S, Pérez-Villalba A, Fernagut P-O, Blesa J, Parent A, Perier C, Fariñas I, Obeso JA, Bezard E, Vila M. Lewy body extracts from Parkinson disease brains trigger α-synuclein pathology and neurodegeneration in mice and monkeys. Ann Neurol 2014a; 75:351–362

Recasens A, Dehay B, Bové J, Carballo-Carbajal I, Dovero S, Pérez-Villalba A, Fernagut PO, Blesa J, Parent A, Perier C, Fariñas I, Obeso JA, Bezard E, Vila M. Lewy body extracts from Parkinson disease brains trigger α-synuclein pathology and neurodegeneration in mice and monkeys. Ann Neurol 2014b; 75:351–362

Reijnders JSAM, Ehrt U, Weber WE, Aarsland D, Leentjens AF. A systematic review of prevalence studies of depression in Parkinson's disease. Mov Disord 2008; 23:183–189

Reyes JF, Olsson TT, Lamberts JT, Devine MJ, Kunath T, Brundin P. A cell culture model for monitoring α-synuclein cell-to-cell transfer. Neurobiol Dis 2015; 77:266–275

Richfield EK, Thiruchelvam MJ, Cory-Slechta DA, Wuertzer C, Gainetdinov RR, Caron MG, Di Monte DA, Federoff HJ. Behavioral and neurochemical effects of wild-type and mutated human alpha-synuclein in transgenic mice. Exp Neurol 2002; 175:35–48

Riew T-R, Kim S, Jin X, Kim HL, Lee J-H, Lee M-Y. Osteopontin and its spatiotemporal relationship with glial cells in the striatum of rats treated with mitochondrial toxin 3-nitropropionic acid: possible involvement in phagocytosis. J Neuroinflammation 2019; 16:99

Rizek P, Kumar N, Jog MS. An update on the diagnosis and treatment of Parkinson disease. CMAJ 2016; 188:1157–1165

Rocha NP, De Miranda AS, Teixeira AL. Insights into neuroinflammation in Parkinson's disease: From biomarkers to anti-inflammatory based therapies. Biomed Res Int 2015; 2015

Rochet JC, Conway KA, Lansbury PT. Inhibition of fibrillization and accumulation of prefibrillar oligomers in mixtures of human and mouse α-synuclein. Biochemistry 2000; 39:10619–10626

Rodriguez JA, Ivanova MI, Sawaya MR, Cascio D, Reyes FE, Shi D, Sangwan S, Guenther EL, Johnson LM, Zhang M, Jiang L, Arbing MA, Nannenga BL, Hattne J, Whitelegge J, Brewster AS, Messerschmidt M, Boutet S, Sauter NK, Gonen T, Eisenberg DS. Structure of the toxic core of α-synuclein from invisible crystals. Nature 2015; 525:486–490

van Rooijen BD, Claessens MMAE, Subramaniam V. Membrane permeabilization by oligomeric α-synuclein: In search of the mechanism. PLoS One 2010; 5

Royo NC, Vandenberghe LH, Ma J-Y, Hauspurg A, Yu L, Maronski M, Johnston J, Dichter MA, Wilson JM, Watson DJ. Specific AAV serotypes stably transduce primary hippocampal and cortical cultures with high efficiency and low toxicity. Brain Res 2008; 1190:15–22

Rusconi R, Ulusoy A, Aboutalebi H, Di Monte DA. Long-lasting pathological consequences of overexpression-induced α-synuclein spreading in the rat brain. Aging Cell 2018; 17

Sasaki Y, Ohsawa K, Kanazawa H, Kohsaka S, Imai Y. Iba1 is an actin-cross-linking protein in macrophages/microglia. Biochem Biophys Res Commun 2001; 286:292–297

Scheiblich H, Dansokho C, Mercan D, Schmidt S V, Bousset L, Wischhof L, Eikens F, Odainic A, Spitzer J, Griep A, Schwartz S, Bano D, Latz E, Melki R, Heneka MT. Microglia jointly degrade fibrillar alpha-synuclein cargo by distribution through tunneling nanotubes. Cell 2021; 184:5089-5106.e21

Schrag A, Horsfall L, Walters K, Noyce A, Petersen I. Prediagnostic presentations of Parkinson's disease in primary care: A case-control study. Lancet Neurol 2015; 14:57–64

Scott D, Roy S. α-Synuclein inhibits intersynaptic vesicle mobility and maintains recycling-pool homeostasis. J Neurosci 2012; 32:10129–10135

Sedelis M, Schwarting RK, Huston JP. Behavioral phenotyping of the MPTP mouse model of Parkinson's disease. Behav Brain Res 2001; 125:109–125

Selvaraj S, Piramanayagam S. Impact of gene mutation in the development of Parkinson's disease. Genes Dis 2019; 6:120–128

Shahmoradian SH, Lewis AJ, Genoud C, Hench J, Moors TE, Navarro PP, Castaño-Díez D, Schweighauser G, Graff-Meyer A, Goldie KN, Sütterlin R, Huisman E, Ingrassia A, Gier Y de, Rozemuller AJM, Wang J, Paepe A De, Erny J, Staempfli A, Hoernschemeyer J, Großerüschkamp F, Niedieker D, El-Mashtoly SF, Quadri M, Van IJcken WFJ, Bonifati V, Gerwert K, Bohrmann B, Frank S, Britschgi M, Stahlberg H, Van de Berg WDJ, Lauer ME. Lewy pathology in Parkinson's disease consists of crowded organelles and lipid membranes. Nat Neurosci 2019; 22:1099–1109

Sharma K, Schmitt S, Bergner CG, Tyanova S, Kannaiyan N, Manrique-Hoyos N, Kongi K, Cantuti L, Hanisch U-K, Philips M-A, Rossner MJ, Mann M, Simons M. Cell type–and brain region–resolved mouse brain proteome. Nat Neurosci 2015; 18:1819–1831

Shin Y-J, Lim Kim H, Choi J-S, Choi J-Y, Cha J-H, Lee M-Y. Osteopontin: Correlation with phagocytosis by brain macrophages in a rat model of stroke. Glia 2011; 59:413–423

Shrivastava AN, Redeker V, Fritz N, Pieri L, Almeida LG, Spolidoro M, Liebmann T, Bousset L, Renner M, Léna C, Aperia A, Melki R, Triller A. α-synuclein assemblies sequester neuronal α3-Na+/K+-ATPase and impair Na+ gradient. EMBO J 2015; 34:2408–2423

Singhal G, Jaehne EJ, Corrigan F, Baune BT. Cellular and molecular mechanisms of immunomodulation in the brain through environmental enrichment. Front Cell

Neurosci 2014; 8:97
Singleton AB, Farrer M, Johnson J, Singleton A, Hague S, Kachergus J, Hulihan M, Peuralinna T, Dutra A, Nussbaum R, Lincoln S, Crawley A, Hanson M, Maraganore D, Adler C, Cookson MR, Muenter M, Baptista M, Miller D, Blancato J, Hardy J, Gwinn-Hardy K. α-Synuclein Locus Triplication Causes Parkinson's Disease. Science 2003; 302:841
Sirevaag AM, Greenough WT. Differential rearing effects on rat visual cortex synapses. III. Neuronal and glial nuclei, boutons, dendrites, and capillaries. Brain Res 1987; 424:320–332
Spillantini MG, Crowther RA, Jakes R, Cairns NJ, Lantos PL, Goedert M. Filamentous alpha-synuclein inclusions link multiple system atrophy with Parkinson's disease and dementia with Lewy bodies. Neurosci Lett 1998; 251:205–208
Spillantini MG, Schmidt ML, Lee VM-Y, Trojanowski JQ, Jakes R, Goedert M. α-Synuclein in Lewy bodies. Nature 1997; 388:839–840
Steiner B, Winter C, Hosman K, Siebert E, Kempermann G, Petrus DS, Kupsch A. Enriched environment induces cellular plasticity in the adult substantia nigra and improves motor behavior function in the 6-OHDA rat model of Parkinson's disease. Exp Neurol 2006; 199:291–300
Stirpe P, Hoffman M, Badiali D, Colosimo C. Constipation: an emerging risk factor for Parkinson's disease? Eur J Neurol 2016; 23:1606–1613
Stöckl MT, Zijlstra N, Subramaniam V. α-Synuclein oligomers: an amyloid pore? Insights into mechanisms of α-synuclein oligomer-lipid interactions. Mol Neurobiol 2013; 47:613–621
Stratoulias V, Venero JL, Tremblay M-È, Joseph B. Microglial subtypes: diversity within the microglial community. EMBO J 2019; 38:e101997
Stuart KE, King AE, King NE, Collins JM, Vickers JC, Ziebell JM. Late-life environmental enrichment preserves short-term memory and may attenuate microglia in male APP/PS1 mice. Neuroscience 2019; 408:282–292
Su X, Federoff HJ, Maguire-Zeiss KA. Mutant alpha-synuclein overexpression mediates early proinflammatory activity. Neurotox Res 2009; 16:238–254
Su X, Maguire-Zeiss KA, Giuliano R, Prifti L, Venkatesh K, Federoff HJ. Synuclein activates microglia in a model of Parkinson's disease. Neurobiol Aging 2008; 29:1690–1701
Sung JY, Kim J, Paik SR, Park JH, Ahn YS, Chung KC. Induction of neuronal cell death by Rab5A-dependent endocytosis of alpha-synuclein. J Biol Chem 2001; 276:27441–27448
Surmeier DJ, Obeso JA, Halliday GM. Parkinson's Disease Is Not Simply a Prion Disorder. J Neurosci 2017a; 37:9799 LP – 9807
Surmeier DJ, Obeso JA, Halliday GM. Selective neuronal vulnerability in Parkinson disease. Nat Rev Neurosci 2017b; 18:101–113
Susanne W, E. BR, Louis D, B. RA, Miwei H, Danny M, J. KM, Julia S, Nahel T, C. AA, Zhanyun F, Samantha N, Eloise H, T. HB. Experimental evidence for the age dependence of tau protein spread in the brain. Sci Adv 2021; 5:eaaw6404
Sveinbjornsdottir S. The clinical symptoms of Parkinson's disease. J Neurochem 2016;318–324
Svensson E, Henderson VW, Borghammer P, Horváth-Puhó E, Sørensen HT. Constipation and risk of Parkinson's disease: A Danish population-based cohort study. Parkinsonism Relat Disord 2016; 28:18–22

Tanik SA, Schultheiss CE, Volpicelli-Daley LA, Brunden KR, Lee VMY. Lewy body-like α-synuclein aggregates resist degradation and impair macroautophagy. J Biol Chem 2013; 288:15194–15210

Tanriöver G, Bacioglu M, Schweighauser M, Mahler J, Wegenast-Braun BM, Skodras A, Obermüller U, Barth M, Kronenberg-Versteeg D, Nilsson KPR, Shimshek DR, Kahle PJ, Eisele YS, Jucker M. Prominent microglial inclusions in transgenic mouse models of α-synucleinopathy that are distinct from neuronal lesions. Acta Neuropathol Commun 2020; 8:133

Theodore S, Cao S, McLean PJ, Standaert DG. Targeted overexpression of human alpha-synuclein triggers microglial activation and an adaptive immune response in a mouse model of Parkinson disease. J Neuropathol Exp Neurol 2008; 67:1149–1158

Tremblay M-È, Zettel ML, Ison JR, Allen PD, Majewska AK. Effects of aging and sensory loss on glial cells in mouse visual and auditory cortices. Glia 2012; 60:541–558

Tremblay ME, Cookson MR, Civiero L. Glial phagocytic clearance in Parkinson's disease. Mol Neurodegener 2019; 14:1–14

Ueda K, Fukushima H, Masliah E, Xia Y, Iwai A, Yoshimoto M, Otero DAC, Kondo J, Ihara Y, Saitoh T. Molecular cloning of cDNA encoding an unrecognized component of amyloid in Alzheimer disease. Proc Natl Acad Sci U S A 1993; 90:11282–11286

Ulmer TS, Bax A, Cole NB, Nussbaum RL. Structure and dynamics of micelle-bound human α-synuclein. J Biol Chem 2005; 280:9595–9603

Ulusoy A, Decressac M, Kirik D, Björklund A. Viral vector-mediated overexpression of α-synuclein as a progressive model of Parkinson's disease. Prog Brain Res 2010; 184:89–111

Ulusoy A, Musgrove RE, Rusconi R, Klinkenberg M, Helwig M, Schneider A, Di Monte DA. Neuron-to-neuron α-synuclein propagation in vivo is independent of neuronal injury. Acta Neuropathol Commun 2015; 3:13

Ulusoy A, Rusconi R, Pérez-Revuelta BI, Musgrove RE, Helwig M, Winzen-Reichert B, Monte DA Di. Caudo-rostral brain spreading of α-synuclein through vagal connections. EMBO Mol Med 2013; 5:1119–1127

Ungerstedt U, Ljungberg T, Steg G. Behavioral, physiological, and neurochemical changes after 6-hydroxydopamine-induced degeneration of the nigro-striatal dopamine neurons. Adv Neurol 1974; 5:421–426

Varkey J, Isas JM, Mizuno N, Jensen MB, Bhatia VK, Jao CC, Petrlova J, Voss JC, Stamou DG, Steven AC, Langen R. Membrane curvature induction and tubulation are common features of synucleins and apolipoproteins. J Biol Chem 2010; 285:32486–32493

Végh MJ, Rausell A, Loos M, Heldring CM, Jurkowski W, van Nierop P, Paliukhovich I, Li KW, del Sol A, Smit AB, Spijker S, van Kesteren RE. Hippocampal extracellular matrix levels and stochasticity in synaptic protein expression increase with age and are associated with age-dependent cognitive decline. Mol Cell Proteomics 2014; 13:2975–2985

Verstraeten A, Theuns J, Van Broeckhoven C. Progress in unraveling the genetic etiology of Parkinson disease in a genomic era. Trends Genet 2015; 31:140–149

Villar-Piqué A, Lopes da Fonseca T, Outeiro TF. Structure, function and toxicity of alpha-synuclein: the Bermuda triangle in synucleinopathies. J Neurochem 2016; 139:240–255

Volles MJ, Lansbury PTJ. Vesicle permeabilization by protofibrillar alpha-synuclein is sensitive to Parkinson's disease-linked mutations and occurs by a pore-like

mechanism. Biochemistry 2002; 41:4595–4602
Wakabayashi K, Matsumoto K, Takayama K, Yoshimoto M, Takahashi H. NACP, a presynaptic protein, immunoreactivity in Lewy bodies in Parkinson's disease. Neurosci Lett 1997; 239:45–48
Wakabayashi K, Tanji K, Odagiri S, Miki Y, Mori F, Takahashi H. The Lewy body in Parkinson's disease and related neurodegenerative disorders. Mol Neurobiol 2013; 47:495–508
Walsh DM, Selkoe DJ. A critical appraisal of the pathogenic protein spread hypothesis of neurodegeneration. Nat Rev Neurosci 2016; 17:251–260
Wang L, Das U, Scott DA, Tang Y, McLean PJ, Roy S. α-synuclein multimers cluster synaptic vesicles and attenuate recycling. Curr Biol 2014; 24:2319–2326
Wang Q, Liu Y, Zhou J. Neuroinflammation in Parkinson's disease and its potential as therapeutic target. Transl Neurodegener 2015; 4:19
Wassouf Z, Hentrich T, Samer S, Rotermund C, Kahle PJ, Ehrlich I, Riess O, Casadei N, Schulze-Hentrich JM. Environmental Enrichment Prevents Transcriptional Disturbances Induced by Alpha-Synuclein Overexpression. Front Cell Neurosci 2018; 12:112
Wassouf Z, Schulze-Hentrich JM. Alpha-synuclein at the nexus of genes and environment: the impact of environmental enrichment and stress on brain health and disease. J Neurochem 2019; 150:591–604
Watson MB, Richter F, Lee SK, Gabby L, Wu J, Masliah E, Effros RB, Chesselet M-F. Regionally-specific microglial activation in young mice over-expressing human wildtype alpha-synuclein. Exp Neurol 2012; 237:318–334
Wi S, Lee JW, Kim M, Park C-H, Cho S-R. An Enriched Environment Ameliorates Oxidative Stress and Olfactory Dysfunction in Parkinson's Disease with α-Synucleinopathy. Cell Transplant 2018; 27:831–839
Winner B, Jappelli R, Maji SK, Desplats PA, Boyer L, Aigner S, Hetzer C, Loher T, Vilar M, Campioni S, Tzitzilonis C, Soragni A, Jessberger S, Mira H, Consiglio A, Pham E, Masliah E, Gage FH, Riek R. In vivo demonstration that alpha-synuclein oligomers are toxic. Proc Natl Acad Sci U S A 2011; 108:4194–4199
Winslow AR, Chen C-W, Corrochano S, Acevedo-Arozena A, Gordon DE, Peden AA, Lichtenberg M, Menzies FM, Ravikumar B, Imarisio S, Brown S, O'Kane CJ, Rubinsztein DC. α-Synuclein impairs macroautophagy: implications for Parkinson's disease. J Cell Biol 2010; 190:1023–1037
Wong WT. Microglial aging in the healthy CNS: phenotypes, drivers, and rejuvenation. Front Cell Neurosci 2013; 7:22
Wong YC, Krainc D. α-synuclein toxicity in neurodegeneration: Mechanism and therapeutic strategies. Nat Med 2017; 23:1–13
Wu KP, Kim S, Fela DA, Baum J. Characterization of Conformational and Dynamic Properties of Natively Unfolded Human and Mouse α-Synuclein Ensembles by NMR: Implication for Aggregation. J Mol Biol 2008; 378:1104–1115
Xia Y, Zhang G, Kou L, Yin S, Han C, Hu J, Wan F, Sun Y, Wu J, Li Y, Huang J, Xiong N, Zhang Z, Wang T. Reactive microglia enhance the transmission of exosomal α-synuclein via toll-like receptor 2. Brain 2021; 144:2024-2037
Xu H, Gelyana E, Rajsombath M, Yang T, Li S, Selkoe D. Environmental Enrichment Potently Prevents Microglia-Mediated Neuroinflammation by Human Amyloid β-Protein Oligomers. J Neurosci 2016; 36:9041–9056
Xu Q, Park Y, Huang X, Hollenbeck A, Blair A, Schatzkin A, Chen H. Physical activities

and future risk of Parkinson disease. Neurology 2010; 75:341–348

Yang F, Lagerros YT, Bellocco R, Adami HO, Fang F, Pedersen NL, Wirdefeldt K. Physical activity and risk of Parkinson's disease in the Swedish National March Cohort. Brain 2015; 138:269–275

Zhang T-Y, Keown CL, Wen X, Li J, Vousden DA, Anacker C, Bhattacharyya U, Ryan R, Diorio J, O'Toole N, Lerch JP, Mukamel EA, Meaney MJ. Environmental enrichment increases transcriptional and epigenetic differentiation between mouse dorsal and ventral dentate gyrus. Nat Commun 2018; 9:298

Zhang W, Wang T, Pei Z, Miller DS, Wu X, Block ML, Wilson B, Zhang W, Zhou Y, Hong J-S, Zhang J. Aggregated α-synuclein activates microglia: a process leading to disease progression in Parkinson's disease. FASEB J 2005; 19:533–542

9 Acknowledgments

First of all, I want to thank my supervisor Prof. Dr. Anja Schneider for giving me the opportunity to pursue my doctoral studies in her group. I am deeply grateful for your scientific guidance, scientific discussions, and your support during the last five years.

I would like to thank Prof. Dr. Tiago Fleming Outeiro and Prof. Dr. Ullrich Wüllner for their willingness to be members of my thesis committee. Many thanks to Prof. Dr. Ina Vorberg for being part of my dissertation committee and for the helpful discussions and ideas at the annual meetings.

I would like to express my special thanks to Prof. Donato di Monte and all lab members for the great collaboration and help to move the project forward. I am grateful for the contribution of Angela, Michael H., and Ayse to my project. I would like to thank Michael K., Michael H., and Laura for showing me all the methods. Special thanks to Ayse for the scientific discussions and ideas during this project.

I would like to thank the animal caretakers at DZNE Bonn who took care of the mice. I would also like to thank Ireen and Hans from the Light Microscope Facility (LMF) at the DZNE in Bonn for their great efforts and solution-oriented support!

I had the opportunity to work together with amazing people in the lab. Many thanks to all former lab members, Belissa, Anne, and Beate who helped me settle in at the lab in the beginning. I appreciated the discussions, ideas, experimental help, and lab dinners with all the current lab members. Thanks to Anna, Kristin, Madhurima, Sally, Loic, and Eva.

I want to thank my friends who always supported and encouraged me during the good and bad times of my PhD. Thank you, Lilly, Eva, Nina, Annika, Beate, and Stephi for the wonderful times and memories inside and outside of the lab. I am also really grateful to have someone in my life who supports me and is always by my side. Thank you, Daniel.

Ich möchte meiner Familie danken für die Unterstützung, die Liebe und den Glauben an mich. Ihr habt mich zu dem Menschen gemacht, der ich heute bin.

10 Publication

Stuendl, A., **Kraus, T.**, Chatterjee, M., Zapke, B., Sadowski, B., Moebius, W., Hobert, M.A., Deuschle, C., Brockmann, K., Maetzler, W., Mollenhauer, B. and Schneider, A. (2021), *α-Synuclein in Plasma-Derived Extracellular Vesicles Is a Potential Biomarker of Parkinson's Disease.* Mov Disord. https://doi.org/10.1002/mds.28639